ISSN 0916-7390

九州大学大学院理学研究院紀要

MEMOIRS

OF THE

FACULTY OF SCIENCES

KYUSHU UNIVERSITY

Series D Earth and Planetary Sciences

VOLUME XXXII

No. 3

FUKUOKA, JAPAN

March, 2011

Contents

All communications relating to this Memoirs should be addressed to the Dean of the Faculty of Sciences, Kyushu University Hakozaki, Fukuoka 812-8581, JAPAN

Mem. Fac. Sci., Kyushu Univ., Ser. D, Earth & Planet. Sci., Vol. XXXII, No. 3,
pp. 1-10, March 10, 2011

Occurrences of radiolarian biostratigraphic markers *Lychnocanoma nipponica sakaii* and *Amphimelissa setosa* in Core YK07-12 PC3B from the Okhotsk Sea

Takahito Ikenoue*, Kozo Takahashi*, Tatsuhiko Sakamoto**,
Saburo Sakai** and Koichi Iijima**

Abstract

Core YK07-12 PC03B obtained from the central Okhotsk plain (52°36'N, 150°08'E ; water depth: 1049 m) was analyzed every 5 cm, focusing on two radiolarian biostratigraphic markers in the late Pleistocene: *Lychnocanoma nipponica sakaii* and *Amphimelissa setosa*. The last occurrence (LO) datum of *A. setosa* at 67 ka conformed with those of the LO of the previously published studies. However, the LO of *L. nipponica sakaii* at 25 ka was off set and significantly younger than those published in the previous studies in the North Pacific and the marginal seas. We introduce herein the conceptual use of the last common occurrence (LCO) of *L. nipponica sakaii* as the LCO conforms with the LO of this taxon published elsewhere and hence more reliable, especially out side of the northern part of the central Okhotsk plain. The LCO of *L. nipponica sakaii* is 46 ka, 21 kyrs older than the LO, but is approximately the same as the LOs published elsewhere. We postulate the LCO as a practical datum which can be compared with the data from out side of the studied region. As alternative explanations, the obtained significantly younger LO than the LOs of other studies from the out side of the study region may stem from the following two reasons. Because that the present study is specifically focused on the two biostratigraphic marker radiolarian taxa with details our microscopic counts are significantly greater than those performed in the previous studies. This may have caused the documentation of the LO with the rare microscopic counts on multiple microslides, which could have been missed had we counted only one microslide. It is also possible that the effect of bioturbation due to upward transport in the slow sedimentation rate regime caused the appearance of the rare specimens of *L. nipponica sakaii* well above the LCO.

Keywords: Radiolarian biostratigraphy, last occurrence (LO), last common occurrence (LCO), *Lychnocanoma nipponica sakaii, Amphimelissa setosa*, Okhotsk Sea, late Pleistocene

1. Introduction

The Okhotsk Sea represents as one of the lowest latitude regions with extensive sea-ice cover in the world. Environmental conditions of the Okhotsk Sea with such sea-ice formation can alter global water circulations because that the formation results in the generation of dense Okhotsk intermediate water which exits into the North Pacific (e.g., Talley, 1991). The Okhotsk Sea is also characterized by a high biological productivity and thus it serves as an efficient biological pump to absorb atmospheric CO_2. Therefore, for further understanding the global carbon cycle it is important to study the region including the past environmental conditions (Takahashi, 1998).

Radiolarians represent as one of the common microzooplankton groups in the pelagic and hemipelagic realms. Their siliceous skeletons are often well preserved in the sediments and hence they can be used in biostratigraphy

Manuscript received on 1 November 2010; accepted on 7 January 2011
* Department of Earth & Planetary Sciences, Graduate School of Sciences, Kyushu University, 6-10-1 Hakozaki, Higashi-ku, Fukuoka 812-8581, JAPAN; Corresponding author's e-mail: ikenoue@geo.kyushu-u.ac.jp
** Earth and Life History Research Program, Institute of Biogeosciences, Japan Agency for Marine-Earth Science and Technology (JAMSTEC), Natsushima-cho 2-15, Yokosuka, 237-0061, JAPAN

of deep-sea sediments and reconstruction of paleoceanographic conditions. Pertinent previous works on radiolarian biostratigraphy in the Okhotsk Sea are, for example, published by Takahashi et al. (2000), Matul et al. (2002, 2009), and Okazaki et al. (2003, 2005). The purpose of this study is to examine radiolarian biostratigraphic markers of the late Pleistocene in detail employing Core YK07-12 PC03B obtained in the northern part of the central Okhotsk plain.

2. Materials and Methods

During Cruise YK07-12 of R/V Yokosuka belonging to Japan Agency for Marine-Earth Science and Technology (JAMSTEC) in summer 2007, Core YK07-12 PC03B was obtained from the northern part of the central Okhotsk plain (52°36'N, 150°08'E ; water depth: 1,049 m; Fig. 1). The recovered core length is 14.09 m. Sediment samples were continuously sliced every 1 cm in thickness throughout the core. In this study, samples were analyzed at every 5 cm interval.

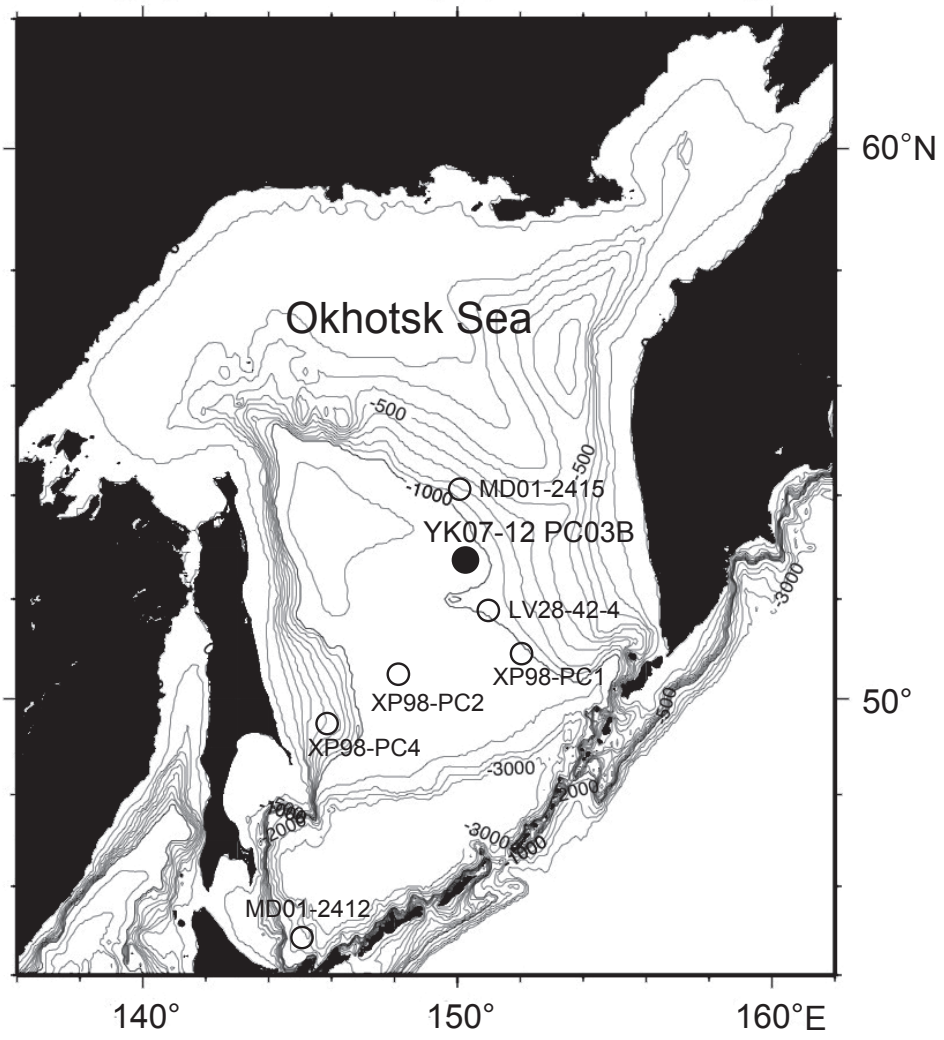

Fig. 1. Location map of Core YK07-12 PC03B (solid circle) together with other relevant cores (open circles) in the Okhotsk Sea.

An age model of Core YK07-12 PC3B was established based on $\delta^{18}O$ stratigraphy with subordinate magnetic susceptibility (MS). Graphic correlations of $\delta^{18}O$ records were established between the $\delta^{18}O$ variations of benthic foraminifer shells (*Uvigerina* spp.) in Core PC3B and the standard curve of LR04 Benthic $\delta^{18}O$ global stack constructed by Lisiecki and Raymo (2005) (Fig. 2). As results of the analyses, Marine Isotope Stages (MIS) 1-12.3 were identified, and it was determined that Core PC3B recorded at least 450 kyrs of the environmental conditions of the northern part of the central Okhotsk plain.

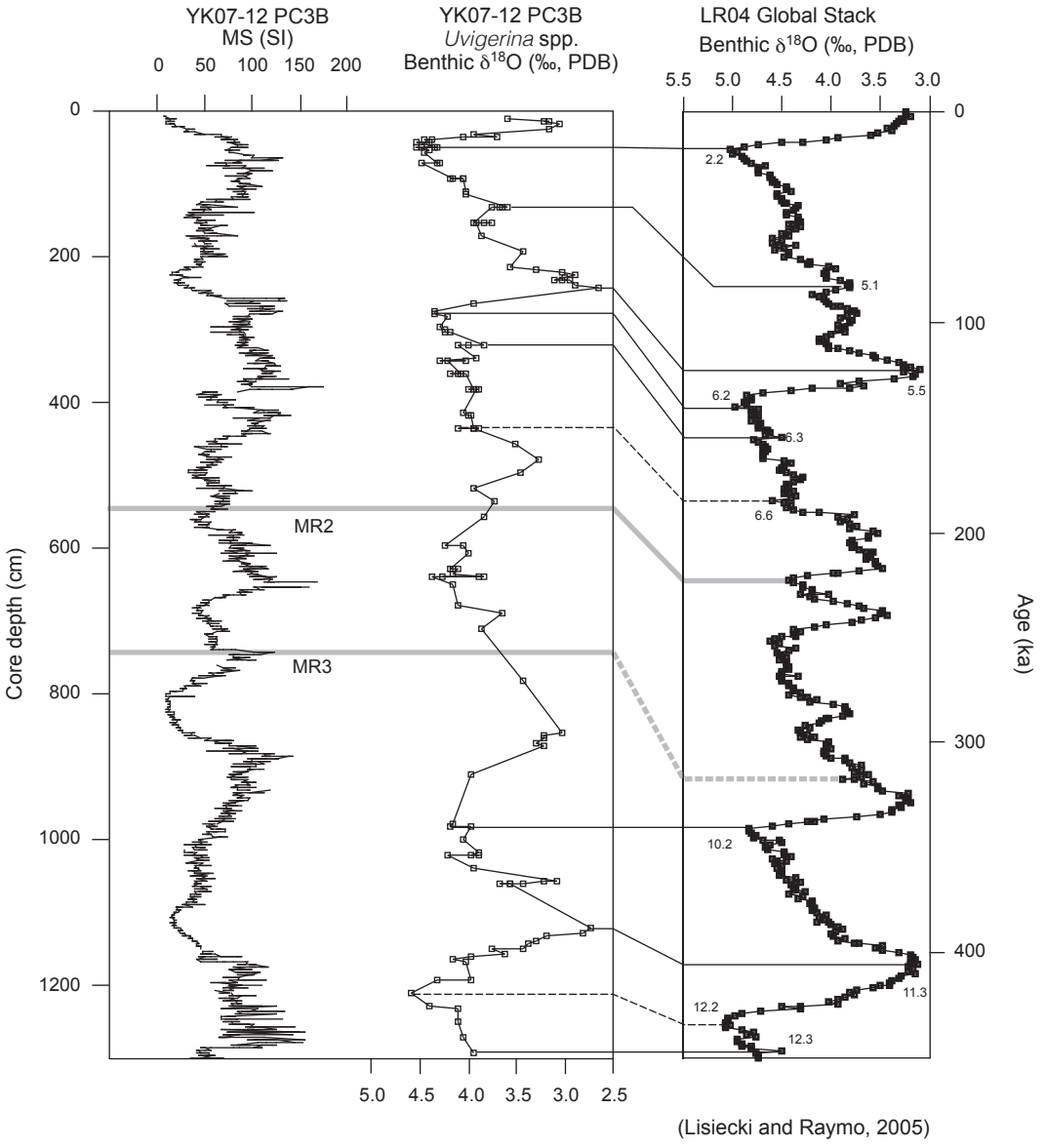

Fig. 2. An age model of Core YK07-12 PC3B based on $\delta^{18}O$ stratigraphy and subordinated by MS. Changes in (a) MS of Core YK07-12-PC3B; (b) benthic foraminiferal (*Uvigerina* spp.) $\delta^{18}O$ of Core YK07-12-PC3B; and (c) stacked benthic foraminiferal oxygen isotope curve LR04 (Lisiecki and Raymo, 2005), Lines MR2 and MR3 are tephra horizons recovered in Core YK07-12 PC3B.

Radiolarian counts were conducted on 53 selected samples whose ages ranged from 133 ka at 264.5 cm depth to the present at the core top. Wet samples of 100-1,100 mg were weighed after freeze-drying for 24 hrs. They were treated with 5 ml of 1N hydrochloric acid, 10 ml of 30% hydrogen peroxide, and heated on a hot plate at 90℃ for 1 hr in order to remove organic matter and calcium carbonate. Then, Calgon® (hexametaphosphate, surfactant) solution was added to the mixture to further disaggregate the sediments. Our samples contained a large amount of lithogenic grains and thus we employed the elutriation method for extracting opal particles from the residues according to Itaki (2003). After the elutriation, samples were sieved through a stainless screen with 45 μm mesh and filtered through Gellman® membrane filters with a nominal pore size of 0.45 μm. The filtered samples were washed with distilled water to remove salts, dried in an oven at 50°C, and then permanently mounted with Canada Balsam® on microslides. We counted the number of all radiolarian specimens on the slides under a compound light-microscope at x100-200 magnifications. Normally, counts were made on an entire area of

Table 1. Radiolarian counts in Core YK07-12 PC3B.

							Total Radiolaria		*Lychnocanoma nipponika sakaii*				*Amphimelissa setosa*			
Section	Total depth at cube center (cm)	Age (ka)	Dry bulk density (g cm^{-3})	SR (cm ky^{-1})	Dry sediment (g)	Number of slides counted	Count	AR (No. rads cm^2 ky^{-1})	Count	AR (No. rads cm^2 ky^{-1})	%	Specimens (g dry sed.$^{-1}$)	Count	AR (No. rads cm^2 ky^{-1})	%	Specimens (g dry sed.$^{-1}$)
1	9.3	0.00	0.324	2.49	0.042	1	434	8381	0	0	0	0	0	0	0	0
1	16.0	2.79	0.459	2.49	0.040	1	630	17896	0	0	0	0	0	0	0	0
1	20.5	5.59	0.564	2.49	0.043	1	563	18559	0	0	0	0	0	0	0	0
1	25.0	8.38	0.617	2.49	0.050	1	323	9901	0	0	0	0	0	0	0	0
1	29.5	11.18	0.526	2.49	0.051	1	130	3374	0	0	0	0	0	0	0	0
1	34.0	13.97	0.742	2.49	0.057	1	168	5418	0	0	0	0	0	0	0	0
1	40.9	16.76	0.976	2.49	0.096	1	34	860	0	0	0	0	0	0	0	0
1	45.4	19.69	1.010	1.43	0.118	1	79	970	0	0	0	0	0	0	0	0
1	50.0	23.16	1.005	1.43	0.413	4	282	981	0	0	0	0	0	0	0	0
1	54.5	26.63	0.968	1.43	0.420	4	426	1404	1	3	0	2	0	0	0	0
1	59.1	30.10	1.057	1.43	0.982	8	721	1110	4	6	0.55	4	0	0	0	0
1	66.0	33.57	1.045	1.43	0.408	3	561	2055	12	44	2.14	29	0	0	0	0
1	70.6	37.03	1.002	1.43	0.419	2	1382	4727	2	7	0	5	0	0	0	0
1	75.2	40.50	0.957	1.43	0.427	2	1600	5134	2	6	0	5	0	0	0	0
1	79.3	43.97	1.058	1.43	0.095	1	239	3819	3	48	1.26	32	0	0	0	0
2	79.3	44.66	1.002	1.43	0.096	1	192	2861	0	0	0	0	0	0	0	0
2	84.8	48.13	1.020	1.43	0.441	2	972	3218	89	295	9.16	202	0	0	0	0
2	89.4	51.60	0.938	1.43	0.491	5	326	891	222	606	68.10	452	0	0	0	0
2	94.0	55.07	0.967	1.43	0.527	5	252	661	122	320	48.41	231	0	0	0	0
2	100.9	58.54	0.966	1.43	0.452	8	309	945	195	596	63.11	432	0	0	0	0
2	105.5	62.01	0.914	1.43	0.407	3	590	1894	335	1075	56.78	823	0	0	0	0
2	110.1	65.47	0.946	1.43	0.071	1	122	2331	35	669	28.69	494	0	0	0	0
2	114.7	68.94	1.151	1.43	0.139	1	189	2235	32	378	16.93	230	1	12	0.53	7
2	119.2	72.41	0.730	1.43	0.066	1	232	3670	38	601	16.38	576	0	0	0	0
2	126.1	75.88	0.700	1.43	0.058	1	305	5304	56	974	18.36	972	2	35	0.66	35
2	130.6	79.20	0.706	1.43	0.057	1	279	4979	60	1071	21.51	1060	2	36	0.72	35
2	135.2	81.15	0.493	2.5	0.027	1	223	10294	41	1893	18.39	1536	4	185	1.79	150
2	139.8	83.10	0.566	2.5	0.049	1	357	10352	63	1827	17.65	1291	3	87	0.84	61
2	144.4	85.06	0.619	2.5	0.046	1	359	12211	44	1497	12.26	967	1	34	0.28	22
2	149.0	87.01	0.584	2.5	0.043	1	194	6522	25	840	12.89	576	4	134	2.06	92
2	155.9	88.97	0.652	2.5	0.060	1	495	13505	48	1310	9.70	804	2	55	0.40	34
2	160.5	90.92	0.502	2.5	0.062	1	631	12741	56	1131	8.87	900	19	384	3.01	305
2	165.1	92.88	0.578	2.5	0.056	1	476	12328	71	1839	14.92	1272	7	181	1.47	125
2	169.7	94.83	0.622	2.5	0.056	1	322	8926	71	1968	22.05	1266	7	194	2.17	125
2	174.3	96.79	0.665	2.5	0.064	1	309	8085	33	863	10.68	520	9	235	2.91	142
3	178.9	98.94	0.724	2.5	0.051	1	366	12984	38	1348	10.38	745	9	319	2.46	176
3	184.6	100.89	0.659	2.5	0.067	1	331	8206	6	149	1.81	90	11	273	3.32	165
3	189.0	102.85	0.595	2.5	0.052	1	790	22408	24	681	3.04	458	42	1191	5.32	802
3	195.8	104.80	0.740	2.5	0.058	1	804	25809	22	706	2.74	382	50	1605	6.22	868
3	200.2	106.75	0.626	2.5	0.063	1	2166	53544	23	569	1.06	363	149	3683	6.88	2354
3	204.8	108.71	0.588	2.5	0.061	1	2522	60421	18	431	0.71	293	199	4768	7.89	3241
3	209.4	110.66	0.575	2.5	0.064	1	4001	89649	26	583	0.65	405	642	14385	16.05	10000
3	214.1	112.62	0.518	2.5	0.037	1	3002	104436	36	1252	1.20	968	578	20108	19.25	15538
3	221.1	114.57	0.510	2.5	0.046	1	2810	78002	30	833	1.07	654	506	14046	18.01	11024
3	225.7	116.53	0.585	2.5	0.049	1	2925	87846	26	781	0.89	534	470	14115	16.07	9651
3	230.3	118.48	0.561	2.5	0.033	1	1939	81672	27	1137	1.39	811	203	8551	10.47	6096
3	234.9	120.44	0.601	2.5	0.043	1	1651	58251	22	776	1.33	516	86	3034	5.21	2019
3	239.5	122.41	0.626	2.5	0.056	1	1367	37905	14	388	1.02	248	111	3078	8.12	1968
3	244.1	124.44	0.638	1.85	0.059	1	557	11132	5	100	0.90	85	48	959	8.62	812
3	250.9	126.47	0.687	1.85	0.059	1	762	16461	9	194	1.18	153	45	972	5.91	765
3	255.5	128.50	0.917	1.85	0.081	1	421	8875	8	169	1.90	99	46	970	10.93	571
3	260.0	130.53	0.973	1.85	0.101	1	278	4934	7	124	2.52	69	21	373	7.55	207
3	264.5	132.56	1.021	1.85	0.076	1	344	8582	3	75	0.87	40	22	549	6.40	291

one microslide with a goal of counting >300 specimens. The counts of <200 specimens were resulted in eight cases out of the total of 55 cases whereas the counts exceeding 500 specimens resulted in 22 cases (11 cases >1,000 specimens) (Table 1). In two extremely cases of rare radiolarian occurrences (Samples 59.1 cm and 100.9 cm) eight microslides were prepared and all the slides were counted in order to fulfill the initial goal of counting sufficient number of specimens. In order to achieve the goal as close as possible, multiple microslides were counted in eleven cases in total (Table 1). The classification of *Lychnocanoma nipponica* (Nakaseko) *sakaii* (Morley and Nigrini) and *Amphimelissa setosa* (Cleve) in the samples follow that of Morley and Nigrini (1995) for the former and Bjørklund et al. for the latter (1998), respectively.

A radiolarian accumulation rate (RAR) was calculated using the following equation: RAR (No. radiolarians cm^{-2} kyr^{-1})= [No. radiolarians g^{-1} dry sediment] (No. g^{-1}) × [dry bulk density] (g cm^{-3}) × [sedimentation rate] (cm kyr^{-1}). Dry bulk density was determined from weights of each of 10 cc sediment samples taken with a polypropylene cube. It was calculated from the wet bulk density multiplied by the water contents (%). The water contents of each sample were determined from weights of the wet and dry samples. The samples were weighed before and after drying in an oven at 50℃ for 24 hrs. Sedimentation rates (SR) were assumed between the age control points.

3. Results and Discussion

The temporal changes in total RAR in Core YK07-12 PC3B are shown in Fig. 3. Its pattern tends to follow the temporal patterns displayed by the global $\delta^{18}O$ changes during the glacial-interglacial cycles (e.g., Lisiecki and Raymo, 2005); total RAR increased during the interglacial periods and decreased during the glacial periods at least for the time span examined. The values during MIS 1 and MIS 5 were relatively high compared to those of the other MIS stages.

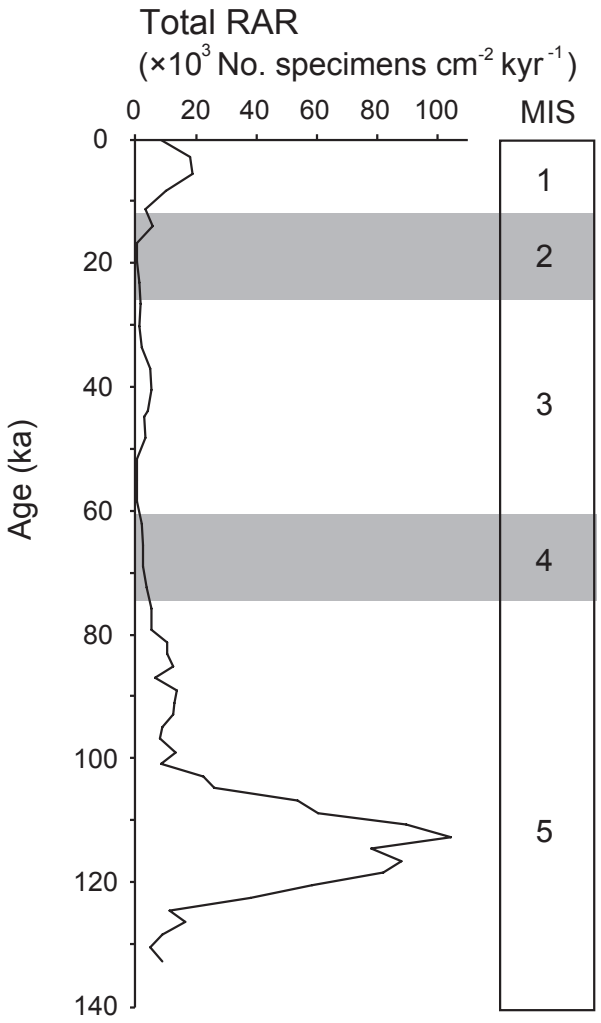

Fig. 3. Changes in total RAR in Core YK07-12 PC3B during the last 130 kyrs. Gray areas indicate cold MIS.

In this study we focused on two important radiolarian taxa as biostratigraphic markers in the late Pleistocene: *Lychnocanoma nipponica* (Nakaseko) *sakaii* (Morley and Nigrini) and *Amphimelissa setosa* (Cleve) (Fig. 4). They are quite useful markers in the North Pacific and marginal seas (Bjørklund and Swanberg, 1987; Morley et al., 1995; Matul et al., 2002). In Core YK07-12 PC3B, the LO of *L. nipponica sakaii* occurred in the upper MIS 3 at 25 ka, and the *L. nipponica sakaii* acme event occurred at 81 ka (Table 1, Fig. 5). Our data displayed several differences compared to the results shown by the previous studies. The LO of *L. nipponica sakaii* in the previous studies are listed in Table 2. Specifically, the LO of *L. nipponica sakaii* was 49 ka (Morley et al., 1982) and 50 ka (Morley et al., 1995) in the North Pacific. Tanaka and Takahashi (2005) and Itaki et al. (2009) dated the LO of *L. nipponica sakaii* at 46-52 ka using sediment samples from the Bering Sea. Itaki et al. (2007) also estimated the LO to be 54 ka using sediment samples from the Japan Sea. The LO in four piston cores XP98-PC1, XP98-PC2, XP98-PC4, MD01-2412 from the Okhotsk Sea were determined also as ca. 50 ka (Takahashi et al., 2000; Okazaki at al., 2005). The locations of these four core sites are further south of the core site of the present study.

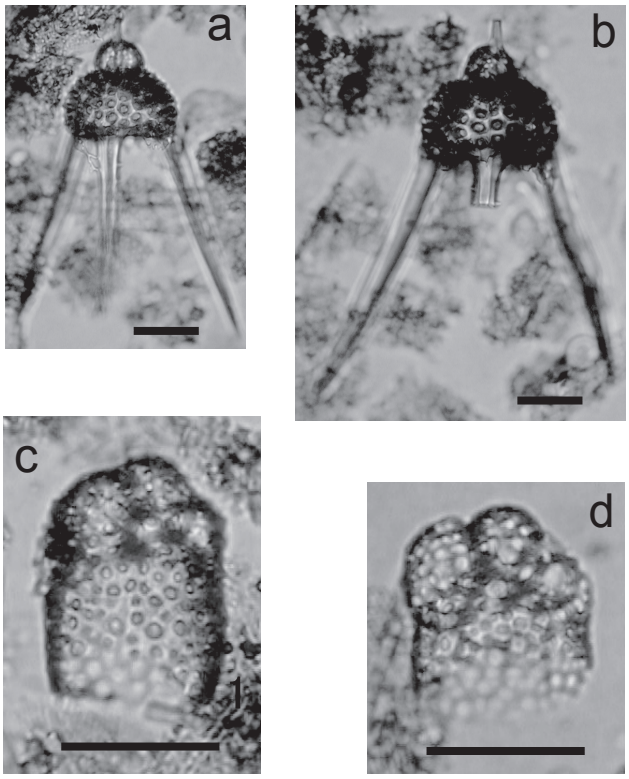

Fig. 4. Radiolarian taxa from Core YK07-12 PC03B discussed in the text. All scale bars equal to 50 μm. a. *Lychnocanoma nipponica* (Nakaseko) *sakaii* (Morley and Nigrini), Sample 230.3 cm. b. *Lychnocanoma nipponica* (Nakaseko) *sakaii* (Morley and Nigrini), Sample 230.3 cm. c. *Amphimelissa setosa* (Cleve), sample 230.3 cm. d. *Amphimelissa setosa* (Cleve), Sample 230.3 cm.

On the contrary to the majority of the LOs of ca, 50 ka mentioned above, Matul et al. (2002) and Matul et al. (2009) proposed the LO to have occurred at 28 ka and 34 ka in the central Okhotsk Sea, which is fundamentally the same region as that in our study. As mentioned earlier, the results of our study also show that the LO to be at 25 ka level, approximately the same age as those in Matul et al. (2002, 2009). These LOs from the three piston cores (LV28-42-4, MD01-2412, and YK07-12 PC03B) from the same general region collectively displayed significantly younger ages than those from other previous studies. While there is a discrepancy in the timing of the LOs between the older (ca. 50 ka) and younger (34-25 ka) groups, the overall patterns of the population change with time appear to be conformable between the two groups. Namely, the AR, abundance and relative abundance of *L. nipponica sakaii* increased steadily from ca. 120 ka towards 50 ka and rapidly declined after 50

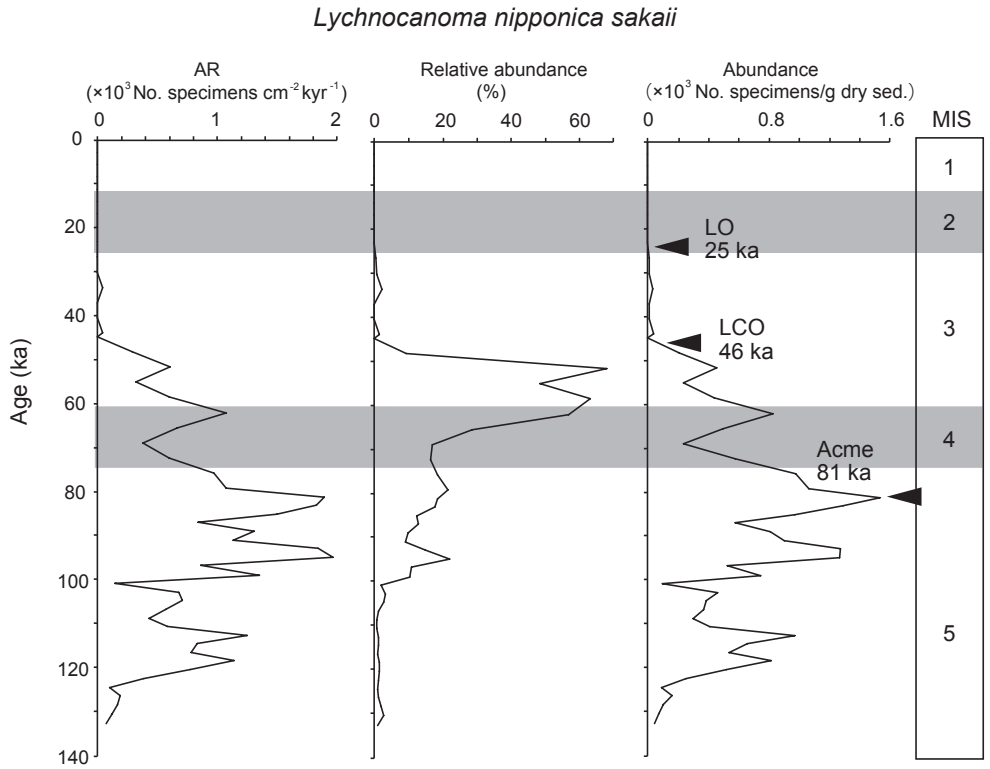

Fig. 5. Changes in AR, relative abundance and abundance of *L. nipponica sakaii* in Core YK07-12 PC03B. The LO, LCO and Acme datums are shown with arrows.

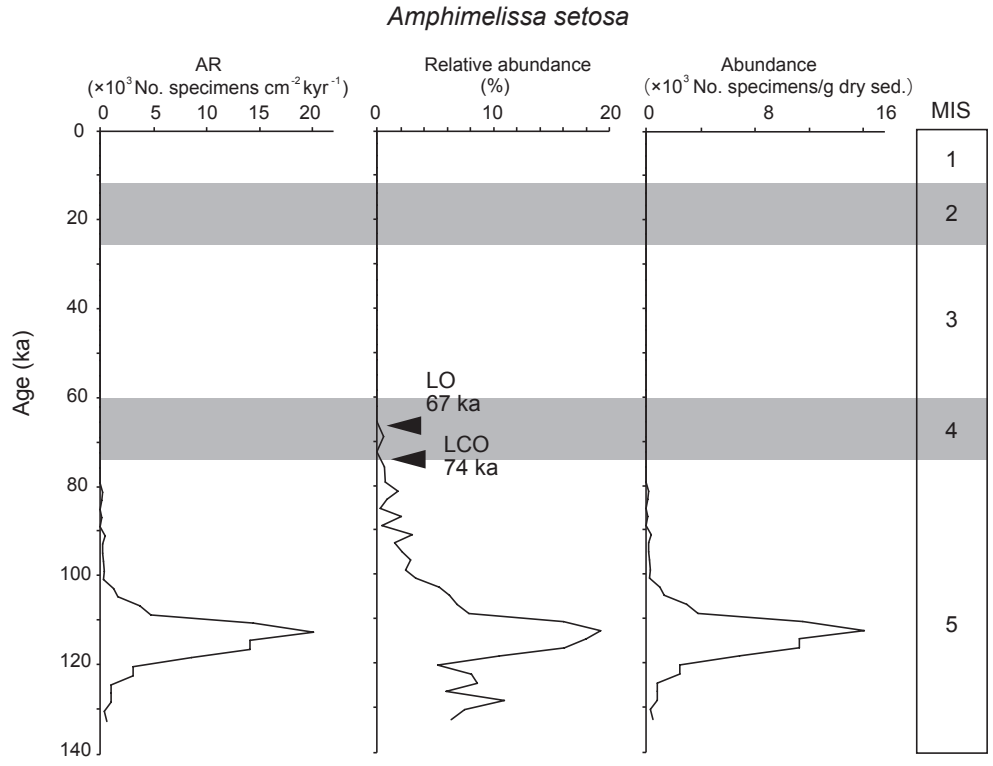

Fig. 6. Changes in AR, relative abundance and abundance of *A. setosa* in Core YK07-12 PC03B. The LO and LCO are shown with arrows.

ka. Thus, the trend of the changes in AR, abundance and relative abundance in our study are roughly conformable with those in the previous studies.

Furthermore, the LO of *A. setosa* is placed at 67 ka within MIS 4, slightly above the MIS 4/5 boundary (Fig. 6). Thus, the LO of *L. nipponica sakaii* and *A. setosa* obtained from Core YK07-12 PC3B correspond to the LOs of Core LV28-42-4 (Matul et al., 2002) fairly well. It is quite possible that the LO of *L. nipponica sakaii* in the northern part of the central Okhotsk plain is diachronous with respect to the LO of this taxon further south in the Okhotsk plain and in other basins, considering the consistency of the LOs from the same region. It is plausible that the environmental conditions between ca. 50 ka and ca. 34-25 ka in the northern part of the central Okhotsk plain were still favorable for the survival of *L. nipponica sakaii* whereas those of the further south were severe enough to cause an extinction of this taxon at ca. 50 ka. This could well be due to the distribution of the sea-ice cover during the interval in question in the region. It is noteworthy to mention here that the sea-ice cover was more extensive at Site XP98-PC1 than Site XP98-PC2 (Fig. 1), according to Okazaki et al. (2005). Shiga and Koizumi (2000) also reported more open water conditions in the eastern Okhotsk Sea than in the western area during the time period around 22 ka and the last glacial maximum. Based on these pieces of information we interpret that the survival of *L. nipponica sakaii* was prolonged at our study site than the western area and perhaps further south in the Okhotsk Sea. Thus, one of the possible three reasons (see below for the remainders) for the significantly young 25 ka as the LO is the diachronous extinction of this taxon within the entire Okhotsk Sea.

As a part of the second explanation of the discrepancy, we herein propose the introduction of "the last common occurrence (LCO)" concept as a practical biostratigraphic datum. This datum should be far more reliable than the LO for the following details which we have encountered in the present piston core. The tail end of the occurrence of *L. nipponica sakaii* prior to ca. 25 ka (Fig. 5) may well be due to the detailed radiolarian counts performed in our study, which is specifically devoted to illustrate the exact occurrences. Specifically, the total radiolarian counts of 426 (4 microslides) at 27 ka and 721 (8 microslides) at 30 ka were performed (Table 1). These values are apparently far more greater than those proceeded in other published data whereas their exact counts were not published nor available in their results. Our microscopic counts for *L. nipponica sakaii* were one specimen at 27 ka and four specimens at 30 ka, respectively (Table 1). These relatively small count values could well have been missed and recorded as zeros, had the significantly smaller counts (1 microslide or portion of it) than the present study were made. In that case our LO would have been 46 ka in stead. Thus, it makes a sense to use the 46 ka level as the LCO, which is graphically illustrated as the rapid decrease interval in AR, abundance and %*L. nipponica sakaii*.

Table 2.

(a) List of the LO / LCO of *L. nipponica sakaii* and SR for cores used in the recent studies.

Core/ Site	Area	Latitude	Longitude	Age (ka)	SR (cm kyr^{-1})	Reference
YK07-12 PC03B	Okhotsk Sea	52°36.01' N	150°08.25' E	25 / 46	2.86	This paper
LV28-42-4	Okhotsk Sea	51°42.89' N	150°59.13' E	28	2-4	Matul et al. (2002)
MD01-2415	Okhotsk Sea	53°57.09' N	149°57.52' E	34	2-4	Matul et al. (2009)
MD01-2412	Okhotsk Sea	44°31' N	145°00' E	47-48	46	Okazaki et al. (2005)
XP98-PC1	Okhotsk Sea	51°00.9' N	152°00.5' E	43-44	8.1	Takahashi et al. (2000)
XP98-PC2	Okhotsk Sea	50°23.7' N	148°19.4' E	53-55	10.5	Takahashi et al. (2000)
XP98-PC4	Okhotsk Sea	49°29.3' N	146°07.7' E	55-56	12.6	Takahashi et al. (2000)
PC-23A	Bering Sea			48.6		Itaki et al. (2009)
ES	Bering Sea			45.9		Tanaka and Takahashi (2005)
BOW-8A	Bering Sea			49.5		Tanaka and Takahashi (2005)
BOW-9A	Bering Sea			49.7		Tanaka and Takahashi (2005)
BOW-12A	Bering Sea			51.7		Tanaka and Takahashi (2005)
MD01-2407 & others	Japan Sea			54		Itaki et al. (2007)
V20-120, RC14-103 & others	North Pacific			49		Morley et al. (1982)
ODP Sites 881, 883 & others	North Pacific			50		Morley et al. (1995)

(b) List of the LO / LCO of *A. setosa* and SR for cores used in the recent studies.

Core/ Site	Area	Latitude	Longitude	Age (ka)	SR (cm kyr^{-1})	Reference
YK07-12 PC03B	Okhotsk Sea	52°36.01' N	150°08.25' E	67 / 74	2.86	This paper
LV28-42-4	Okhotsk Sea	51°42.89' N	150°59.13' E	72	2-4	Matul et al. (2002)
MD01-2415	Okhotsk Sea	53°57.09' N	149°57.52' E	64	2-4	Matul et al. (2009)
ES	Bering Sea			85.1		Tanaka and Takahashi (2005)
BOW-8A	Bering Sea			111.5		Tanaka and Takahashi (2005)
BOW-9A	Bering Sea			68		Tanaka and Takahashi (2005)
GAT-3A	Bering Sea			82.6		Tanaka and Takahashi (2005)
	North Pacific			70		Bjørklund and Swanberg (1987)

As a second alternative, the slow SR observed in the central Okhotsk Sea may have caused the discrepancy in the LO levels. Itaki et al. (2009) speculated that the delay of the LO of *L. nipponica sakaii* by Matul et al. (2002) might be due to the effect of bioturbation in the slow SR environment. When sedimentation rates are slow fossil radiolarian specimens initially located at several cm deep (or even deeper sometimes) in sediments, for example, could have been subsequently transported upward to the sediment surface or nearby by organisms living near the surface or within sediments, causing a bioturbation. Such an activity can alter the sequentially deposited initial signature in a drastic manner. On the other hand, the chances of the effect in high SR regime can minimize such an action because faster burial than the artifact of the bioturbation. The sedimentation rates of the previously studied cores from the Okhotsk Sea are shown in Table 2. The sediment cores with higher SRs than the three piston cores (LV28-42-4, MD01-2412, and PC03B) may have led the LO of *L. nipponica sakaii* to be ca. 50 ka. Thus, the time lag of the LO of *L. nipponica sakaii* with respect to the LCO in YK07-12 PC03B could possibly be due to the effect of bioturbation in the slow SR regime. Note that the first disappearances of *L. nipponica sakaii* and *A. setosa* after the major occurrence maxima are 46 ka and 74 ka, respectively. These ages are nearly equal to the LO of other previously published studies. One drawback of such an explanation with the slow SR is that the LO of *A. setosa* at 68 ka did not cause any significant time lag compared to the data from the fast SR regimes. Because that the occurrence of total radiolarians is about the same at both at 25 ka and 67 ka (Table 1, Fig. 3) it is difficult to explain why we did not encounter a time lag problem in the LO of *A. setosa* in the present piston core.

4. Conclusions

A focused detailed study on two important radiolarian biostratigraphic markers of the late Pleistocene was performed in the northern part of the central Okhotsk plain: *Lychnocanoma nipponica* (Nakaseko) *sakaii* (Morley and Nigrini) and *Amphimelissa setosa* (Cleve). We have employed Core YK07-12 PC3B from the northern part of the central Okhotsk plain with the aid of benthic foraminiferal $\delta^{18}O$ stratigraphy. The introduction of the concept of "the last common occurrence (LCO)" makes a sense where the LO and the LCO differ significantly in age, especially in the case of the present study. The LCO of the 46 ka in the present study serves as a comparable datum with respect to the LO at ca. 50 ka of *L. nipponica sakaii* found further south in the Okhotsk Sea and elsewhere in the marginal seas of the North Pacific and subarctic Pacific. It is possible that the extinction datum of *L. nipponica sakaii* in the northern part of the central Okhotsk plain (25 ka) specifically lagged behind of that of elsewhere by ca. 25 kyrs. This may well have caused the diachronous LO compared to those of elsewhere. We interpret that the sea-ice conditions were favorable to allow the survival of *L. nipponica sakaii* for additional ca. 16-25 kyrs in the study region compared to elsewhere. As alternative explanations for the discrepancy in the LOs, we also offer (1) the detailed counts of the radiolarians in this devoted study; and (2) the slow SR where bioturbation may have caused the apparent time lag of the LO at 25 ka compared to the LO of ca. 50 ka in the studies performed other than in the northern part of the central Okhotsk plain. Furthermore, the LO of *Amphimelissa setosa* at 67 ka obtained from the present study was conformable with that of Core LV28-42-4.

5. Acknowledgments

We thank scientists, Captain and crew participated in Cruise YK07-12 of R/V Yokosuka who assisted us on board for this work. We thank Dr. Yusuke Okazaki of JAMSTEC for his constructive review of an early draft of this paper as well as further discussion. The senior author received and benefitted by the Professor Tatsuro Matsumoto Scholarship Fund.

6. References

Bjørklund, K.R., and Swanberg, N.R. (1987) The distribution of two morphotypes of the radiolarian *Amphimelissa setosa* Cleve (Nassellarida): a result of environmental variability. *Sarsia*, **72**, 245-254.

Bjørklund, K.R., Cortese, G., Swanberg, N., and Schrader, H.J. (1998) Radiolarian faunal provinces in surface sediments of the Greenland, Iceland and Norwegian (GIN) Seas. *Marine Micropaleontology*, **35**, 105-140.

Itaki, T. (2003) Elutriation technique for the extraction of radiolarian skeletons from sandy sediment. *Fossils*, **73**,

38-41.

Itaki, T., Komatsu, N., and Motoyama, I. (2007) Orbital- and millennial-scale changes of radiolarian assemblages during the last 220 kyrs in the Japan Sea. *Palaeogeography, Palaeoclimatology, Palaeoecology*, **247**, 115-130.

Itaki, T., Uchida, M., Kim, S., Shin, H-S., and Tada, R. (2009) Late Pleistocene stratigraphy and palaeoceanographic implications in northern Bering Sea slope sediments: evidence from the radiolarian species *Cycladophora davisiana*. *Journal of Quaternary Science*, **24**, 856-865.

Lisiecki. L.E., and Raymo, M.E., 2005. A Plio-Pleistocene stack of 57 globally distributed benthic $\delta^{18}O$ records. *Paleoceanography*, **20**, 1003.

Morley, J.J., and Nigrini, J.D. (1995) Miocene to Pleistocene radiolarian biostratigraphy of North Pacific sites 881, 884, 885, 886, and 887. In: Rea, D.K., Basov, I.A., Scholl, D.W., Allan, J.F. (Eds.), *Proc. ODP, Sci. Results*, **145**, College Station, TX (Ocean Drilling Program), 55-91.

Morley, J.J., Hays, J.D., and Robertson, J.H. (1982) Stratigraphic framework for the late Pleistocene in the northwest Pacific Ocean. *Deep-Sea Research*, **29**, 1485-1499.

Morley, J.J., Tiase, V.L., Ashby, M.M., and Kashgarian, M. (1995) A high-resolution stratigraphy for Pleistocene sediments from North Pacific Sites 881, 883, and 887 based on abundance variations of the radiolarian *Cycladophora davisiana*. In: Rea, D.K, Basov, I.A, Scholl D.W., Allen, J.F. (Eds), *Proc. ODP, Sci. Results*, **145**, College Station, TX (Ocean Drilling Program), 133-140.

Matul, A., Abelmann, A., Tiedemann, R., Kaiser, A., and Nürnberg, D. (2002) Late Quaternary polycystine radiolarian datum events in the Sea of Okhotsk. *Geo-Marine Letters*, **22(1)**, 25-32.

Matul, A., Abelmann, A., Nürnberg, D., and Tiedemann, R. (2009) Stratigraphy and major paleoenvironmental changes in the Sea of Okhotsk during the last million years inferred from radiolarian data. *Oceanology*, **49(1)**, 93-100.

Okazaki, Y., Takahashi, K., Yoshitani, H., Nakatsuka, T., Ikehara, M., and Wakatsuchi, M. (2003) Radiolarians under the seasonally sea-ice covered conditions in the Okhotsk Sea: flux and their implications for paleoceanography. *Marine Micropaleontology*, **49(3)**, 195-230.

Okazaki, Y., Takahashi, K., Katsuki, K., Ono, A., Hori, J., Sakamoto, T., Uchida, M., Shibata, Y., Ikehara, M., and Aoki, K. (2005) Late Quaternary paleoceanographic changes in the southwestern Okhotsk Sea: evidence from geochemical, radiolarian, and diatom records. *Deep-Sea Research II*, **52**, 2332-2350.

Shiga, K., and Koizumi, I., (2000) Latest Quaternary oceanographic changes in the Okhotsk Sea based on diatom records. *Mar. Micropaleontol*. **38**, 91-117.

Takahashi, K. (1998) The Bering and Okhotsk Seas: modern and past paleoceanographic changes and gateway impact. *Journal Asian Earth Science*, **16**, 49-58.

Takahashi, K., Okazaki, Y., and Yoshitani, H. (2000) Radiolarian fossils and paleoceanography: accumulation changes in the Okhotsk Sea. *Chikyu Monthly*. **22**, 623-630. [in Japanese]

Talley, L. D. (1991) An Okhotsk Sea water anomaly: implications for ventilation in the North Pacific. *Deep-Sea Research*, **38**, S171-S190.

Tanaka, S. and Takahashi, K. (2005) Late Quaternary paleoceanographic changes in the Bering Sea and the western subarctic Pacific based on radiolarian assemblage. *Deep-Sea Research II*, **52**, 2131-2149.

Mem. Fac. Sci., Kyushu Univ., Ser. D, Earth & Planet. Sci., Vol. XXXII, No. 3,
pp. 11-26, March 10, 2011

Chemosynthetic fossil molluscan faunas from the Neogene Taishu Group, distributed in Tsushima Islands, Nagasaki Prefecture, the southwest Japan

Takashi Ninomiya*

Abstract

The middle of the Neogene Taishu Group, distributed in Tsushima Islands, Nagasaki Prefecture, the southwest Japan, is considered to include the authigenic carbonates originated from cold-seep and the chemosynthetic molluscan faunas deposited in deep sea environment of greater than 500 m depth. In this study, the author examined classification of the bivalves occurred in the middle of the Taishu Group. Consequently, the molluscan faunas are assigned into the following ten species belonging to seven genera: *Bathymodiolus* sp., *Adipicola* sp., *Calyptogena* spp., *Acharax* spp., *Acila* sp., *Nuculana* sp., and *Yoldia* sp.

Keywords: the Neogene Taishu Group, deep sea environment, chemosynthetic molluscan faunas

1. Introduction

The formation of the Sea of Japan is thought to be the results of the following processes. (1) The east margin of the Eurasian Continent subsided in the late Cenozoic; (2) the spreading of the Sea of Japan reached the climax opening stage in the Early Miocene; and (3) the Japanese Archipelago was formed in the middle Miocene (Otofuji and Matsuda, 1983, 1985). The Taishu Group distributed in Tsushima Islands, which is located in the southwest part of the Sea of Japan, has been regarded as the conformable marine deposits and they can be compared with the Paleogene strata distributed in the northwest Kyushu (Nakajo and Funakawa, 1996; Nakajo et al., 2006). Therefore, Tsushima Islands are important area in reconstructing the formation history of the Sea of Japan and the Japanese Archipelago. However, our knowledge concerning the sedimentary environments of the Taishu Group was fragmental and there are many unsettled discussions about the formation age (Okada and Fujiyama, 1970; Nakajo and Maejima, 1998; Nakajo et al., 2006; Yamaguchi and Oho, 2007). Furthermore, the maga-fossils found in the Taishu Group are of mainly shallow marine fossil faunas. However, the maga-fossils are scarce and poorly preserved (Matsumoto, 1969; Masuda, 1970; Takahashi and Nishida, 1975). The author has been studying about the Taishu Group distributed in Tsushima Islands to understand the formation processes of the Sea of Japan and the depositional environments of the deep sea sediments in the southwestern Sea of Japan. Recently, small-scale carbonate and fossil assemblages are found successively in the middle of the Taishu Group (Aoki and Nishida, 1999; Ninomiya et al., 2008). In our study, it has been shown that they are authigenic carbonates originated from cold-seep and that the fossil molluscan faunas are chemosynthetically formed (Ninomiya et al., 2008). They state that the middle of the Taishu Group was deposited in deep-sea environments at greater than 500 m depth (Ninomiya et al., 2010). Therefore, cold-seep carbonates and chemosynthetic fossil assemblages from the Taishu Group are important in deciphering the paleoenvironments of the opening stage of the Sea of Japan. The author reports the classification of chemosynthetic bivalves occurred from the Taishu Group in this paper.

Manuscript received on 24 December 2010; accepted on 27 January 2011
* Department of Earth and Planetary Sciences, Graduate School of Science, Kyushu University, Hakozaki6-10-1, Fukuoka, 812-8581, JAPAN; author's e-mail: sc308031@s.kyushu-u.ac.jp

2. Geological setting of Tsushima Islands

Tsushima Islands are located at 120 km off Kyushu in the southwestern Sea of Japan (Fig. 1). The Taishu Group is conformable marine formation with the thickness of greater than 5,400 m and it is classified into the Lower Formation, Middle Formation and Upper Formation based on lithology and distribution of T3 Tuff (MITI, 1973). The layer of T3 Tuff can be tracked in distance of greater than 40 km (Fig. 2). Anticlinorium and synclinorium structures with a northeast-southwest axis are observed in Tsushima Islands. In the south of Tsushima Islands, where granite as intrusive rock is observed the Taishu Group was affected by contact metamorphism. Also observed are rhyolite, quartz porphyry, plagiophyre and dolerite as intrusive rocks. The formation age of the Taishu Group has been regarded as the early Eocene-early Miocene (Ibaragi, 1994; Nakajo and Funakawa, 1996; Sakai and Yuasa, 1998). However, the author and his colleagues dated T3 Tuff and subaqueous pyroclastics of the Upper Formation. Consequently, we learned that the main part of the Taishu Group was deposited at approximately 16 Ma which was in the middle Miocene (Ninomiya et al., 2010). Furthermore, the lower most of the Taishu Group with the reported early Eocene radiolarians may be compared with the Paleogene strata distributed in the northwest Kyushu.

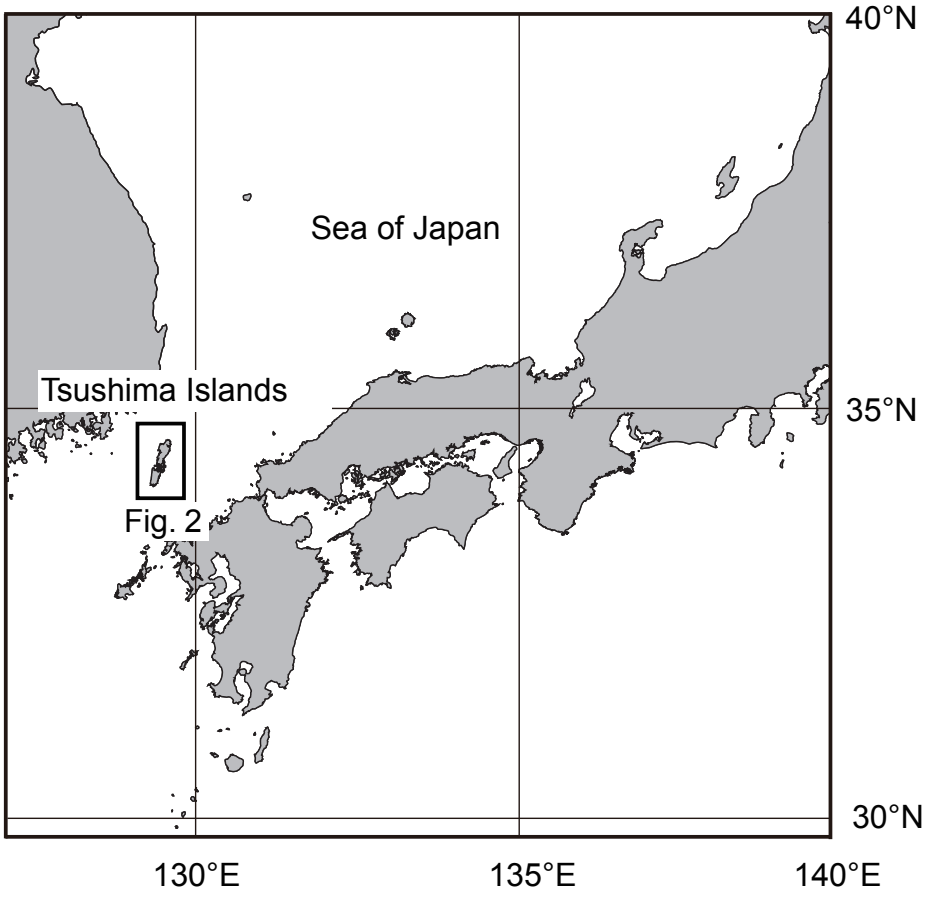

Fig. 1. Location of Tsushima Islands.

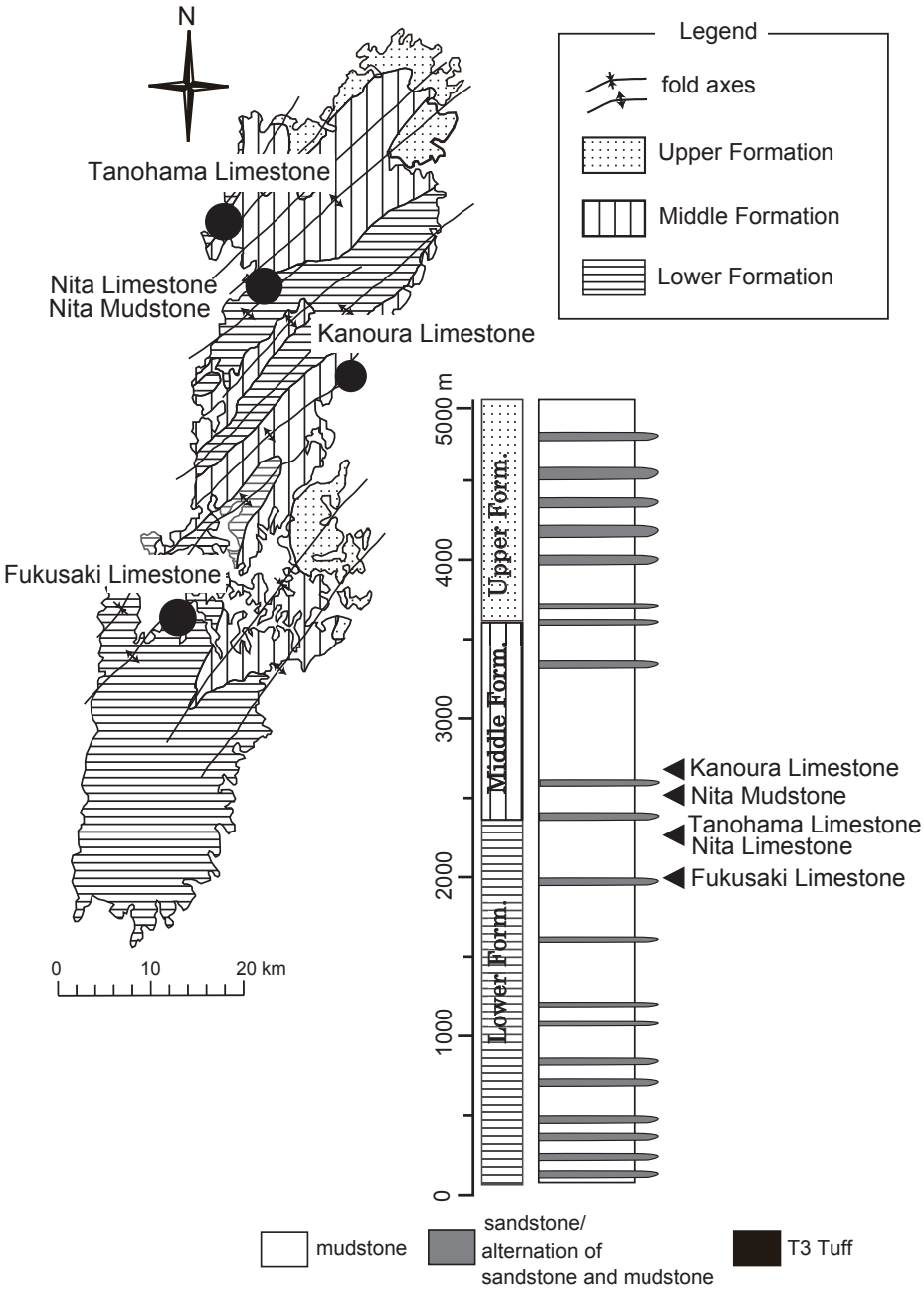

Fig. 2. Geologic map of Tsushima Islands and lithological column of the Taishu Group based on MITI (1972, 1973, 1974). Circles show the locality of limestone and chemosynthetic fossil assemblages.

3. Chemosynthetic bivalves from the Taishu Group

MITI (1972) reported *Adulomya* cf. *uchimuraensis, Calyptogena akanudaensis* from the limestone boulder at Tanohama, where the upper part of the Lower Formation is located. Aoki and Nishida (1999) found a lenticular limestone including small *Adulomya* sp. from the same horizon. Moreover, fossil molluscan faunas are dominated by *Acharax* spp. with occurrences of *Sacella*, *Yoldia* and *Portlandia*. These fossil molluscan faunas are quite dense in population and they are regarded as chemosynthetic fossil assemblages.

Ninomiya et al. (2010) reported that fossil assemblages of the authigenic cold-seep carbonates and mudstone are chemosynthetic bivalves which are mytilids, vesicomyids and solemyids. As Aoki and Nishida (1999) indicated, the calcareous shells are absent in mudstones but are preserved in carbonates. Based on these conditions, the middle part of the Taishu Group is considered to be deposited at deep-sea floor greater than 500 m depth (Ninomiya et al., 2010).

4. Description of molluscan fossils

Class Bivalvia Linnaeus, 1758
Family Solemyidae Gray, 1840
Genus *Acharax* Dall, 1908
Type species: *Solemya johnsoni* Dall, 1891; Recent, Northeast Pacific.

***Acharax* sp. A**
Plate 1, fig. 1

Acharax sp. A, Aoki and Nishida, 1999.

Locality: Nita (Basal part of the Middle Formation; Aoki and Nishida, 1999)

Measurements (in mm) :

Sumple No.	valve	Length	La	Height	Height/ Length	La/L	Rib number	Plate
Aok-001	right balve	49.7	14.2	23.7	0.48	0.29	20	Plate 1, fig. 1

La: Length of anterior margin.

Description: Shell is of middle size. Ligament external. Dorsal margin straight, antero-postero margin rounded. Ventral margin nearly straight. Umbo located at anterior one and third of valve of shell length. Radial ribs count 18-20, and marginal portion degitated beyond shell margin. The ribs are strong at anterior-posterior end, but weak and obscure at center of valve.

Remarks: According to Aoki and Nishida (1999), this species resembles *Acharax tokunagai*. As Sasaki et al. (2005) indicated, *Solemya* (*Acharax*) *agasizii, Solemya tokunagai, Solemya* (*Acharax*) *tibai,* and *Solemya tokunagai elongata* are synonymyzed with *Solemya johnsoni* (Coan et al., 2000). This species resembles *Acharax johnsoni* in many points. However, umbo of *Acharax johnsoni* situates posteriorly, 78%. Therefore, this species may be distinguished from *Acharax johnsoni*.

***Acharax* sp. B**
Plate 1, figs. 2-6

Acharax sp. B, Aoki and Nishida, 1999.

Locality: Nita (Basal part of the Middle Formation; Aoki and Nishida, 1999)

Measurements (in mm) :

Sumple No.	valve	Length	La	Height	Height/ Length	La/L	Rib number	Plate
Aok-002	right balve	38.3	8.8	13.8	0.36	0.23	17	Plate 1, fig. 2
GK-L12000	left valve	29.4	8.2	10.4	0.35	0.28	17	Plate 1, fig. 3
Aok-003	right balve	44.2	10.6	13.3	0.30	0.24	15+	Plate 1, fig. 4
GK-L12001	right balve	59.5+	16.1	—	—	—	18	Plate 1, fig. 5, 6

Description: Shell is small to middle size and elongated. Ligament external. Dorsal margin straight, antero-postero margin rounded. Ventral margin nearly straight. Umbo located at anterior about three of quarter of valve length. Radial ribs count 17, and marginal portion digitated beyond shell margin. The ribs are strong at anterior-posterior end, but weak and obscure at center of valve.

Remarks: Bivalves of geneus *Acharax* is reported at least in eight species (Baba, 1990; Hatai and Koike1956; Kamada, 1962; Kanehara, 1937; Kanno, 1960; Kanie and Kuramochi, 1995; Kanie et al, 1995; Kanie et al., 1999; Natori, 1964). This species resembles *Acharax yessoensis, Acharax dalli, Acharax muroensis*, and *Acharax gigas*. However, radial rib numbers of *A. yessoensis* are 18-20. Shell length of *A. dalli* is smaller than that of this species and radial rib numbers are 10-11. Shell length of *A. muroensis* is less than that of this species. *Acharax bosoana* is larger than *Acharax* sp. B and has 10-11 ribs. Shell size of *Acharax gigas* is much larger than those of *A. yessoensis, A. dalli, A. muroensis* and *Acharax* sp. B. Therefore, *Acharax* sp. B can clearly be distinguished from other species. It appears necessary in the future to discuss about the possibility of erecting this taxon as a new species.

***Acharax* sp. C**
Plate 2, figs. 1-2

Locality: Kanoura (Lower part of the Middle Formation)

Description: Shell size and outline unknown. Ligament is external. Radial ribs marginal portion digitated beyond shell margin. Frequently, this species is observed in mudstones around Kanoura Limestone. However, shells are imperfect, shell outline is unknown. This species may be identified as *Acharax* sp. A or *Acharax* sp. B. In this paper, the author assigns this taxon as *Acharax* sp. C.

Class Bivalvia Linnaeus, 1758
Family Nuculidae Adams and Adams, 1858
Genus *Acila* Adams and Adams, 1858
Type species: Nucula divaricata Hinds, 1843; Recent, China

***Acila* sp.**
Plate 2, fig. 3

Locality: mudstone around Fukusaki Limestone (Upper part of the Lower Formation)

Measurements (in mm):

Sample No.	valve	Length	Height	Plate
GK-L12004	left valve	26+	34.7+	Plate 2, fig. 3

Description: Shell length greater than 26 mm and height reaching about 35 mm. Shell subovate, inequilateral, not so inflated well-defined rostral portion. Posterior side is very short. Umbo located at nearly posterior margin. Anterior dorsal margin gently sloping, but anterior end is absent. Ventral margin regularly arched. Posterior margin form and lunula cannot be observed. Sculpture consisting of divaricating oblique threads, the line of main devarication is slightly posterior to the middle.

Remarks: This species resembles *Acila submirabilis* and is common in the Neogene of Japan. However, umbo, linule and posterior margin forms are unknown. Therefore, the author tentatively assigns this taxon as *Acila* sp. until well-preserved specimens with visible structures are studied.

Family Nuculanidae Adams and Adams, 1858
Genus *Nuculana* Link, 1807
Type species: *Arca rostrata* Bruguière, 1791= *Mya pernula* Müller, 1779; Recent, North Atlantic.

***Nuculana* sp.**
Plate 2, fig. 4

Locality: Nita (Basal part of the Middle Formation; Aoki and Nishida, 1999).

Measurements (in mm):

Sample No.	valve	Length	La	Plate
Aok-004	left valve	8.7	3.2	Plate 2, fig. 4

Description: Shell small, long-ovate, inflated, nearly veneriform. Escutcheon is obscure. Umbo located at nearly anterior margin. Strong concentric regular growth line presents on surface. Hinge structure unknown.

Remarks: Shell form and only growth line are observed on surface. However, hinge structure is unknown. Therefore, the author assigns this taxon as *Nuculana* sp. until well-preserved specimens are studied.

Genus *Yoldia* Möller, 1842
Type species: *Yoldia hyperbore* Torell, 1859= *Nucula hyperborea* Gould, 1841; Recent, North Atlantic.

***Yoldia* sp.**
Plate 2, figs. 5-6
Locality: Nita (Basal part of the Middle Formation; Aoki and Nishida, 1999).

Measurements (in mm):

Sample No.	valve	Length	La	Height	Height/ Length	Plate
Aok-005	right valve	13.7	3.2	10.1	0.74	Plate 2, fig. 5
Aok-006	left valve	14.9	5.0	8.2	0.55	Plate 2, fig. 6

Description: Shell small, long-ovate, anterior margin rounded, anterior side slightly shorter than posterior side. Postero-dorsal corner pointed. Postero-dorsal border concaved. Strong concentric regular growth line is observed on surface. Hinge structure and escutcheon are unknown.

Remarks: Shells are deformed, umbo area structures cannot be observed. Therefore, the author assigns this taxon as *Yoldia* sp.

Unidentified species
Plate 2, fig. 6

Locality: Nita (Basal part of the Middle Formation; Aoki and Nishida, 1999).

Measurements (in mm):

Sample No.	valve	Length	La	Plate
GK-L12005	left valve	42.1+	13.2	Plate 2, fig. 6

Description: Shell moderate, elongated, anterior margin rounded, ventral margin slightly arcuated. Posterior dorsal margin is straight. Strong concentric regular growth line presents on surface. Hinge structure is unknown. Therefore, it will be necessary to describe more details in the future based on well-preserved specimens whose structures can be observed.

Class Bivalvia Linnaeus, 1758
Order Mytiloida Férussac, 1822
Family Mytilidae Rafinesque, 1815
Subfamily Bathymodiolinae Kenk and Wilson, 1985
Genus *Bathymodiolus* Kenk and Wilson, 1985
Type species: *Bathymodiolus thermophilis* Kenk and Wilson, 1985; Recent, Galapagos Rift zone.

***Bathymodiolus* sp.**
Plate 3, figs. 1-6

Locality: Fukusaki Limestone (Upper part of the Lower Formation).

Measurements (in mm):

Sample No.	valve	Length	La	Height	Plate
GK-L12006	right valve	36	1.3	−	Plate 3, fig. 1
GK-L12007	right valve	38.1+	4.6	21.8	Plate 3, fig. 2
GK-L12008	right valve	41.5	−	−	Plate 3, fig. 3
GK-L12009	left valve	29.5+	−	17.7	Plate 3, fig. 4
GK-L12010	right valve	46.7+	−	−	Plate 3, fig. 5
GK-L12011	left valve	33.0+	−	17.5	Plate 3, fig. 6

Description: The largest one reaches about 47 mm in length, although the present specimen is broken at anterior, posterior, and dorsal sides. All the specimens are imperfect and height/length ratio and width/length ratio unknown. Shell rather thick and solid, modioliform, inflated, elliptical equivalve. Umbo subterminal, prosogyrated at nearly anterior margin. Anterior margin is located slightly forward than umbo. Anterior margin rounded, dorsal margin convex, postero-dorsal corner rounded, posterior margin broadly rounded, ventral margin straight. Feeble radial threads present in mid-portion. Inner structures are unknown.

Remarks: This species resembles *Bathymodiolus platifrons, B. japonicus* and *B. hirtus* described by Hashimoto and Okutani (1994) and Okutani et al. (2004) from Japanese waters. However, this species is distinguished from the similar taxa listed above based on umbo projection from anterior margin, strait ventral margin, as well as shell length of 50 mm. Nobuhara et al. (2008) indicated that bathymodiolin became large in the middle Miocene. However, this species is 50 mm in shell length. It may be necessary in the future to discuss about the possibility of erecting this taxon as a new species.

Genus *Adipicola* Dautzenberg, 1927
Type species: *Myrina denhami* Adams and Adams, 1854 =*Modiolus pelagica* Woodward, 1854 (by monotypy); Recent, South Atlantic.

***Adipicola* sp.**
Plate 3, fig. 7

Locality: Kanoura (Lower part of the Middle Formation).

Measurements (in mm):

Sample No.	valve	Length	La	Height	Height/ Length	Plate
GK-L12012	right valve	37.4	11.2	14	0.37	Plate 3, fig. 7

Description: Shell small (length: 37.4 mm), elongate quadrangular, ligament external. Antero-postero dorsal margin nearly straight. Anterior margin slightly narrow, rounded, posterior margin smoothly rounded, ventral margin slightly concave. Umbo directed forwards, situated at between anterior about one and third. Growth line distinct at posterior margin of shell.

Remarks: Bivalves belonging to genus *Adipicola* are known as whale-fall community of the present or the past (Amano and Little, 2005; Dell, 1995; Okutani et al., 2004; Tsuchida and Tabakotani, 1997). Okutani and Miyazaki (2007) described *Benthomodiolus geikotsucola* from deep sea floor of the northeast Pacific. This species closely resembles *Adipicola pacifica*. However, the calcareous shell has not been preserved and thus the inner structure cannot be observed. This species occurred from the mudstone around Kanoura Limestone which is the authigenic cold-seep carbonate. Consequently, in this study, the author assigns this taxon as *Adipicola* sp. until well-preserved specimens with structures are studied.

Class Bivalvia Linnaeus, 1758
Order Veneroida Adams and Adams, 1856
Superfamily Glossaceae Gray, 1847
Family Vesicomyidae Dall and Simpson, 1901
Genus *Calyptogena* Dall, 1891
Type species: *Calyptogena pacifica* Dall, 1891 (by monotypy); Recent, East Pacific.

***Calyptogena* sp. A**
Plate 4, figs. 1-4, Plate 5, figs. 1-6, Plate 6, figs. 1-4

Locality: Kanoura Limestone (Lower part of the Middle Formation), Tanohama Limestone (Upper part of the Lower Formation) and mudstone around Kanoura Limestone (Lower part of the Middle Formation).

Measurements (in mm):

Sample No.	valve	Length	La	Height	Height/ Length	Width	Plate
GK-L12013	left valve	41.9	6.9	16.5	0.39	−	Plate 4, fig. 1
Aok-007	right valve	40.3+	9.6	−	−	−	Plate 4, fig. 2
Aok-008	left valve	39.0+	−	13.2	−	−	Plate 4, fig. 3
GK-L12014	right valve	44.4+	−	−	−	−	Plate 4, fig. 4
GK-L12015	right valve	45.4	6.1	18.2	−	13.2	Plate 5, figs. 1, 2
GK-L12016	left valve	35.3	5.1	15.3	0.43	−	Plate 5, figs. 3, 4
GK-L12017	right valve	32.7+	4.9	17.3	−	−	Plate 5, fig. 5
GK-L12018	right valve	37.9+	−	15.5	−	−	Plate 5, fig. 6
GK-L12020	right valve	37.3	8.5	−	−	−	Plate 6, fig. 1
GK-L12021	left valve	37.5+	6.5	11.3	−	−	Plate 6, fig. 2
GK-L12022	left valve	36.9+	−	9.1	−	−	Plate 6, fig. 3
GK-L12023	left valve	46.5	6.3	11.3	−	−	Plate 6, fig. 4

Description: The largest one can be measured about 47mm in length, although it is deformed. Shell thick, not so inflated, elongated slightly inequivalve.

Ligament external. Anterior margin rounded, ventral margin strait. Posterior margin slightly broad, smoothly rounded. Postero-dorsal margin nearly straight. Umbo low, reaching slightly above hinge line and is located at between anterior about one sixth of valve length. Hinge structures are unknown.

***Calyptogena* sp. B**
Plate 4, figs. 5-6, Plate 5, figs.7-8, Plate 6, fig. 5

Locality: Kanoura Limestone (Lower part of the Middle Formation), Tanohama Limestone (Upper part of the Lower Formation) and mudstone around Kanoura Limestone (Lower part of the Middle Formation)

Measurements (in mm):

Sample No.	valve	Length	La	Height	Width	Plate
Aok-009	right valve	51.1+	7.5	15.5	8.5	Plate 4, fig. 5, 6
GK-L12019	right valve	32.1+	4.2	12.4	8.5	Plate 5, fig. 7, 8
GK-L12024	right valve	43.9	5	−	−	Plate 6, fig. 5

Description: The largest one can be measured about 51 mm in length, although posterior end is not observed. Shell rather thick, antero-posteriorly significantly elongated, inequilateral slightly inequivalve. Ligament is external along dorsal side. Anterior margin rounded, ventral margin long, rather strongly concave centrally. Anterior dorsal margin descending at an angle of about 30° from umbo. Umbo quite low, reaching slightly above hinge line and located at anterior side and one seventh of valve length. Hinge structure is unknown.

Remarks on *Calyptogena spp*.: In Japan, many fossil species and present species of *Calyptogena* are described thus far (Amano and Kiel, 2006; Kanno et al., 1998; Métivier et al., 1986; Kojima and Ohta, 1997; Kuroda, 1943; Okutani, 1957, 2000, 2008; Okutani and Métivier, 1986; Okutani et al., 1992, 1993, 1996, 1997, 2000, 2002).

Calyptogena sp. A closely resembles *Calyptogena* (*Archivesica*) *similaris* described by Okutani et al. (1997). However, there are differences in that *Calyptogena* sp. A of shell length is a half size or less and anterior margin and antero-dorsal margin are rounded. *Adulomya* cf. *uchimuraensis* reported by MITI (1972) is long as 150 mm (Kanno et al., 1998). And *Calyptogena* sp. A is more elongated than *C. akanudaensis*. Therefore, this species is different from these two species. This species closely resembles *Adulomya hokkaidoensis* in shell length and form, which is described by Amano and Kiel (2006) from the Miocene Chikubetsu Formation as a part of whale-fall community. However, *Adulomya hokkaidoensis* is known only from the whale-fall community. However, hinge structure of *Calyptogena* sp. A cannot be observed. Consequently, in this study, the author assigns this taxon as *Calyptogena* sp. A. Most of fossil bivalves from mudstone around Kanoura Limestone are considered as this species, although they are deformed.

Calyptogena sp. B resembles the modern species *Calyptogena* (*Ectenagena*) *phaseoliformis*. However, *Calyptogena* sp. B is distinguished from the thick shell and 50 mm or less in shell length. *Adulomya uchimuraensis* is different from this species because that ventral margin is straight or only a little concave toward dorsal. It is considered that this species is the same as that occurred from mudstone, but the specimen is significantly deformed. Hinge structure cannot be observed. Therefore, in this study, the author assigns this taxon as *Calyptogena* sp. B.

5. Conclusions

The middle part of the Neogene Taishu Group including the cold-seep carbonates was originated from the authigenic chemosynthetic fossil molluscan faunas, which are distributed in Tsushima Islands, Nagasaki Prefecture. It is considered that the Taishu Group was deposited in deep sea environments of greater than 500 m depth. In this paper, the author classified the bivalves from the cold-seep carbonates and mudstones. The assemblages are identified as ten species belonging to seven genera as follows: *Bathymodiolus* sp., *Adipicola* sp., *Calyptogena* spp., *Acharax* spp., *Acila* sp., *Nuculana* sp., and *Yoldia* sp. These fossil bivalves may be considered to be new species pending on further studies. It will be necessary in the future to classify them based on detailed hinge structures of well-preserved specimens.

6. Acknowledgements

The author is grateful to Mr. Takahiro Aoki (Shinwa Techno Co., Ltd.) for lending many specimens from his collections. Dr. Shoichi Shimoyama (Kyushu University) is gratefully acknowledged for providing helpful advice and suggestions. Thanks are extended to Dr. Kozo Takahashi (Kyushu University) for providing opportunity to write this manuscript and for his helpful suggestions and improving the English text. The author is also greatly

indebted to Dr. Tamio Nishida (Professor Emeritus of Saga University), who acted as an external reviewer, for providing valuable comments and suggestions.

7. References

Adams, H., and Adams, A. (1853-1859) The genera of Recent Mollusca arranged according to their organization. vol. **1**, 484 pp., vol. **2**, 660 pp. Publisher John Van Voorst, London.

Amano, K., and Kiel, S. (2006) Fossil vesicomyid bivalves from the North Pacific region. *The Veliger*, **49**, 270-293.

Amano, K., and Little, C.T.S. (2005) Miocene whale-fall community from Hokkaido, northern Japan. *Palaeogeography, Palaeoclimatology, Palaeoecology*, **215**, 345-356.

Aoki, T., and Nishida, T. (1999) Chemosynthetic molluscan fauna found from the basal part of the Middle Formation of the Taishu Group. *Proceedings of The Nishinihon Branch, Geological Society of Japan*, **114**, 19-20. (In Japanese)

Baba, K. (1990) Molluscan fossil assemblages of the Kazusa Group, south Kwanto, central Japan. 445 pp, Keio Yochisha. (In Japanese)

Bruguière, J.G. (1789-1816) Encyclopédic méthodique ou par ordre de matières. Histoire naturelle de Vers des Mollusques. 758 pp. Charles Joseph Panckoucke, Paris.

Clark, W. (1851) On the classification of the British marine testaceous Mollusca. *The Annals and Magazine of Natural History, sec. 2*, **7**, 469-481.

Coan, E.V., Scott, P. V., and Bernard, F. R. (2000) Bivalve seashells of western North America. Santa Barbara Museum of Natural History, 764 pp.

Dall, W.H. (1891) Scientific results of explorations by the U. S. Fish Commision Steamaer Albatross. XX. On some new or interesting West American shells obtained from dredgings of the U.S. fish commission streamer Albatross in 1888. *Proceedings of the U. S. National Museum*, **14**, 174-191.

Dall, W.H. (1908) Reports on the dredging operations off the west coast of Central Amarica … The Mollusca and Brachiopoda. *Bulletin of the Museum of Comparative Zoology at Harvard University*, **43**, 205-487.

Dall, W.H., and Simpson, C.T. (1901) The Mollusca of Porto Rico. *Bulltin of the U. S. Fish and Fisheries Commision*, **20**, 351-524.

Dautzenberg, P. (1927) Mollusques provenant des campagnes scientifiques du Prince Albert Ier de Monaco dans l'Ocean Altantique et dans le Golfe de Gascogne. *Résultats des Campagnes Scientifiques accomplies par Albert Ier*, **72**, 1-400.

Dell, R.K. (1995) New species and records of deep-water mollusca from off New Zealand. *Tuhinga (Records of the Museum of New Zealand Te Papa Tongarewa)*, **2**, 1-26.

Férrusac, A.E.de. (1822) Tableaux systématiques des animaux mollusques. Classés en families naturelles, dans lequels on a établi la concordance de tous les systémes; suivis d'un prodrome general pour tous les mollusques terrestres ou fluviatiles, vivants ou fossils. 111 pp. Berntland, Paris.

Gould, A.A. (1841) Reports on the Invertebrate of Massachusetts, comprising the Mollusca, Crutacea, Annelida and Radiata. 373 pp. Cambridge, Folsom, Wells and Thurston.

Gray, J.E. (1840) Synopsis of the Contents of the British Museum. 370 pp. G. Woodfall, London.

Gray, J.E. (1847) A list of the genera of Recent Mollusca, their synonyma and types. *Proceedings of the Zoological Society of London*, **15**, 129-219.

Hashimoto, J., and Okutani, T. (1994) Four new species mytilid mussels associated with deep-sea chemosynthetic communities around Japan. *Venus (Japanese Journal of Malacology)*, **53**, 61-83.

Hatai, K., and Koike, K. (1957) On fossil mollusca from Chiba Prefecture, Japan. *Japanese Journal of Geology and Geography*, **28**, 77-90.

Hinds, R.B. (1843) Descriptions of new species of *Nucula*, from the collections of Captain Sir Edward Belcher, during the years 1836-42. Vol. 2, Mollusca, 72 pp. Smith, Elder and Co., London.

Ibaraki, M. (1994) Ages and paleoenvironments of Tertiary in northwestern Kyushu the view point of planktonic foraminifer assemblages. *The Earth Monthly (Gekkan Chikyu)*, **16**, 150-153. (In Japanese)

Kamada, Y. (1962) Tertiary marine Mollusca from the Joban coal-field, Japan. *Special Papers, Paleontological Society of Japan*, **8**, 1-187.

Kanehara, K. (1937) On some Tertiary fossil shells from Hokkaido (Yesso). *Japanese Journal of Geology* and *Geography*, **14**, 155-161. (In Japanese)

Kanie, Y., and Kuramochi, T. (1995) *Acharax yokosukensis* n. sp. (gigantic Bivalve) from the Miocene Hayama Formation of the Miura Peninsula, south-central Japan. *Science Report of Yokosuka City Museum*, (**43**), 51-57.

Kanie, Y., Kuramochi, T., Asami, S., and Kanno, S. (1995) Solemyid pelecypod of Miocene Hayama Group in Miura Peninsula. *Report of Culture and Natural Treasury, Yokosuka City*, (**29**), 57-61. (In Japanese)

Kanie, Y., Kuramochi, T., Kanno, S., Mizota, C., Shimizu, M., and Takakuwa, Y. (1999) New occurrence and shell from of Middle Miocene *Acharax gigas* (Bivalvia: Solemyidae) in Gunma Prefecture. *Bulletin of Gunma Museum Natural History*, (**3**), 17-23. (In Japanese with English abstract)

Kanno, S. (1960) The Tertiary System of the Chichibu Basin, Saitama Prefecture, central Japan. Part 2. Paleontology, 123-196. Japanese Society Promotion Science.

Kanno, S., Tanaka, K., Koike, K., Narita, K., and Endo, T. (1998) *Adulomya uchimuraensis* Kuroda (Bivalvia) from the Miocene Bessho Formation in Shiga-mura, Nagano Prefecture, Japan. *Research Report of the Shinshu- shinmachi Fossil Museum*, **1**, 17-28.

Kenk, V.C., and Wilson, B.R. (1985) A new mussel (Bivalvia, Mytilidae) from hydrothermal vents in the Galapagos Rift zone. *Malacologia*, **26**, 253-271.

Kojima, S., and Ohta, S. (1997) *Calyptogena okutanii* n. sp., a sibling species of *Calyptogena soyoae* Okutani, 1957 (Bivalvia: Vesicomyidae). *Venus (Japanese Journal of Malacology)*, **56**, 189-195.

Kuroda, T. (1943) *Akebiconcha*, a new pelecypod genus. *Venus (Japanese Journal of Malacology)*, **13**, 14-18. (In Japanese with English description)

Link, H.F. (1806-1808) Beschreibung der Naturalian. 1, 160 p., 2, 30 pp., 3, 38 pp. *Sammlung der Universität zu Rostock*, Rostock.

Linnaeus, C. (1758) Systema naturae per regna tria naturae, secundum classes, ordines, genera, species, cum characteribus, diffrentiis, synonymis, locis. Tomus 1, edition decimal, reformata, 824 pp. Laurentius Salvius, Stockholm.

Masuda, K. (1970) Molluscan fauna from the Taishu Group, Tsushima Islands, Nagasaki Prefecture, Japan. *Memoirs of Natural Science Museum Tokyo*, **3**, 25-32

Matsumoto, T. (1969) Geology of Tsushima and Relevant Problems. *Memoirs of Natural Science Museum Tokyo*, **2**, 4-18. (In Japanese with English abstract)

Métivier, B. Okutani, T., and Ohta, S. (1986) *Calyptogena* (*Ectenagena*) *phaseoliformis* n. sp., an unusual vesicomyid bivalve collected by the submersible Nautil from abyssal depths of the Japan and Kurile Trenches. *Venus (Japanese Journal of Malacology)*, **45**, 161-168.

MITI (The Ministry of International Trade and Industry) (1972) Report on the regional geological survey, Tsushima, Kamiagata district of the 1971' fiscal year. pp. 29. (In Japanese)

MITI (The Ministry of International Trade and Industry) (1972) Report on the regional geological survey, Tsushima, Kamiagata district of the 1972' fiscal year. pp. 34. (In Japanese)

MITI (The Ministry of International Trade and Industry) (1973) Report on the regional geological survey, Tsushima, Kamiagata district of the 1973' fiscal year. pp. 52. (In Japanese)

Möller, H. (1842) Index Molluscorum Groenlandiae. *Naturhistorisk Tidsskrft*, **4**, 76-97.

Müller, O.F. (1779) Von zwoen wenig bekannten Muscheln, der Schinkenarche und der gerunzeltenMahlermuschel. *Beschäftigungen der Berlinischen Gesellschaft naturforschender Freunde*, **4**, 55-59.

Nakajo, T., and Funakawa, T. (1996) Eocene radiolarians from the Lower Formation of the Taishu Group. *Journal of Geological. Society of Japan*, **102**, 751-754 (In Japanese)

Nakajo, T., and Maejima, W. (1998) Morpho-dynamics development and facies organization of the Tertiary delta system in the Taishu Group Tsushima Islands, southwestern Japan. *Journal of Geological. Society of Japan*, **104**, 749-763.

Nakajo, T., Yamaguchi, Y., Komatsubara, J., and Ohtake, S. (2006) Sedimentation and tectonics of the Tertiary delta to basin successions in the Tsushima Islands, off northwestern Kyushu, Japan. *In*: Ito, M., Yagishita, K., Ikehara, K. and Matsuda, H. (Eds.), *Field Excursion Guidebook, 17th International Sedimentological Congress,Fukuoka, Japan,* Sedimentological Society of Japan, FE-B11, 1-12.

Natori, H. (1964) Some molluscan fossils from the Tertiary Muro Group in Kii Peninsula, Japan. *Transctions and Proceedings of the. Palaeontological Socity of Japan, New Series*, **55**, 247-255.

Ninomiya, T., Miyata, Y., Taniguchi, S., Shimoyama, S., Matsuda, H., Yamanaka, T., Aoki, T., and Nishida, T. (2008) Cold-seep carbonates and chemosynthetic assemblages from the Taishu Group, in the Tsushima Islands. Japan Geoscience Union, 2008 Meeting, abstract.

Ninomiya, T., Taniguchi, S., Shimoyama, S., Miyata, Y., Daniel, D. J., Matsuda, H., Yamanaka, T., Aoki, T., Nishida, T., and Ichihara, T. (2010) Sedimentary environment of the Neogene Taishu Group, Nagasaki Prefecture, Southwest Japan. Annual Meeting of Geological Society of Japan, p. 68. (In Japanese)

Nobuhara, T., Imaizumi, I., Kaneko, T., Koike, H.,Narita, K., and Amano, K. (2008) Btahymodiolin bivalves from the Middle Miocene cold-seep carbonate in Bessho Formation, Nagano Prefecture. Abstracts with Programs The 157th Regular Meeting, the Palaeontological Society of Japan, p. 30. (In Japanese)

Okada, H., and Fujiyama, I. (1970) Sedimentation of the Taishu Group, in the Shiohama Area, Central Tsushima, Kyushu. *Memoirs of Natural Science Museum Tokyo*, **3**, 9-21. (In Japanese with English abstract)

Okutani, T. (1957) Two new species of bivalves from deep water in Sagami Bay by the R. V. Soyo-Maru. *Bulletin of the Tokai Regional Fisheries Research Laboratory*, **17**, 27-30.

Okutani, T. (2000) Vesicomyidae. In: Okutani, T. (Ed.), *Marine Mollusks in Japan*. Tokai University Press, Tokyo, 996-999.

Okutani, T. (2008) Mollusca. In: Fujikura, K., Okutani, T. and Maruyama, T. (Eds.), *Deep-sea Life-Biological observations using research submersibles*. Tokai University Press, Tokyo, 99-142. (In Japanese)

Okutani, T., and Miyazaki, J. (2007) Benthomodiolus geikotsucola n. sp.: a mussel colonizing deep-sea whale bones in the northwest Pacific (Bivalvia: Mytilidae). *Venus (Japanese Journal of Malacology)*, **66**, 49-55.

Okutani, T., and Métivier, B. (1986) Descriptions of three new species of vesicomyid bivalves collected by submersible Nautile from abyssal depths off Honshu, Japan. *Venus (Japanese Journal of Malacology)*, **45**, 147-160.

Okutani, T., Kojima, S., and Ashi, J. (1996) An unusual vesicomyid bivalve, *Calyptogena nankaiensis* n. sp. from bathyal depth off Honshu, Japan. *Venus (Japanese Journal of Malacology)*, **55**, 257-263.

Okutani, T., Kojima, S., and Ashi, J. (1997) Further discovery of a new taxon of vesicomyid clam, Nankai Trough, off Honshu, Japan. *Venus (Japanese Journal of Malacology)*, **56**, 185-188.

Okutani, T., Kojima, S., and Iwasaki, N. (2002) New and known vesicomyid bivalves recently collected from the western and central Nankai Trough off Shikoku and Honshu, by deep sea research systems of Japan Marine Science and Technology Center. *Venus (Japanese Journal of Malacology)*, **61**, 129-140.

Okutani, T., Fujikura, K. and Hashimoto, J. (1993) Another new species of Calyptogena (Bivalvia: Vesicomyidae) from the bathyal depth in Suruga Bay, Japan. *Venus (Japanese Journal of Malacology)*, **52**, 121-126.

Okutani, T., Fujikura, K., and Kojima S. (2000) New taxa and review of vesicomyid bivalves collected from the northwest Pacific by deep sea research systems of Japan Marine Science and Technology Center. *Venus (Japanese Journal of Malacology)*, **59**, 83-101.

Okutani, T., Fujikura, K. and Sasaki, T. (2004) Two new species of *Bathymodiolus* (Bivalvia: Mytilidae) from methane seeps on the Kuroshima Knoll off the Yaeyama Islands, southwestern Japan. *Venus (Japanese Journal of Malacology)*, **62**, 97-110.

Okutani, T., Fujiwara, Y., Fujikura, K., Miyake, H., and Kawato, M. (2004) A mass aggregation of the mussel *Adipicola pacifica* (Bivalvia: Mytilidae) on submerged whale bones. *Venus (Japanese Journal of Malacology)*, **63**, 61-64.

Okutani, T., Hashimoto J., and Fujikura, K. (1992) A new species of vesicomyid bivalve associated with hydrothermal vents near Amami-Ohshima Island, Japan. *Venus (Japanese Journal of Malacology)*, **51**, 225-233.

Otofuji, Y., and Matsuda, T. (1983) Paleomagnetic evidence for the clockwise rotation of Southwest Japan. *Earth and Planetary Science Letters*, **62**, 349-359.

Otofuji, Y., and Matsuda, T. (1987) Amount of clockwise rotation of Southwest Japan-fan shape opening of the southwestern part of the Japan Sea. *Earth and Planetary Science Letters*, **85**, 289-301.

Rafinesque, C.S. (1815) Analyse de la nature ou tableau de l'univers et des corps organisés. 224 pp. Barravecheia, Palermo.

Sakai, H., and Yuasa, T. (1998) K-Ar Ages of the Mogi and Ugetsuiwa Subaqueous Pyroclastic Flow Deposits in the Taishu Group, Tsushima Islands. *Memoirs of Natural Science Museum Tokyo*, **31**, 23-28

Sasaki, T., Okutani, T., and Fujikura, K. (2005) Molluscs from hydrothermal vents and cold seeps in Japan: A review of taxa recorded in twenty recent years (1984-2004). *Venus (Japanese Journal of Malacology)*, **64**, 87-133.

Takahashi, K., and Nishida, T. (1974) On the molluscan fossils from the Lower Formation of the Taishu Group in the Kamiagata district of Tsushima Islands. *Bulletin of Faculty of Liberal Arts, Nagasaki University. Natural science*, **15**, 15-21. (In Japanese with English abstract)

Torell, O.M. (1859) Bidrag till Spitsbergen Mollusk-fauna. Jemte en allman oversigt af Arktiska regionens naturforahallanden och forntida ubtredning, 154 pp. Boktrycheri, Stocholm.

Tsuchida, E., and Tabakotani, Y. (1997) Deep-sea mytilid bivalve assemblage on whale bone collected from the entrance of Tokyo Bay. *Venus (Journal of Malacological Society of Japan)*, **56**, 77-78. (In Japanese)

Woodward, S.P. (1851-1856) *A manual of the Mollusca; or a rudimentary treatise on Recent and fossil shells*, 486 pp. John Weale, London.

Yamaguchi, Y., and Oho, Y. (2007) Sedimentological history of Tertiary slope facies in the northern area of the Tsushima Islands, Japan. *Journal of Geological Society of Japan*, **113**, 113-126. (In Japanese with English abstract)

Plate 1

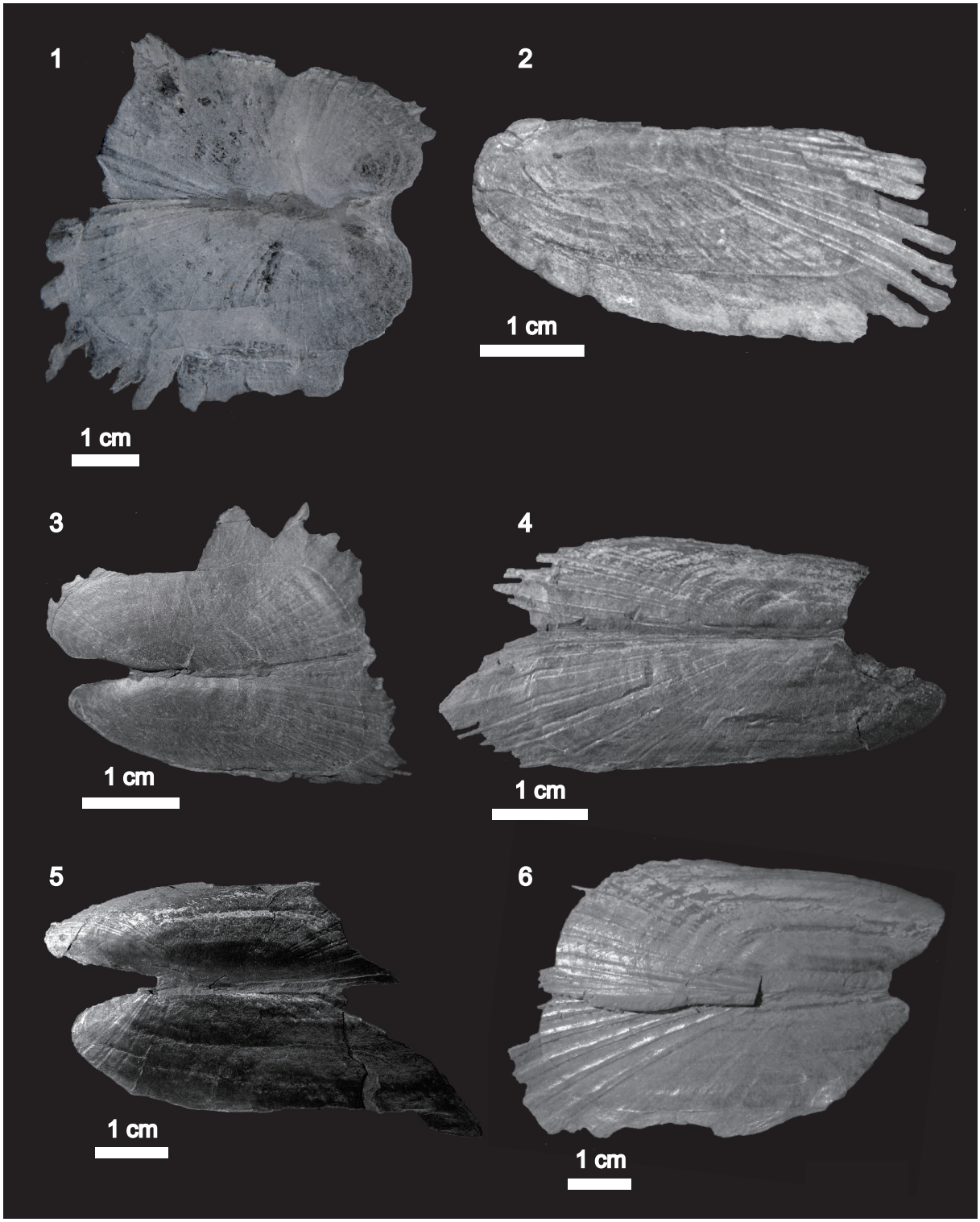

Plate 1. **1-6**. ***Acharax* spp**. from Nita (fig. 1: *Acharax* sp. A [Sample ID: Aok-001]; fig. 2: *Acharax* sp. B [Aok-002]; fig. 3: Left valve of *Acharax* sp. B [GK-L12000]; fig. 4: *Acharax* sp. B [Aok-003]; figs. 5, 6: *Acharax* sp. B [GK-L12001], fig. 5: Anterior side; fig. 6: Posterior side).

Plate 2

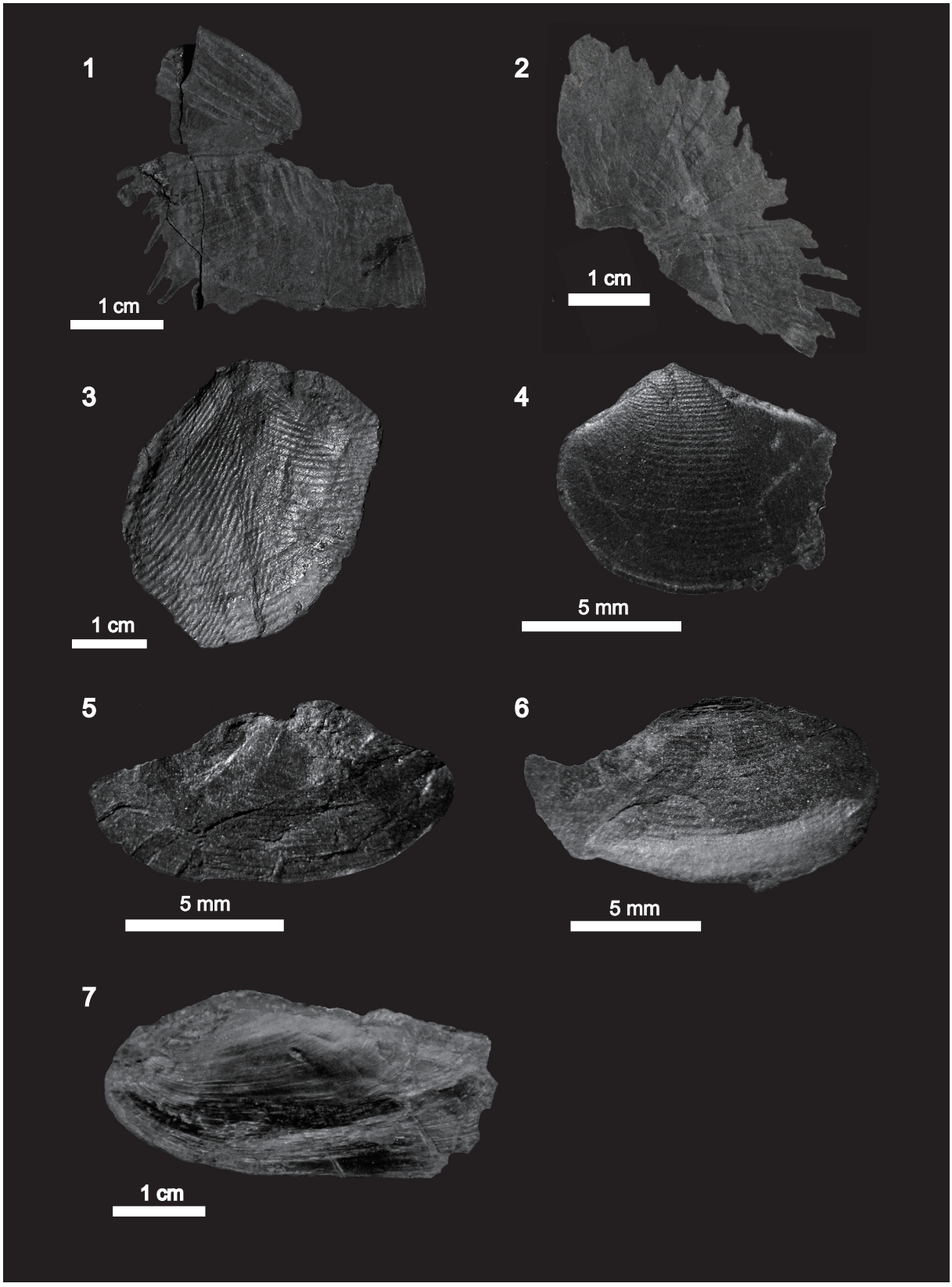

Plate 2. **1, 2. *Acharax* sp. C** from Kanoura (fig. 1: *Acharax* sp. C [GK-L12002]; fig. 2: *Acharax* sp. C [GK-L12003]), **3. *Acila* sp.** from Fukusaki [GK-L12004], **4-7. Nuculanidiae,** Unidentified species from Nita (fig. 4: Left valve of *Nuculana* sp. [Aok-003]; fig. 5: Right valve of *Yoldia* sp. [Aok-004]; fig. 6: Right valve of *Yoldia* sp. [Aok-005]; fig. 7: Unidentified species [GK-L12005]).

Plate 3

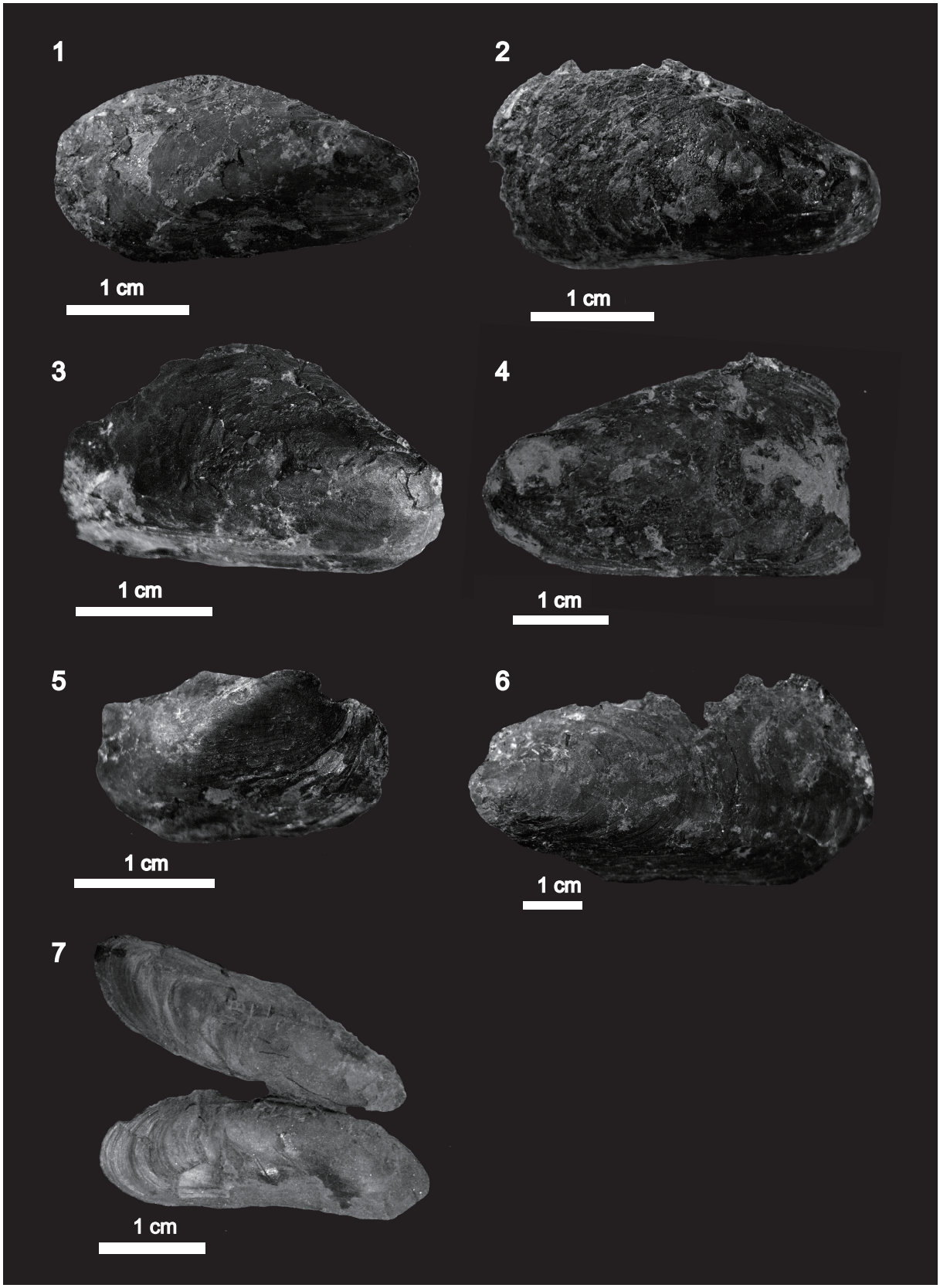

Plate 3. **1-6. *Bathymodiolus* sp.** from Fukusaki Limestone (fig. 1: Right valve [GK-L12006]; fig. 2: Right valve [GK-L12007]; fig. 3: Right valve [GK-L12008]; fig. 4: Left valve [GK-L12009]; fig. 5: Right valve [GK-L12010]; fig. 6: Left valve [GK-L12011]]]), **7. *Adipicola* sp.** [GK-L12012].

Plate 4

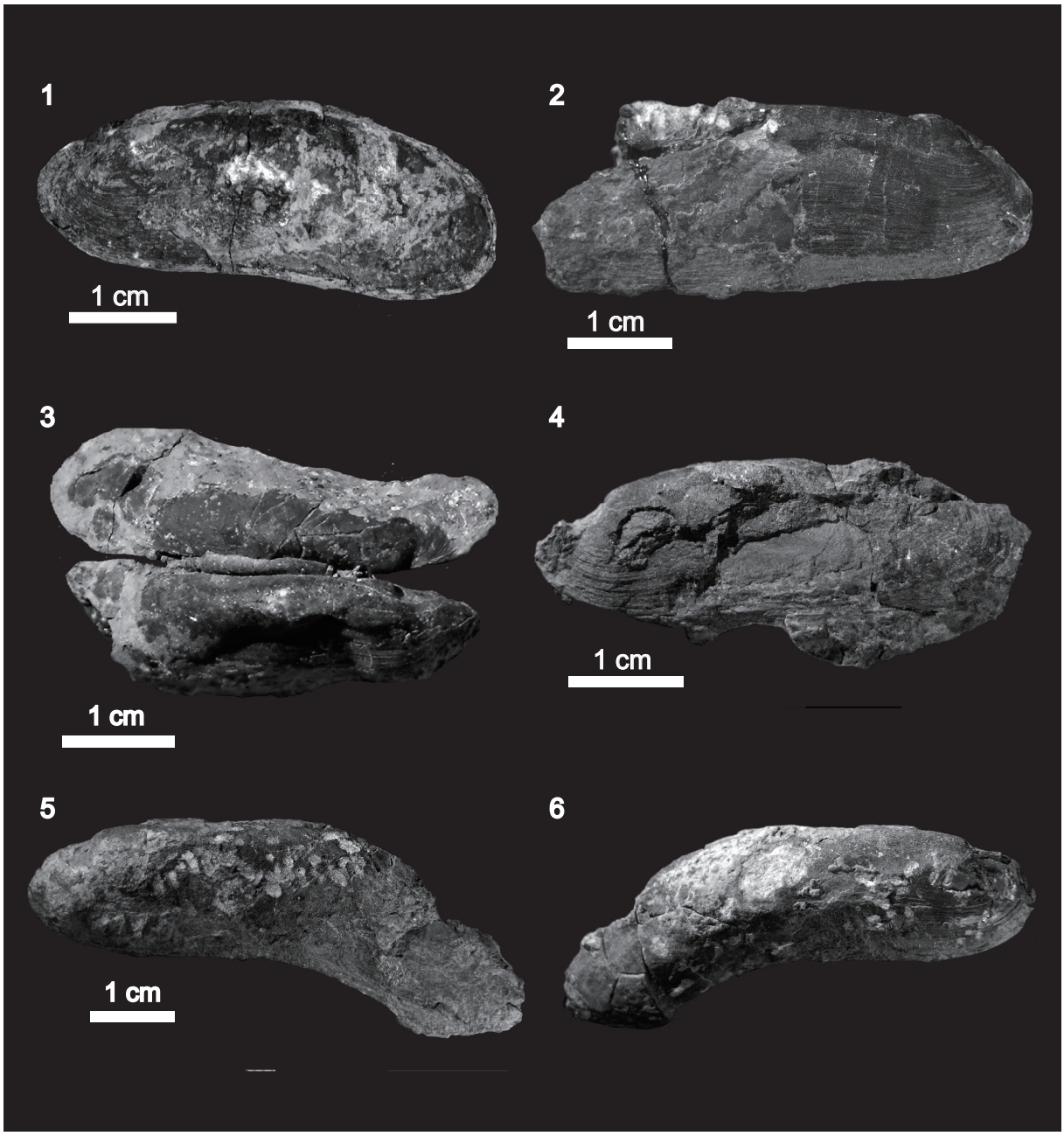

Plate 4. ***Calyptogena*** **spp.** from Kanoura Limestone. **1-4.** ***Calyptogena*** **sp. A** (fig. 1: Left valve [GK-L12013]; fig. 2: Right valve [Aok-007]; fig. 3: Dorsal side (Aok-008). fig. 4: Left valve (GK-L12014)), **5, 6.** ***Calyptogena*** **sp. B** [Aok-009] (fig. 5: Right valve; fig. 6. Left valve).

Plate 5

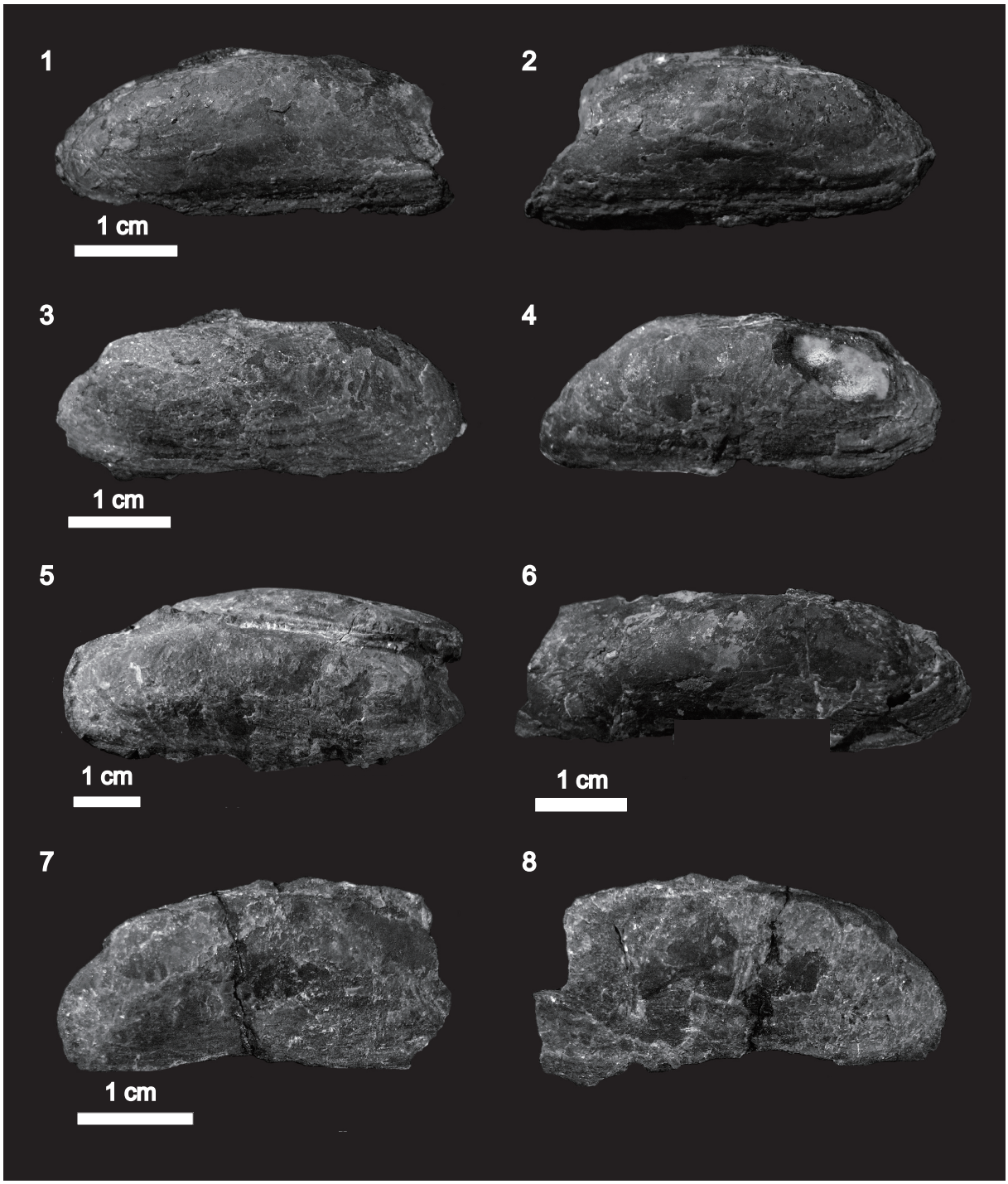

Plate 5. ***Calyptogena*** **spp.** from Tanohama Limestone. **1-6.** ***Calyptogena*** **sp. A. 1, 2.** ***Calyptogena*** **sp. A** ([GK-L12015]: fig. 1: Right valve; fig. 2: Left valve), **3, 4.** ***Calyptogena*** **sp. A** ([GK-L12016]: fig. 3: Right valve; fig. 4: Left valve), **5.** ***Calyptogena*** **sp. A** [GK-L12017]. **6.** ***Calyptogena*** **sp. A** [GK-L12018], **7, 8.** ***Calyptogena*** **sp. B** ([GK-L12019]: fig. 7: Right valve; fig. 8: Left valve).

Plate 6

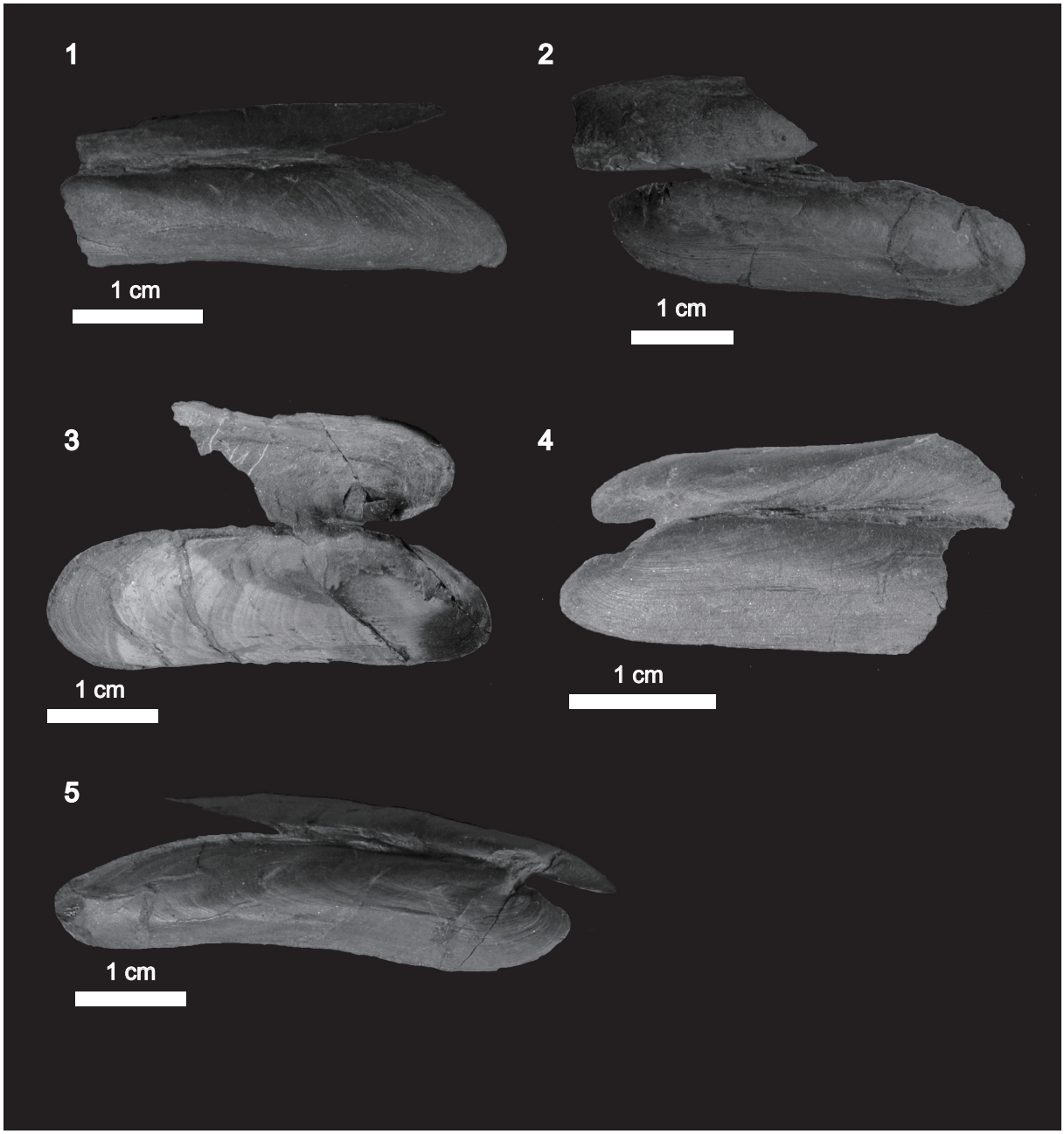

Plate 6. ***Calyptogena*** **spp.** from mudstone around Kanoura Limestone. **1-4.** ***Calyptogena*** **sp. A** (fig. 1: Right valve [GK-L12020]; fig. 2: Right valve [GK-L12021]; fig. 3: Left valve Right valve [GK-L12022]; fig. 4: Left valve [GK-L12023]), fig. 5. Left valve of ***Calyptogena*** **sp. B** [GK-L12024].

Mem. Fac. Sci., Kyushu Univ., Ser. D, Earth & Planet. Sci., Vol. XXXII, No. 3,
pp. 27-38, March 10, 2011

Cell size variation of *Anoplosolenia brasiliensis* (calcareous nannoplankton) in the central equatorial Pacific Ocean

Hideto Tsutsui and Kozo Takahashi*

Abstract

A morphometric analysis on *Anoplosolenia brasiliensis* (calcareous nannoplankton) was conducted employing samples obtained from 0 to 120 m water depths in the central equatorial Pacific Ocean along the equator ranging from 166.3°E to 170.1°W. Measured cell length of *A. brasiliensis* showed the minimum of 39 μm to the maximum of 165 μm. The cell width ranged from the minimum of 1 μm to the maximum of 10 μm. Measured cell volumes ranged from the minimum of 28.3 μm^3 to the maximum of 2,741 μm^3. In addition, length/width ratios ranged from the minimum of 6.8 to the maximum of 37.5. The cell size of this taxon is very large compared to that of other calcareous nannoplankton taxa such as *Emiliania huxleyi*. Related factors for such a large cell size appears to be: (1) population density of the own taxon; (2) ambient temperature; (3) ambient dissolved oxygen concentration; and (4) other phytoplankton population density such as that of *E. huxleyi*. The life adaptation of *A. brasiliensis* is interpreted as fundamentally pursuing a K-strategy, but this taxon is also pursuing an r-strategy when appropriate situation arises. The population density of this taxon may be related to ambient nutrient concentrations, intricate balance among several species of nutrients, and competitions with other coccolithophore taxa such as *E. huxleyi*.

Keywords: *Anoplosolenia brasiliensis*, calcareous nannoplankton, morphometrics, cell size, K-strategy, central equatorial Pacific Ocean

1. Introduction

In the recent years, we have seen a steady progress in morphometric studies (e.g., de Meuter and Symons, 1975; Lazarus, 1986a; Lazarus, 1986b; Lazarus, 1986c; Kurihara and Takahashi, 2002; Schmidt et al., 2004; Tsutsui and Takahashi, 2009a; Tsutsui et al., 2009b). However, these studies were limited by the following reasons. (1) In general, the plankton groups included in the above-cited literature are microscopic in size. Therefore, the work concerning size measurement requires substantial labor employing a light microscope (LM) or a scanning electronic microscope (SEM) under high magnifications. (2) Significant amount of time must be expended when one wisheds to employ an SEM.

Calcareous nannoplankton can be very useful as indicators for deciphering environmental conditions in oceanography and paleoceanography. It is important to characterize basic information for population, distribution, and/or cell size since the nannoplankton can tell us about environmental conditions such as nutrient concentrations.

Therefore, our present study is focused on morphometric analysis of *Anoplosolenia brasiliensis*. This taxon has a comparatively large-sized cell among many calcareous nannoplankton taxa and hence measurements are easier compared to that of other nannoplankton taxa. The cell form of this taxon appears as a very slim figure like the shape of a javelin. Simply put, the exterior calcareous shield of this taxon is composed of a large number of very slim rhomboids, which are geometrically arranged in an orderly manner (Fig. 2). Each member of such a shield is classified as a 'scapholith' type. A scapholith of this taxon represents an appearance like hair comb slits in the central area called as a 'lath' (Winter and Siesser, 1994). The first description of this species was given by

Manuscript received on 27 December 2010; accepted on 10 February 2011
* Department of Earth and Planetary Sciences, Graduate School of Sciences, Kyushu University, Hakozaki6-10-1, Fukuoka, 812-8581, JAPAN; Corresponding author's e-mail: hideto@geo.kyushu-u.ac.jp

Lohmann (1919), followed by a re-description by Deflandre (1952). In recent years, Young et al. (2003) transferred and emended *A. brasiliensis* into genus *Calciosolenia* due to the significant similarity in fine coccolith structure of *Calciosolenia murrayi*. Furthermore, Young et al. (2003) also discussed about classification of *A. brasiliensis* based on the presence/absence by dimorphism: *Anoplosolenia brasiliensis* represents a monomorphic stage, and C. *murrayi* represents a dimorphic stage. In our study, we respect the differences in the coccoliths and coccosphere morphology by lath and cell form of genus *Anoplosolenia* and genus *Calciosolenia*, thus this species in question is tentatively defined as *A. brasiliensis* as done by Deflandre (1952). This species belongs to Kingdom Protista, Phylum Haptophyta, Class Haptophyceae, Order Coccolithophorales, Family Calciosoleniaceae (Manton and Oates, 1985; Jordan and Kelijne, 1994; Heimdal, 1997; Young et al., 2003; Edvardsen and Medlin, 2007). *Anoplosolenia brasiliensis* belongs to heterococcolithophores group (Jordan and Kelijne, 1994). Rutten (1972) discussed about this species based on sediment trap samples collected at approximately 3,000 m depth at Station UM15 in the Bannock basin in the Mediterranean Sea and *A. brasiliensis* was described as a member of calcareous nannoplankton fluxes. Nishida (1979) discussed about this species from the central Pacific Ocean. Manton and Oates (1985) studied morphology of this species in the Galapagos Islands. Manton and Oates (1985) sampled *A. brasiliensis* and *Calciosolenia* aff. *murrayi* from 8 to 19 m depths from Academy Bay, Barrington (Fernandina) Island of the Galapagos Islands. Manton and Oates (1985) discussed fine structures including lath employing LM, SEM and transmission electron microscopy (TEM) and suggested a morphological difference between genus *Anoplosolenia* and genus *Calciosolenia*. Steinmetz (1991) reported about this species in the flux material collected by sediment traps deployed in the equatorial Atlantic, central Pacific and Panama Basin. Nishida et al. (2000) investigated the assemblages and populations of nannoplankton in the central equatorial Pacific Ocean and discussed about this species among other nannoplankton taxa. Ziveri and Thunell (2000) discussed and described this species as a member of coccolithophore flux in sediment trap samples collected from the Gulf of California. Malinverno (2004) observed fine coccolith morphology of *A. brasiliensis* employing an SEM and discussed/classified the results of scapholith morphometrics. The scapholith length of *A. brasiliensis* is 5.8 to 7 μm and the width is 1.9 to 2.3 μm (Malinverno, 2004). In contrast, when *A. brasilieneis* is living in the modern ocean, *A. brasilieneis* has large cell size compared to major calcareous nannoplankton taxa such as genus *Emiliania* and genus *Gephyrocapsa*, but fine details of *A. brasiliensis* size is not well understood. If a population of *A. brasiliensis* were found in a sediment trap sample, it would be possible to predict that the total mass flux of that sample would be very large for the reasons discussed in Discussion section of this paper. Therefore, we discuss about the variations in *A. brasiliensis* population and cell size of living *A. brasiliensis* in the modern ocean.

2. Materials and Methods

2.1. Sampling logistics

Seawater samples containing nannoplankton were collected on R/V Mirai of JAMSTEC during Cruise MR99-K07, November to December 1999 in the central equatorial Pacific Ocean (Nishida et al., 2000). The sampled depths were limited down to 200 m and the sample water volumes were approximately two to three liters. The sampled stations are shown (Fig. 1). Cruise MR99-K07 started at 04.2°N/135.6°E as Station 1 and the ship steamed along the equator from 145°E to 170.1°W in the central equatorial Pacific Ocean. Stations 1 to 12 were assigned from the east to west as identification numbers (ID) for the samples. Significantly large populations of *A. brasiliensis* were observed at Stations 7, 8, 9 and 12 and hence the populations of *A. brasiliensis* at the four stations were used for a morphometric analysis. Size variations of this taxon can effectively be measured at the four stations by the following reasons: (1) The populations present are sufficient at the four stations among Stations 1 to 12 with statistically satisfactory numbers. (2) The area of high population density is found at Stations 8 and 9 and Station 7 is located at the margin of the high density. Therefore, the cell size variations of *A. brasiliensis* are set to be measured at the three stations plus Station 12, which provides a fair population density.

The logistics for sampling is given (Table 1). Our study depths for *A. brasiliensis* ranged as follows: 0, 10, 30, 40, 50, 60, 80, 100 and 120 m. This is because that below 120 m depth the population density of this taxon was expected to be nearly zero and thus there was no need of taking additional samples from further down depths. The pertinent environmental data such as water temperature, salinity and nutrients were summarized by Kawano (2000).

The seawater samples were filtered and sieved through 200 μm stainless steel mesh and large-sized plankton particles were excluded: no filtered seawater samples include, for example, copepods and planktonic foraminifers. Finally, the calcareous nannoplankton samples were filtered onto Millipore^{R} HA type membrane filters with a nominal pore size of 0.45 μm. After this process, the filters were dried at room temperature in the shipboard

laboratory.

After the filters were brought back to the shore laboratory, circular subsamples of 6 mm in diameter were cut off. The observation for *A. brasiliensis* was conducted on an SEM. The logistic details of the SEM observation are as follows: JSM-6300PS with the acceleration voltage of 10 to 15 kv; and samples coated with carbon vapor using JFE-400 carbon coater (both made by Japan Electron Optics Laboratory (JEOL)).

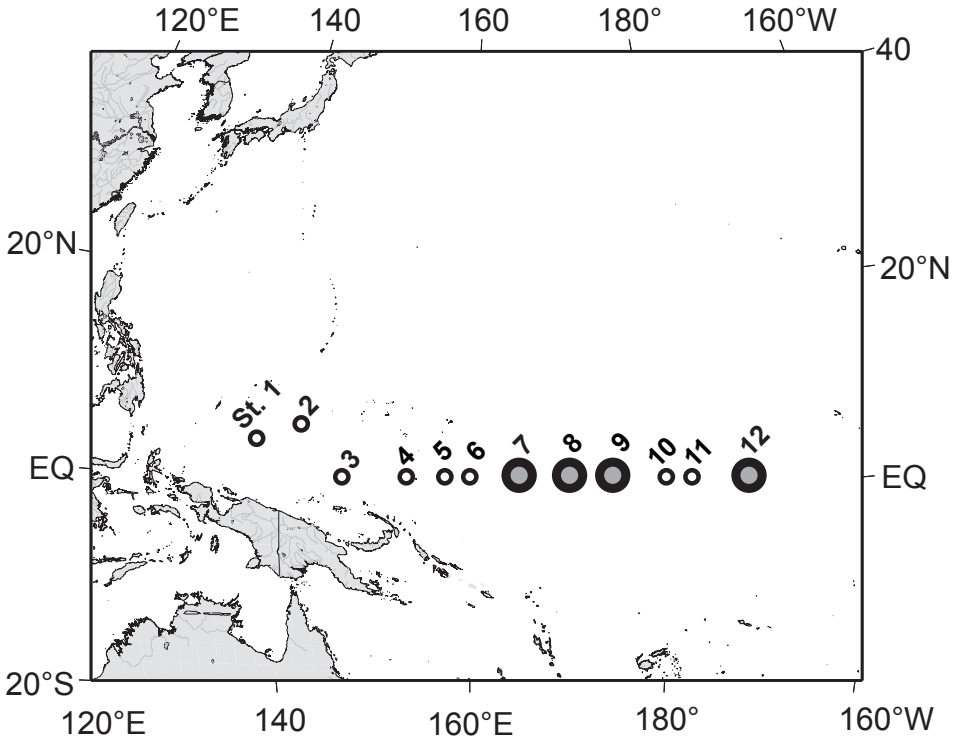

Fig. 1. Map showing the sampled locations

Table 1. Logistics for the sampling.

Station ID	Longitude (all at the Equartor)	Sampled Date (all 1999)	Sampled Time
St. 7	166.3°E	4 Dec.	10:33-11:20
8	171.4°E	5 Dec.	10:35-11:16
9	174.5°E	6 Dec.	11:05-11:43
12	170.1°W	9 Dec.	10:30-11:32

2.2. Morphometric technique

SEM images of *A. brasiliensis* are shown (Fig 2). The morphometric techniques are kept as simplest and fastest as possible in this study. We focused on measuring cell "length", scaling the distance from one tip to the opposite tip. Analogously, "width" represents the widest part of a cell. In practice, *A. brasiliensis* often exhibits a bending feature like an arch. In that case, the length is manually measured with a flexible lead ruler on a TV screen of the SEM. The morphometric concept employed here is illustrated (Fig. 3). Cell volumes can be calculated based on the measurements of length and width, assuming a cell is made of a pair of ideal geometric cones. The numerical formula for a cell volume is also shown (Fig. 3).

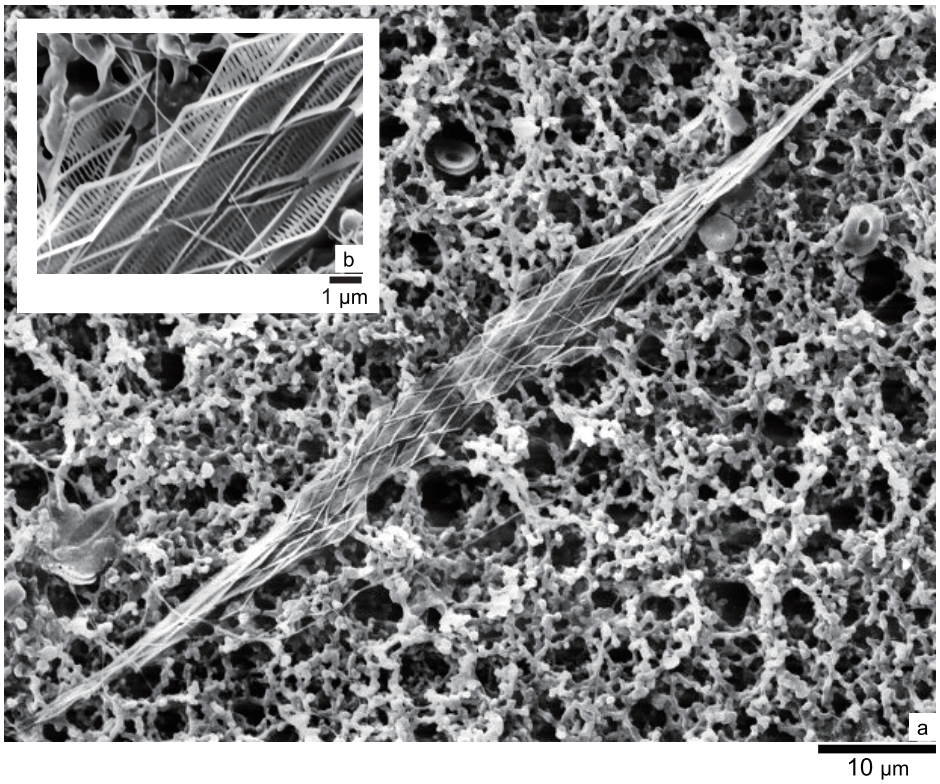

Fig. 2. (a) SEM photograph of *Anoplosolenia brasiliensis* from the equatorial Pacific Ocean (the Equator, 178°05.26W), at 50 m depth at Station 10. (b) An enlarged view of the thickest part of photograph (a).

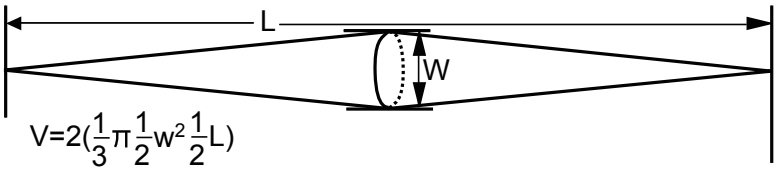

Fig. 3. Graphic representation of the morphometric method. 'V' is a cell volume.

3. Results

3.1. Population of A. brasiliensis along the equator

Distribution of *A. brasiliensis* during Cruise MR99-K07 is illustrated (Fig. 4). Among all sampled stations, the maximum population density of calcareous nannoplankton was 3,333 individuals ℓ^{-1}, and the mean value throughout all stations was 614 individuals ℓ^{-1}. The depth of the maximum population found was at 40 m at Station 8 (171.4°E). The samples from Station 8 and Station 9 (174.5°E) represented 43% of the specimens of total populations, followed by Station 12 (170.1°W) as the third rank representing 14% of the total. The remaining 43% of the population was represented by those from Stations 1 through 6, 10 and 11 (Fig. 4).

On the other hand, when we pay our attention to vertical distribution, 85% of the population concentrations are located between 0 to 70 m depths (Fig. 4). The highest population density is found at 50 m, contributing 15% of total at all depths. The population contributions at 40 m and 60 m are 12% at both depths. In summary, from the surface to 50 m depth the populations increased gradually, but below 50 m the populations decreased and the populations became very small representing only less than 1% below 100 m.

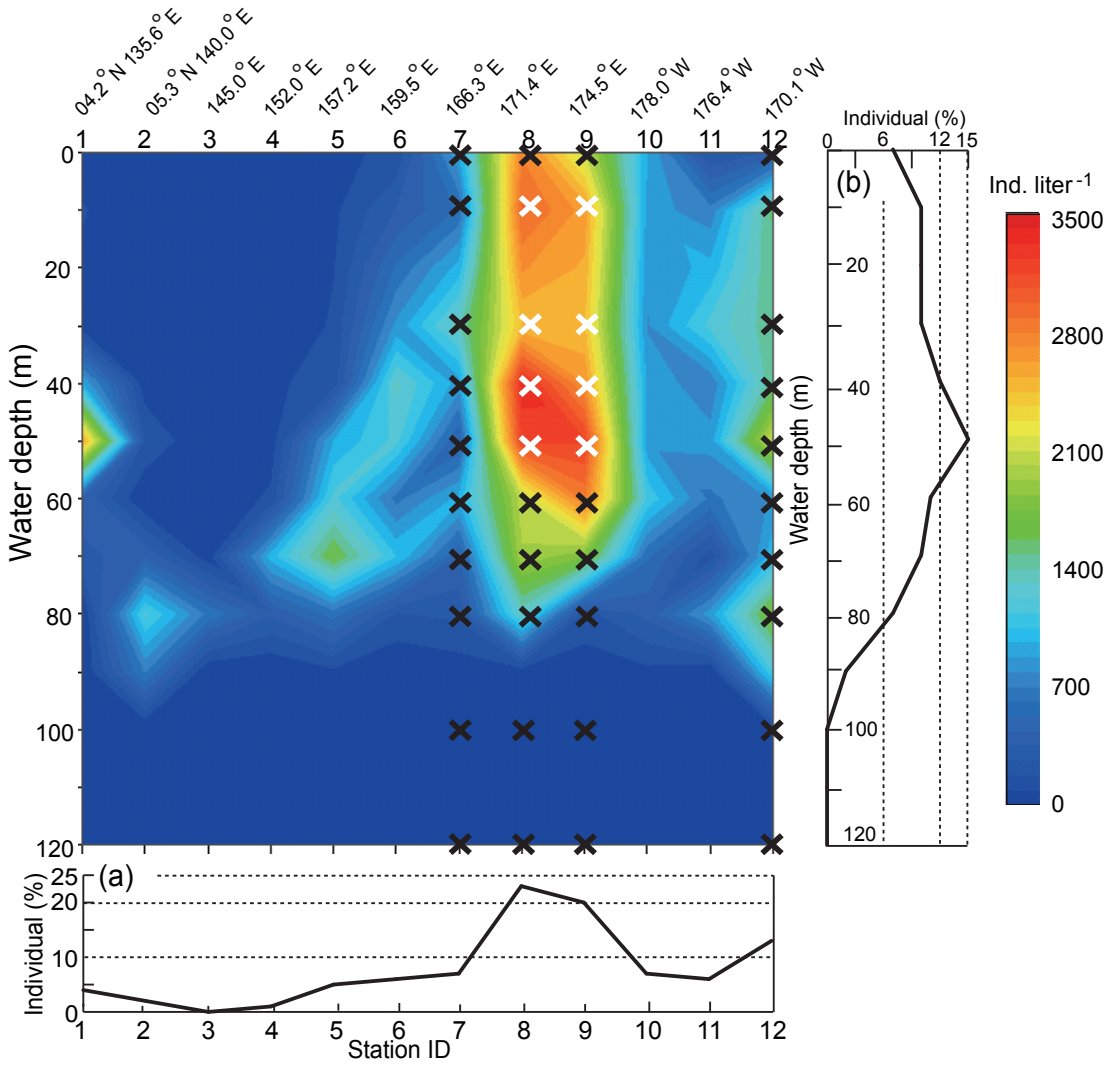

Fig. 4. Distribution of *A. brasiliensis* populations. Crosses represent sampled locations/depths.
Bottom line graph: % contribution by each station in total populations throughout the stations; left line graph: % contribution by each depth in total populations throughout the depths.

3.2. Morphometric results

A total of 1,026 of *A. brasiliensis* specimens were initially attempted to measure for size. Some specimens were, however, physically damaged and the seriously damaged specimens were rejected in the analysis, making the number of valid specimens 963 individuals for length and 1,003 for width. The statistical results of the morphometrics are based on total specimens from all depths and they are summarized including the following parameters: minimum, maximum, mean, standard deviation (S.D.), skewness and kurtosis (Table 2). The results in skewness and kurtosis represent good proxies for the measure of normal distribution (Ichikawa and Ohashi, 1987).

The measured cell length ranged from a minimum of 39 µm to a maximum of 165 µm. At Station 8 (171.4°E) cell length showed a wide range of values compared to that from other stations. The mean cell length also showed a wide range compared to other parameters: the mean value was approximately 10 µm; and the S.D. was greater than 15 µm. In contrast, width showed a narrow range compared to length: the measured cell width ranged from a minimum of 1 µm to a maximum of 10 µm. The mean width also showed a narrow range: the mean value was approximately 5 µm; and the S.D. was approximately 1 µm. In summary, the measured length varied significantly greater than that of the width. The cell length and width can be used to calculate cell volume (Table 2). At Station 7 (166.3°E) and Station 9 (174.5°E) the mean cell volume is greater than 700 µm^3. On the other hand, the mean

cell volumes at Station 8 and Station 12 (170.1°W) showed both approximately 300 μm³, which was roughly one half of the volume measured at the other two stations. The measured kurtosis values are very large except at Station 9.

Table 2. Summary of the statistical analysis performed.

Station ID	Longitude	(a) Length							(b) Width						
		N	Min. (μm)	Max. (μm)	Mean (μm)	S.D. (μm)	Skewness	Kurtosis	N	Min. (μm)	Max. (μm)	Mean (μm)	S.D. (μm)	Skewness	Kurtosis
Statistics		963	39	165	83.1	17.4	0.62	1.02	1003	1	10	5.5	1.1	0.50	1.02
St. 7	166.3°E	119	55	147	90.7	17.9	0.49	-0.07	124	3	10	5.6	1.1	0.91	2.48
St. 8	171.4°E	286	42	165	83.8	17.0	0.86	2.15	297	2	9	5.4	0.9	0.51	1.20
St. 9	174.5°E	395	39	149	79.2	16.4	0.46	0.50	408	3	9	5.8	1.1	0.59	0.43
St. 12	170.1°W	163	46	162	85.4	17.9	0.62	1.20	174	1	7	5.0	1.0	0.04	0.46

		(c) Length/Width							(d) Cell volume						
		N	Min.	Max.	Mean	S.D.	Skewness	Kurtosis	N	Min. (μm^3)	Max. (μm^3)	Mean (μm^3)	S.D. (μm^3)	Skewness	Kurtosis
Statistics		963	6.8	37.5	15.4	3.9	0.87	1.48	963	28.3	2741.0	702.2	354.1	1.62	4.39
St. 7	166.3°E	119	9.3	25.1	16.4	3.8	0.32	-0.68	119	234.8	2734.5	789.4	398.3	2.19	7.56
St. 8	171.4°E	286	7.3	28.7	15.6	3.7	0.54	0.47	286	120.6	2741.0	329.2	329.2	1.98	7.01
St. 9	174.5°E	395	7.2	28.0	13.9	3.2	0.83	1.36	395	200.9	2092.8	731.3	367.2	1.18	1.40
St. 12	170.1°W	163	6.8	37.4	17.4	4.5	1.00	2.04	163	28.3	2056.3	298.8	298.8	1.36	3.49

3.3. Relationship between length and width and summarized results for a normal distribution

The plot for length versus width is illustrated (Fig. 5). The two morphometric parameters did not show any strong correlations each other, but a vague trend can be read along two lines drawn at the upper and lower ends. The morphometric results of *A. brasiliensis* are summarized (Fig. 6). The high kurtosis value for cell length at Station 8 (Table 2) is represented by a sharp peak compared to those at other stations. The frequency distribution curves indicate a dull shape at the top compared to those at other stations, but almost all of the peaks are concentrated between 90 μm and 100 μm in length. In addition, the values for width are concentrated between 5 μm and 6 μm. The peaks for a normal distribution columns are shifted to the left side.

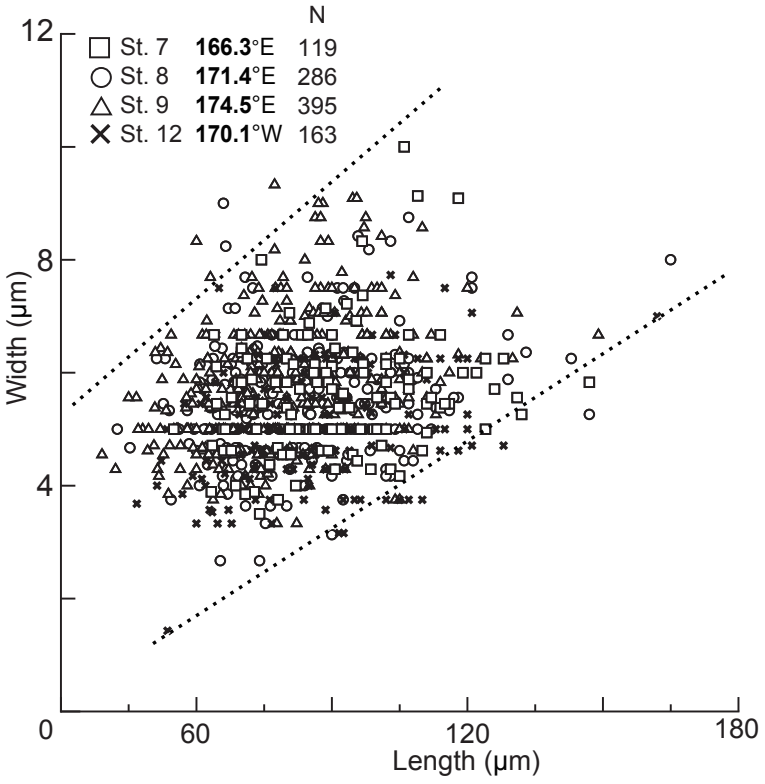

Fig. 5. Plot for length vs. width.

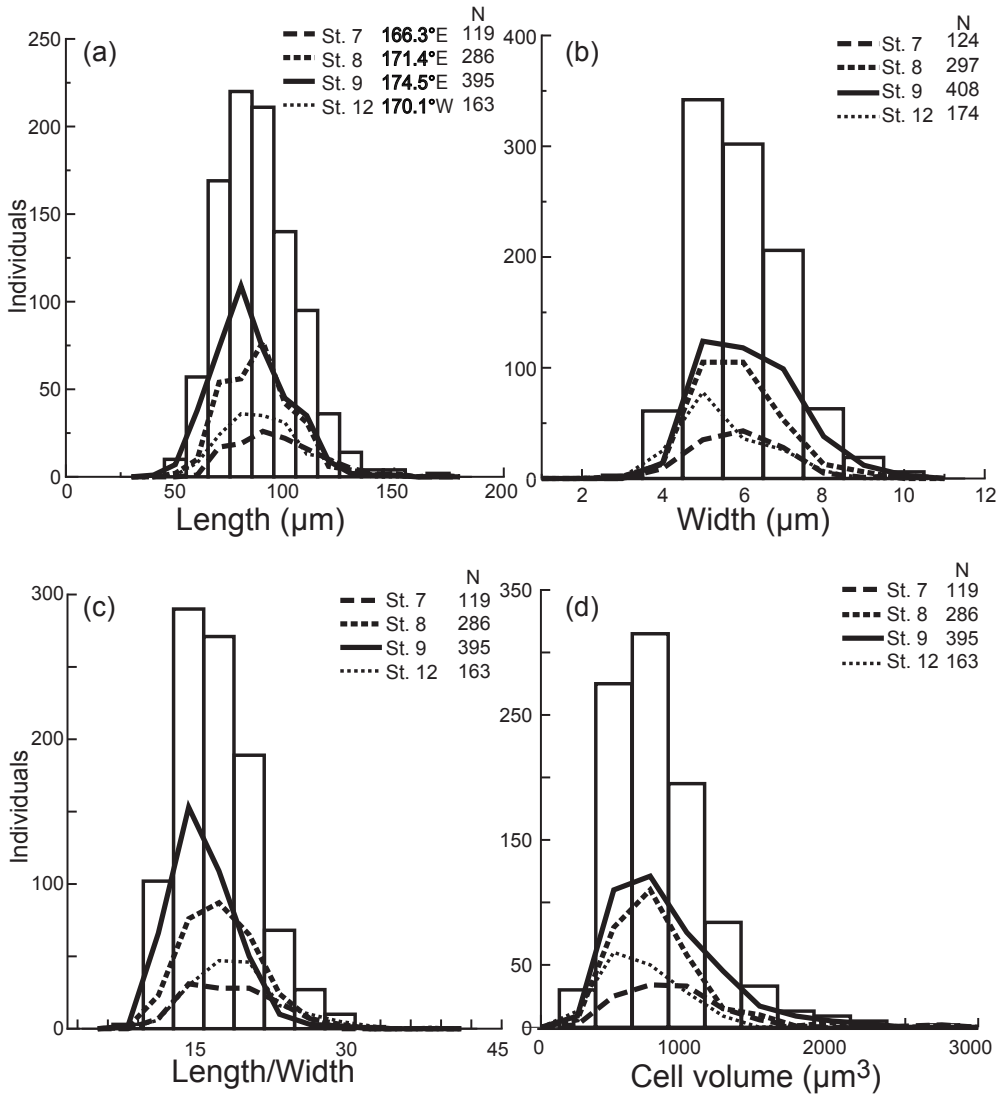

Fig. 6. Histograms for length, width, length/width and cell volume, respectively (columns: sum of the four stations); each of the line graphs represents a histogram curve for a given sampled station.

4. Discussion

4.1. Difference in cell volume at each station

At this step, the variations in cell volume of *A. brasiliensis* are confirmed by t-test: a statistical difference in length can be evaluated depending on depth and station. The results of t-value are summarized (Table 3). First, the results of t-test suggest that there is a statistical difference between the verge point covered by Station 7 and the dense populations covering Station 8 to Station 9. In contrast, the t-test results between Station 8 and Station 9 shows no statistical difference.

Therefore, concerning the cell volume of *A. barasiliensis* belonging to three discrete sample groups we performed another round of t-test again: Station 7, Station 12 and the group of high population density consisting of Stations 8 and 9. The results are summarized in Table 3. The cell volumes of *A. brasiliensis* appear different depending on the verge point of high population density at Station 7 or the dense population group represented by Stations 8 and 9. Therefore, we performed a third round of t-test of *A. brasiliensis* cell volume in opposite sides: the cell volumes in low and high population density, respectively. The borderline between the low population and high population density appears approximately at 1,000 individuals ℓ^{-1}. The results of the t-test show a statistical difference in *A. brasiliensis* cell volume between the values less than 1,000 individuals ℓ^{-1} and greater than 1,000

individuals ℓ^{-1}. The relationship between cell length and population density is illustrated (Fig. 6). The density of 1,000 individuals ℓ^{-1} appears to represent a reasonable boundary between the following two cases. The case with fewer than 1,000 individuals ℓ^{-1} shows a wide range in length from approximately 55 to 110 μm. For the case with greater than 1,000 individuals ℓ^{-1}, the measured cell length is concentrated at approximately 75 to 100 μm. In summary, the variation in cell length of *A. brasiliensis* can be represented by two separate modes depending on high or low population density.

Table 3. Results of t-test matrix: (a) among four stations; (b) among Station 7, Station 12, and the sum of Stations 8 and 9; and (c) between the population density <1,000 individuals ℓ^{-1} and >1,000 individuals ℓ^{-1}. The results with significant differences are shown in bold face.

(a) among four stations

Class	St. 8	St. 9	St. 12
St. 7	**2.72****	**1.47**	**4.58****
St. 8	——	-1.70	**2.75****
St. 9	——	——	**4.09****

(b)

Class	St. 8+St. 9
St. 7	**-2.16***
St. 12	**4.18****

(c)

Class	>1000 ind. liter^{-1}
<1000	**2.58***

Prob.: ** (1%), * (5%)

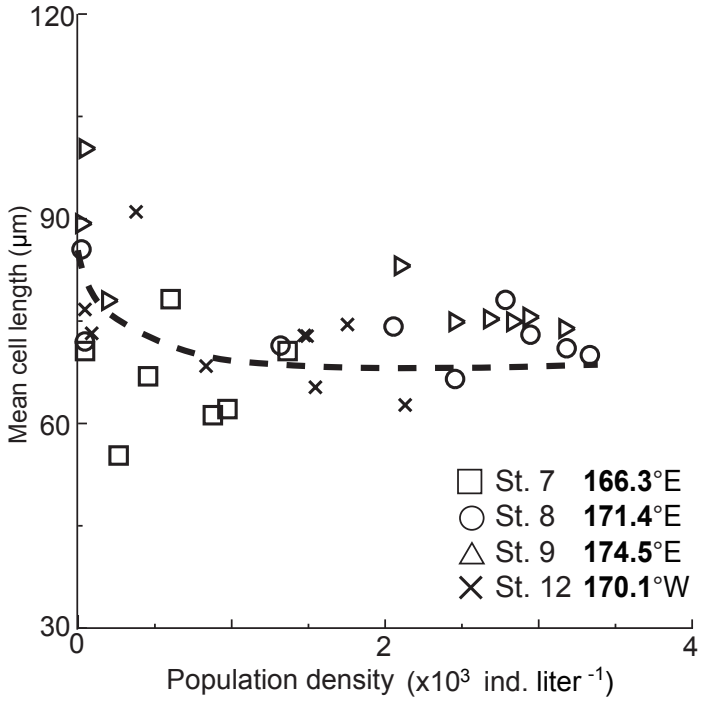

Fig. 7. Relationship between mean cell length and population density. The dashed line is the result of a regression analysis.

4.2. Environmental conditions as related factors for cell size

In general, nannoplankton-sized marine life requires metabolic substance from ambient waters such as nutrients for growth. The obtained cell volumes of *A. brasiliensis* at the four stations are compared with the

measured pertinent oceanographic conditions acquired during Cruise MR99-K07 (Fig. 1): temperature and dissolved oxygen (DO) among many parameters available (Kawano, 2000). In the case of temperature, approximately 27°C appears as the most popular level accounting for the majority of the populations that we investigated. Approximately 190 μmol kg^{-1} is the most popular condition for DO (Fig. 8). Temperature is an important factor as a prerequisite, but the relationships with cell volume variations and DO are unknown. Related factors for cell volumes of *A. brasiliensis* are the followings: (1) population density of this own taxon; (2) water temperature; and (3) DO. Nishida et al. (2000) discussed the changes in population density of the major calcareous nannoplankton taxa encountered in the same samples as this study: they are *Umbellosphaera irregularis, Emiliania huxleyi, Florisphaera profunda* and *Thorosphaera flabellate*. The relationship between the populations of *A. brasiliensis* and *E. huxleyi* is of interested and illustrated (Fig. 9). It is quite cleat that these two distinctively different taxa in shape and size were behaving quite differently each other. When the population density of the latter is fairly high (Stations 7, 11-12) that of the former is low. On the contrary to this, the former picks up its populations at Station 8-9 where the latter declines its populations. Such a mirror image trend observed from Stations 12 to 7 may be a hint showing a biological competition for nutrient uptake while it is hard to prove. For example, *Gephyrocapsa oceanica* is one of the major taxa in population besides *E. huxleyi*, but the population of *G. oceanica* decreased from Station 9 to the west towards Station 7 (not shown). The nutrient level of PO_4 is the highest at Station 12, which is located within the equatorial upwelling region (Fig. 9). There is a general decreasing trend in nutrient concentrations from Station 12 to the west towards Station 1. However, from Station 9 to the west towards Station 6 significant changes are observed in trend and ranks of nutrient concentrations for NH_3 and NO_2, especially relative to those of PO_4 (Fig. 9). The maximum concentrations for NH_3 and NO_2, are found at Station 8 and Station 7, respectively. It may be that *A. brasiliensis* expands its population density at the nutrient level somewhat intermediate rather than the highest. Whether the biological competition is important or ambient nutrient concentrations are more influential must be evaluated in light of further data in future studies.

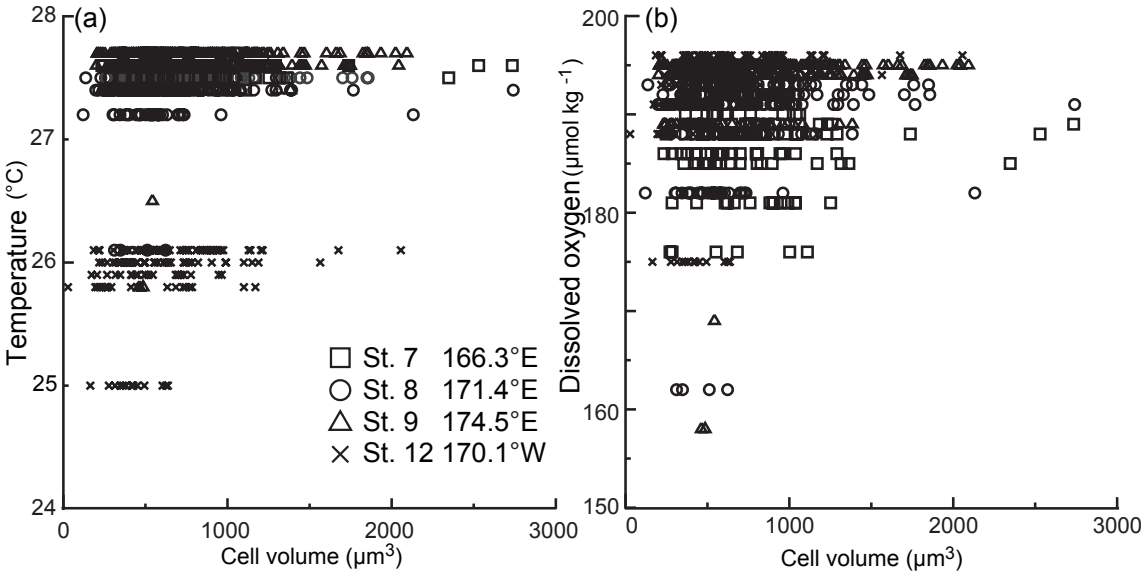

Fig. 8. Relationships between cell volumes and temperature as well as DO as environmental indices.

4.4. Reproductive strategy of A. brasiliensis

Organisms are surrounded by environments and thus they are depended on the ambient conditions. *Anoplosolenia brasiliensis,* a coccolithophore taxon, is not an exception for such dependency on environments. *Anoplosolenia brasiliensis* pursues an adaptation strategy called a ”K-strategy”, which is a commonly used term in ecology. The following features, which are encountered in this taxon, fit in a K-strategy: (1) large body size (Table 2, Figs. 5, 6); (2) low population density compared to that of an r-strategy type (low population density shown at Stations 1 through 12, with respect to those of *E. huxleyi* except for at Stations 8-9 (Figs. 4, 9)); (3)

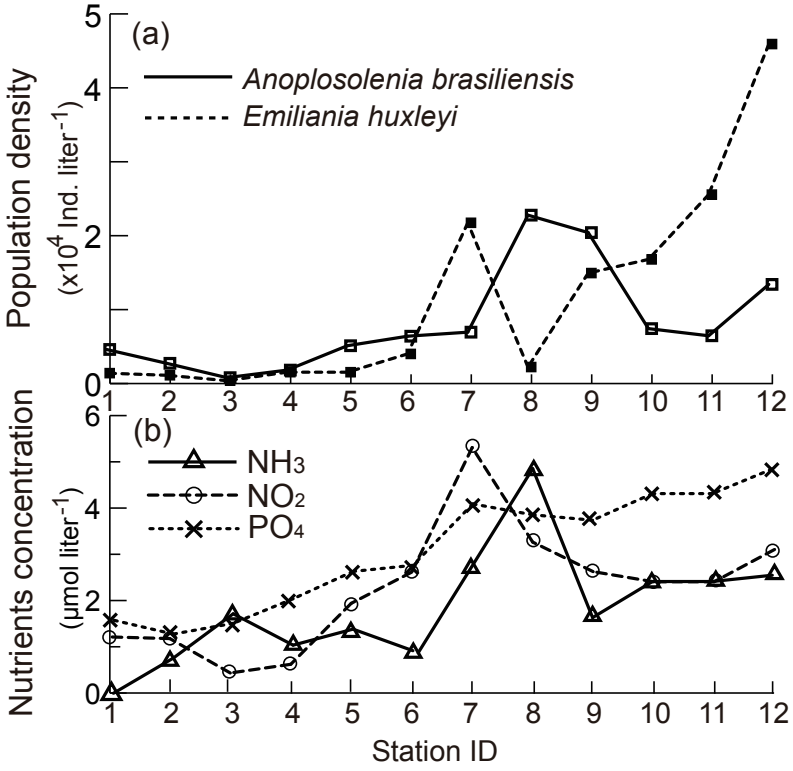

Fig. 9. (a) Changes in population density of *A. brasiliensis* and *E. huxleyi* for Cruise MR99-K07. (b) Also potted are nutrients concentrations for NH_3, NO_2, and PO_4 obtained during Cruise MR99-K07 (Kawano, 2000).

possessing a monomorphic stage; and (4) responsive to low nutrient concentrations (e.g., Foster, 1964; MacArthur and Wilson, 1967; Kimoto, 1979; Tuomi, 1980; Iwasa, 1981; Young et al., 2003; Malinverno, 2004 and Litchman et al., 2007). Young et al. (2003) and Malinverno (2004) described this taxon as possessing a haploid, and this taxon did not show any positive response for specific nutrients (Fig. 9). The above four features represent as evidence for a K-strategy. In addition to a K-strategy, MacArthur and Wilson (1967) proposed another way of life adaptation as an ”r-strategy”. With an r-strategy in stable environments organisms adapt opposite features and characteristics with respect to those of a K-strategy such as high fecundity, small body size, early maturity, and short generation time. A K-strategy can also be seen in other coccolithophore taxa than *A. brasiliensis*. For example, it is known that *Coccolithus braarudi* represents two different ecological niches depending on environmental conditions, representing a haploid stage when nutrient concentrations are low and a diploid stage when nutrient concentrations are high (Houdan et al., 2006).

However, at Stations 8 and 9 *A. brasiliensis* showed remarkably large populations compared to that of other stations (Fig. 4). When the population density of *A. brasiliensis* is greater than 1,000 individuals ℓ^{-1}, cell length decrease ca. 25% from low to high population density groups along the regressions line (Fig. 7). When the population density of *A. brasiliensis* is greater than 1,000 individuals ℓ^{-1}, this taxon appears to have modified growth strategy for adaptation. In other word, the greater the population density becomes, smaller the variance of cell length becomes. We interpret that this taxon has adapted an r-strategy in the situation with relatively high population density. Such a trend can also be observed in body size and litter size of mammals (Tuomi, 1980). Moreover, it is known that major phytoplankton groups and size classes use skillful tactics for nutrient utilization along nutrient availability gradients (Litchman et al., 2007). When the major species of coccolithophores such as *A. brasiliensis* and *E. huxleyi* swapped their population maxima between Stations 8 and 9, *A. brasiliensis* appeared to have won the competition against *E. huxleyi*. Therefore, *A. brasiliensis* fundamentally pursues a K-strategy, but this taxon is also pursuing an r-strategy when the situations become appropriate such as in the above case. According to Lewis (1985), natural selection in phytoplankton could optimize the utilization and storage of nitrogen and phosphorus, and render an advantage to haploid organisms with lower requirements of

these elements in ambient environmental conditions. Margalef (1978) and Houdan et al. (2006) strongly recommended needs for observations on nutrient response in r-strategy and K-strategy in phytoplankton.

5. Summary

The maximum population density of *Anopsolenia brasiliensis* was 3,333 individuals ℓ^{-1} located at 40 m depth at Station 8. A total of 963 individuals were measured for size analysis. The measured cell length ranged from the minimum of 39 μm to the maximum of 165 μm; width from the minimum of 1 μm to the maximum of 10 μm; and cell volume from the minimum of 28 μm^3 to the maximum of 2,741 μm^3. The length/width ratios showed the minimum of seven to the maximum of thirty-seven. One of the related factors for cell length of *A. brasiliensis* appears to be own population density. When the population density is less than 1,000 individuals ℓ^{-1} the measured cell length ranged from 55 to 110 μm. In contrast, when the population density is greater than 1,000 individuals ℓ^{-1}, the values for cell length are clustered in the range of 75 to 100 μm. As other related factors attributing to such a large cell size, the following hydrographic conditions appear important enough to report among many parameters available: water temperature is ca. 27°C; and DO is ca. 190 μmol kg^{-1}. The cell volume variations in *A. brasiliensis* may be negatively influenced by the presence of *E. huxleyi* populations. Intricate nutrient levels with a balance among nutrient species must be considered as one of the factors contributing in high population density of *A. brasiliensis* encountered at Stations 8 and 9. Fundamentally, *A. brasiliensis* pursues a K-strategy for survival because that this taxon presents: (1) large cell size; (2) low population density compared to that of *E. huxleyi*; and (3) responsive to low nutrient conditions. Nevertheless, this taxon is also pursuing an r-strategy when ambient situation becomes appropriate.

6. Acknowledgements

We thank Associate Professor Yutaka Wada of Department of Earth Sciences, Faculty of Education at Nara University of Education; he provided a use of SEM JSM-6300PS and carbon coater JFE-400 for this work. Professor Niichi Nishiwaki of Faculty of Sociology, at Nara University checked the statistic results in the manuscript and provided useful discussions as the first reviewer. Professor Emeritus Shiro Nishida of Nara University of Education provided critical comments and discussions as the second reviewer. Professor Tetsukazu Yahara of Department of Biology, Faculty of Sciences at Kyushu University, who guided us on life strategy and function of phytoplankton, including providing useful references. Ms. Chiho Yamamoto, the technical engineer of the Aero Asahi Corp., checked English in early draft. Ms. Hisako Miyazaki, the CEO and Vice President Ms. Masako Ito of the Miyazaki Insurance Firm and Co., Ltd., helped the senior author with a private scholarship. We also thank Mr. and Ms. Muraoka for their kind assistance in lodging for the senior author while the work on the SEM observation was conducted.

7. References

Colmenero-Hidalgo, E., Flores, J.A., and Sierro, F.J. (2002) Biometry of *Emiliania huxleyi* and its biostratigraphic significance in the Eastern North Atlantic Ocean and Western Mediterranean Sea in the last 20000 years. *Mar. Micropaleontology*, **46**, 247-263.

Deflandre, G. (1952). Class de Coccolithophoridés (Coccolithophoridae Lohmann, 1902). *In*: Grassé, P.P., (Ed.), *Traité de Zoologie, Phylogénie, Protozoaires: généralités. Flagellés*. Paris, Masson et Cie., **1** (1), 439-470.

Foster, J.B. (1964) Evolution of mammals on islands. *Nature*, **202**, 234-235.

Fraguas, Á., and Erba, E. (2010) Biometric analyses as a tool for the differentiation of two coccolith species of the genus *Crepidolithus* (Pliensbachian, Lower Jurassic) in the Basque-Cantabrian Basin (Northern Spain). *Mar. Micropaleontology*, **77**, 125-136.

Gastald, R.A. (2001) Terrestrial plants. *In: Paleobiology* **2**, Briggs, D.E.G., and Clowther, P.R. (Eds.), Blackwell Science, Ltd., 312-314.

Houdan, A., Probert, I., Zatylny, C., Vernon, B., and Billard, C. (2006) Ecology of oceanic coccolithophores. I. Nutritional preferences of the two stages in the life cycles of *Coccolithus braarudii* and *Calcidiscus leptoporus*. *Aquatic Microbial Ecology*, 44, 291-301.

Ichikawa, S., and Ohashi, Y. (1987). *Data analysis by SAS*. Edited by Takeuchi, Tokyo University Press, 241 pp. (In Japanese)

Iwasa, Y. (1981) *Adaptation strategy of life. In:* Katsuma, D., Yamaguchi, M., and Okada, S. (Eds.). The Science Printing Co., Ltd., 229pp. (In Japanese)

Jordan, R.W., and Kleijne, A. (1994). A classification system for living coccolithophores. *In*: Winter, A. and Siesser, W.G., (Eds.), *Coccolithophores*, Cambridge University Press, 83-105.

Kawano, K. (2000) *MR99-K07 Cruise Report*. Japan Marine Science and Technology Center, 183 pp.

Kimoto, S. (1979) *The wildlife in a south islands - biogeography on an island.* Kyoritsu printing, Co., Ltd., 209pp. (In Japanese)

Kurihara, M., and Takahashi, K. (2002) Long-term size variation and life cycle patterns of a predominant diatom *Neodenticula seminae* in the subarctic Pacific and the Bering Sea. *Bulletin of Plankton Society of Japan*, **49** (2), 77-87 (In Japanese with English abstract).

Lazarus, D.B. (1986a). Three-dimensional measurement of microfossil morphology. *Journal of Paleontology*, **60** (4), 960-964.

Lazarus, D.B. (1986b). Tempo and mode of morphologic evolution near the origin of the radiolarian lineage *P. prismatium. Paleobiology*, **12** (2), 175-189.

Lazarus, D.B. (1986c) MEASURE: a program for morphometric measurements. *WHOI Technical Report*, WHOI-86-40, 55 pp.

Lewis, W.M.J. (1985) Nutrient scarcity as an evolution cause of haploidy. *American Naturalist,* **125**, 692-701.

Litchman, E., Klausmeier, C.A., Schofield, O.M., and Falkowski, P.G. (2007) The role of functional traits and trade-offs in structuring phytoplankton communities: scaling from cellular to ecosystem level. *Ecology letters*, **10**, 1170-1181.

Lohmann, H. (1919) Die Bevölkerung des Ozeans mit Plankton nach den Ergebnisse der Zenttrifungenfänge währendder Ausreise der 'Deutchland' 1911. *Archiv für Biontologie*, **4** (3), 617pp.

Malinverno, E. (2004) Morphological variability within the genus *Calciosolenia* (coccolithophorids) from the eastern Mediterranean Sea. *Micropaleontology*, **50**, supplement No. 1, 81-91.

Manton, I., and Oates, K., (1985) Calsciosoleniaceae (Coccolithophorids) from the Galapagos Islands: Unmineralized components and coccolith morphology in *Anopsolenia* and *Calciosolenia*, with a comparative analysis of equivalents in the unmineralized genus *Navisolenia* (Haptophyceae=Prymnesiophyceae). *Philosophical Transactions of the Royal Society of London*, Series B, **309**, 461-477.

de Meuter, F.J.C., and Symons, F.E. (1975) A multivariate analysis of the morphological variability in the foraminiferal species *Florilus boueanus* (d'Orbigny, 1846) from the "Neogene" of the northern Belgium. *Micropaleontology*, **21** (4), 460-470.

Ninomiya, S. (1988). *Statistical analysis system*. Management infomatics, **14**. OHM printing, Co., Ltd., 232 pp. (In Japanese)

Nishida, S. (1979). Atlas of Pacific Nannoplanktons. *News Osaka Micropaleontology*, Special Paper, **3**, 1-31.

Nishida, S., Kawano, K., Matsumoto, K., and Tsutsui, H. (2000). Low and middle latitude western Pacific Coccolithophorids during R/V Mirai MR99-K07 Cruise. *Report of Japan Marine Science and Technology Center*, **42**, 29-55. (In Japanese with English abstract)

Rutten, A. (1972) Fluxes, diagenesis and preservation of recent and Holocene sediments in the eastern Mediterranean. *Mededelingen van de Faculteit ardwetenschappen*, Universiteit Utrecht, Geologica Ultraiectina. 176 pp.

Schmidt, D.N., Thierstein, H.R., and Bolmann, J. (2004). The evolutionary history of size variation of planktonic foraminiferal assembelages in the Cenozoic. *Palaeogeography, Palaeoclimatology, Palaeoecology*, **212**, 159-180.

Steinmetz, J. C. (1991) Calcareous nannoplankton biocoenosis: Sediment trap studies in the Equatorial Atlantic, Central Pacific, and Panama Basin. *In*: Honjo, S., (Ed.), *Ocean Biocoenosis Series*, **1**, Woods Hole Oceanographic Institution, 85 pp.

Tsutsui, H., and Takahashi, K. (2009a) Biometry of *Distephanus medianoctisol* (Silicoflagellata) in the sea-ice covered environment of the central Arctic Ocean, summer 2004. *Memoirs of the Faculty of Science, Kyushu University. Series D, Earth and planetary sciences*, **32** (2), 57-68.

Tsutsui, H., Takahashi, K., Nishida, S., and Nishiwaki, N. (2009b). Intraspecific morphological variation with biometry of *Distephanus speculum* (Silicoflagellata). *Mar. Micropaleontology*, **72**, 239-250.

Ziveri, P., and Thunell, R.C. (2000) Coccolithophore export production in Guaymas Basin, Gulf of California: response to climate forcing. *Deep-Sea Research II*, **47**, 2073-2100.

Winter, A., and Siesser, W.G. (1994) Composition and morphology of coccolithophore skeletons. In: Winter, A. and Siesser, W.G., (Eds.), *Coccollithophores*, Cambridge University Press, 51-62.

Young, J.R., Geisen, M., Cros, L., Kleijne, A., Sprengel, C., Probeit, I., and Ostergaard, J. (2003) A guide to extant coccolithophore taxonomy. *Jounral of Nannoplankton Research*, Special Issue 1, 125pp.

Mem. Fac. Sci., Kyushu Univ., Ser. D, Earth & Planet. Sci., Vol. XXXII, No. 3,
pp. 39-61, March 10, 2011

Distribution of polycystine Radiolaria, Phaeodaria and Acantharia in the Kuroshio Current off Shikoku Island and Tosa Bay during Cruise KT07-19 in August 2007

Jonaotaro Onodera*, Yusuke Okazaki*, Kozo Takahashi**, Kei Okamura***, and Masafumi Murayama***

Abstract

The occurrences of polycystine Radiolaria, Phaeodaria, and Acantharia are reported from plankton net samples, which were obtained in the transect covering from the Kuroshio Current off Shikoku Island to Tosa Bay during Cruise KT07-19 in August 2007. We employed 100 μm as the mesh size of the plankton nets, which was coarser than the mesh size of many recent radiolarian studies (e.g., 44 or 63 μm). The obtained specimens in the samples were categorized into 130 polycystine radiolarian, and 17 phaeodarian, and 3 acantharian taxa. The marked similarity of the polycystine radiolarian assemblages encountered in this study to those reported from the tropical and subtropical oceans in the literature clearly indicates the significant influence by the warm Kuroshio Current. Furthermore, the observed polycystine radiolarian assemblages are similar to those of the previous result from the same specific study area. However, the vertical distribution patterns of some of the major polycystine radiolarian and phaeodarian taxa are different from the previous results from the same region. The differences in vertical distribution may be primarily due to the differences in vertical water mass conditions due to different sampling seasons. In spite of the lengthy sample storage for seven months after the sampling in the shore laboratory, many acantharian specimens were still preserved and encountered in the laboratory census, representing the acantharian presence in the summer sea surface waters in the Kuroshio Current area.

Keywords: Radiolaria, Phaeodaria, Acantharia, Kuroshio, MTD-net, subtropical assemblage

1. Introduction

In the subtropical oceans Radiolaria normally represent one of the major biosiliceous planktonic particles (e.g., Boltovskoy et al., 2010; Ishitani and Takahashi, 2007). In addition to calcareous microplankton particles, together with diatoms the siliceous skeletons of Radiolaria and Phaeodaria significantly contribute as the ballast of sinking particles to the vertical transport of organic material to the interior of the deep oceans (Honjo et al., 2008). Thus, it is important to study them in detail. However, the information concerning the distributio of Radiolaria and related groups in the water column is still meager and hence further studies are warranted. Phaeodaria had been traditionally considered as one group of Radiolaria (see discussion in Takahashi and Anderson, 2002) whereas it has recently been often treated as one of Cercozoa (Poulet et al., 2004). As the taxonomy of polycystine Radiolaria, Class Polycystinea is one of the representative groups in Subphylum Radiolaria (Müller) Cavalier-Smith 1993. Class Polycystinea is subdivided into two Orders: Spumellaria Ehrenberg 1875 and Nassellaria Ehrenberg 1875 (Anderson et al., 2002). Class Acantharia, which is classified into Radiolaria with recent substantial molecular support, was traditionally treated separately from Radiolaria. This is because that they bear celestite ($SrSO_4$) skeletons, which are different from polycystine Radiolaria with biogenic opal skeletons. Although there have been many studies on polycystine Radiolaria, works concerning

Manuscript received on 1 Dember 2010; accepted on 20 January 2011
* Research Institute for Global Change, Japan Agency for Marine Earth Science and Technology, Natsushima-cho 2-15, Yokosuka, 237-0061, JAPAN; Corresponding author's e-mail: onoderaj@jamstec.go.jp
** Department of Earth and Planetary Sciences, Graduate School of Science, Kyushu University, Hakozaki6-10-1, Fukuoka, 812-8581, JAPAN
*** Center for Advanced Marine Core Research, Kochi University, B200 Monobe, Nankoku, 783-8502, JAPAN

Acantharia are quite limited due to readily dissolved nature of their celestite skeletons. However, in the viewpoint of geochemical cycle, acantharian production in the subtropical oceans may significantly influence, for instance, the distribution of Sr/Ca ratios in the upper water column (De Deckker, 2004). Based on the microscopic examinations on plankton tow and surficial bottom sediment samples we report the distribution of polycystine Radiolaria, Phaeodaria and Acantharia in this paper in order to serve a basis for the future studies.

2. Materials and Methods

2.1. Study Materials

The study area is located off Shikoku Island and Tosa Bay in the western North Pacific (Fig. 1). While this is in the temperate region with northern latitude of the Tropic of Cancer the watermasses here are largely influencd by the northernly flow of the Kuroship Current and hence this region is conceptually close to the subtropics. The studied materials were obtained at six sites during Cruise KT07-19 on board R/V Tansei-Maru of Japan Agency for Marine Earth Science and Technology (JAMSTEC), which took place during 8-10 August 2007 (Table 1; Fig. 1). One of the two microplankton sampling methods was proceeded, employing a standard twin North Pacific net (NORPAC net: Motoda, 1957), at Sites M1, M2, and M3. The other sampling method employed involves Motoda horizontal nets (MTD plankton net; lateral tow: Motoda, 1971); the plankton tow samples were obtained from seven discrete depth layers at Sites M5, M7, and M9. During the lateral towing of the MTD plankton nets for a half an hour, the ship speed was controlled (~2 knot) in order to keep the wire angle of 45°. The applied mesh size of the plankton nets for the both moethods is 100 μm because of the primary objective in foraminifer sampling. The obtained plankton samples were immediately fixed by 5% sample volume of buffered (pH 7.8) formaldehyde with sodium tetraborate. The rose bengal stain was added to the MTD samples in order to distinguish live specimens (stained) from dead specimens (stain-free). The twin NORPAC net was towed without a flow meter

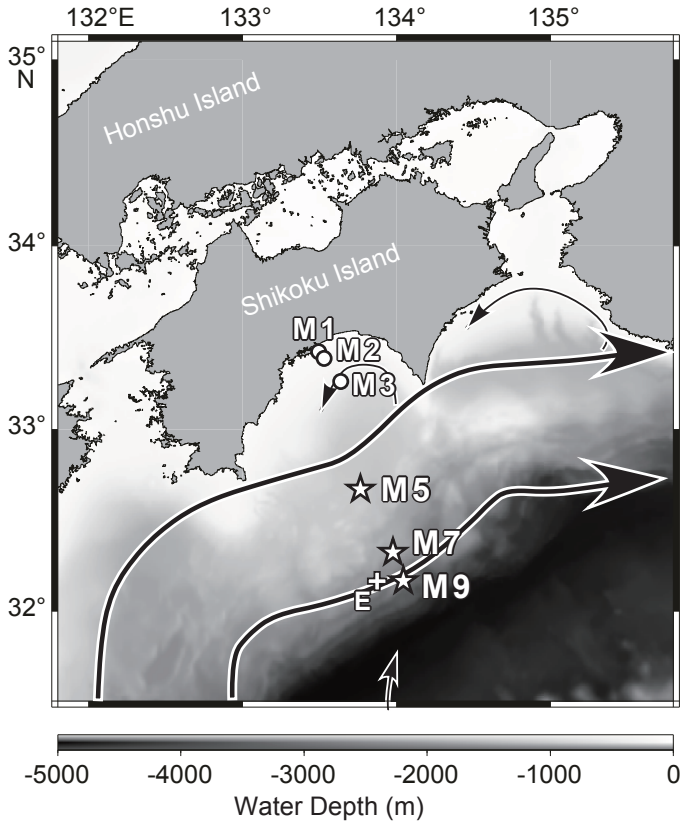

Fig. 1. Map of the studied area configured with GMT. The symbol with circles represents the sampling locations for the vertical towing. The symbol with stars represents the locations for the lateral towing (MTD) and surface sediment sampling. The symbol with a cross is the location where Station E was occupied in a previous study (Ishitani and Takahashi, 2007). Two bold arrows designate the northern and southern boundaries of the Kuroshio Current on 7 August 2007, among the arrows representing the estimated lines of sea surface stream, (JHOD, JCG, 2007).

attached. Furthermore, a flow meter test for the MTD net could not be conducted due to the limited ship time. Therefore, reliable standing stocks cannot be estimated in this study. The results of specimen counts are shown as relative abundance in total numbers of encountered polycystine radiolarian, phaeodarian and acantharian specimens. Unexpected small number of live sea surface and subsurface dwellers were observed in deep MTD samples. Such rare occurrences are considered as the result of contamination in the upper water column during the cast of the net from sea surface to the deep depth. Therefore, some sampling error is included in the obtained % data in deep MTD samples.

Table 1. Summary for microzooplankton and microfossil samples obtained during Cruise KT07-19 of R/V Tansei-maru.

Site ID	Coordinate	Start Date and Time (yr/m/d, JST)	Water Depth (m)	Sample Type	Towing Speed	Target Depth (m)	Flow Meter Read
M1	33°26'N 133°30'E	2007/8/8 9:40	31	Twin NORPAC (mesh: 100μm)	0.5 m/s	0-20	---
M2	33°24'N 133°32'E	2007/8/8 7:20	70	Twin NORPAC (mesh: 100μm)	0.5 m/s	0-50	---
M3	33°14'N 133°38'E	2007/8/10 5:10	231	Twin NORPAC (mesh: 100μm)	0.5 m/s	0-50	---
M5	32°40'N 133°46'E	2007/8/8 21:30	990	Closing MTD + open net at 0m (mesh: 100μm); surface sediment by Multiple Core sampler (MC)	2 knot	0	2869
						50	4345
						100	442 [a]
						200	14475
						300	3522 [a]
						500	21460
						750	24280
M7	32°20'N 134°00'E	2007/8/9 13:55	1935	Closing MTD + open net at 0m (mesh: 100μm); MC	2 knot	0	4162
						50	7522 [b]
						100	17513
						200	13038
						300	28240
						500	245
						1000	3395
M9	33°09'N 134°03'E	2007/8/9 22:00	2750	Closing MTD + open net at 0m (mesh: 100μm); MC	2 knot	0	4501
						50	7045
						100	369
						200	919
						300	1482
						500	732 [a]
						750	5611 [b]

[a]: plankton net tangled during towing; [b]: plankton net mesh was torn during towing

The obtained samples had been kept in a refrigerator (4°C) in a shore laboratory. All of the sample treatment for this study was conducted in March 2008, seven months after the collection at sea. Portions of samples were sieved through stainless screens of 1000, 500, and 63 μm mesh size, respectively. The residue on these mesh sizes was filtered onto a membrane filter (with 3 mm grid printed) and desalted. The filter was dried in an oven at 40˚C and the sample was mounted on a glass slide with Canada Balsam^{R}. In order to observe skeletons of polycystine Radiolaria and Phaeodaria employing a field emission scanning electron microscope (FE-SEM), portions of plankton net samples and surface sediments taken by multiple core sampler (MC) were treated with hydrogen peroxide and sodium hexametaphosphate. The skeletal counts were proceeded under a light microscope (LM) to distinguish the live/dead status of each of the specimens. The polycystine radiolarian and phaeodarian skeletons were normally identified at genus or family level based on the illustrations published by Boltovskoy and Riedel (1987) and Takahashi (1991). Concerning the encountered living specimens of a radiolarian *Sphaerozoum*, both numbers of their spicules and protoplasm were counted (Table 2).

Table 2. The %species represent the values in the grand sum of total Spumellaria, total Nassellaria, total Acantharia, and total Phaeodaria. The blank and the symbol "+" represent no record or less than 1%, respectively.

Site ID (KT07-19)	Sampled Depth (m)	Live/Dead/Total	Total of Counted Skeletons	Acanthosphaera actinota	Acrosphaera murrayana	A. spinosa	Actinomma antarcticum Gr.	A. arcadophorum	A. arcadophorum ?	A. medianum	Actinomma spp.	Actinommidae spp.	Actinosphaera spp.	Amphirhopalum straussii	Arachnosphaera myriacantha	Astrosphaera hexagonalis	Axoprunum stauraxonium	Cenosphaera spp.	Cladococcus cervicornis	C. scoparius	C. viminalis	Collosphaera macropora	C. tuberosa	Dictyocoryne spp.	Didymocyrtis tetrathalamus tetrathalamus	Druppatractus sp.	Drymosphaera dendrophora	Ethmosphaeridae spp.	Euchitonia elegans	Euchitonia sp.	Heliodiscus asterícus	H. echiniscus ?	H. macrococcus	Heliodiscus spp.	Hexacontium hostile	H. melpomene	Hexacontium spp.	Hexalonche amphisiphon	Larcopyle buetschlii	Larcospira quadrangula	Litheliidae spp.	Litherius sp. ?	Myelastrum trinibrachium ?	Plegmosphaera entodictyon	Plegmosphaera sp.	Siphonosphaera spp.	Solenosphaera quadrata	S. zanquebarica	Solenosphaera spp.	Sphaerozoum spp. Spicules
M1	0-20	TOTAL	71			+						2													4				4																				
M2	0-50	TOTAL	120								+	8	+												4		2		2				+				3				3		+				
M3	0-50	TOTAL	209	+							1	4				+								2	3			4	+						+								+				
M5	0	LIVE	1361			+				+	1	+					+						+		+	+	+			+				+							+		+			10
M5	0	DEAD	9		+						+		+																					+													
M5	50	LIVE	50				+	1				10				+	2			1	+		+	2	2		+		+		1				2	+	2				2		3			3
M5	50	DEAD	62								+	1				+	1							2	+		+										2						+			
M5	100	LIVE	21								2	6								12				2	2					2													6			
M5	100	DEAD	15									4								6																											
M5	200	LIVE	51									3													+																					
M5	200	DEAD	117			+						5	+								2			+	2				+							3	+	+				1		+			
M5	300	LIVE	87								1	6				+								4	2			1	1	+						1						13					
M5	300	DEAD	30								3	2															+	1	1																	
M5	500	LIVE	91								1	2	+				+					+		+	2							+			+	+						+				
M5	500	DEAD	115	+					2		+	3	+									+		7	3		+	+	2						+	2	+	+				2				+	
M5	750	LIVE	56			+			+			2					2								+												+									
M5	750	DEAD	108			1			1		1	3						+						8	1				2	+		+		+		+	+		+			1				
M7	0	LIVE	329			+				+	+	2				+							+	+	+	+	+		+			+								+	+					
M7	0	DEAD	573									+									+			+		+						+														
M7	50	LIVE	498										+			+	1				+				+	+		+		+		+				+	+					+				54
M7	50	DEAD	56									+													+	+								+				+									
M7	100	LIVE	404	+			+	+			+	1		+		+	+				+		1	+		+						+		+	+	2		+	+		+	+		+	9		5	10
M7	100	DEAD	192				+				+	1	+			+					1				1	3		1		+		+			+	+	+					2	+				+	
M7	200	LIVE	97	+		+		+			+	1										9		+																					1	+	4	
M7	200	DEAD	136			+						+	+				+					+			1	2				1			+				4		+				1					
M7	300	LIVE	30																			2				+		+								+		+		3					2			
M7	300	DEAD	98			+					2	4												+	4				+					+		4									3		
M7	500	LIVE	23									5												2	1																					1		
M7	500	DEAD	38								6	1												5	4				16							1											
M7	1000	LIVE	110			+	+		+			5	+											4	4		+		1	1	+				1						+	2				1	2	
M7	1000	DEAD	55						+			3	+											+	4		1		1													2						
M9	0	LIVE	122			+																	+		+		+																	3	+		2	
M9	0	DEAD	379																																											+		+	75
M9	50	LIVE	345			+	+		+		+	4	+								+		+	+	5				2	+						4		+				+		2		+	21
M9	50	DEAD	65						+																+		+		+							1	+										2
M9	100	LIVE	65									5	1							2	1				6				2							2									1		4
M9	100	DEAD	29	1								1												1																			1					7
M9	200	LIVE	15																						11					1																	
M9	200	DEAD	23																						5													1						5	5		
M9	300	LIVE	26								1	4																								4		1									
M9	300	DEAD	30								1		2																																			
M9	500	LIVE	29									2					1								15											1											
M9	500	DEAD	21									1					1							5	16																						
M9	750	LIVE	32									3													5		+								+	2										
M9	750	DEAD	40			+						5													5		2		+																	

Table 2. (cont.)

Sphaerozoum spp. Protoplasm ?	Spongaster tetras tetras	Spongodiscidae spp.	Spongodiscus spp.	Spongosphaera polycantha	S. streptacantha	Spongurus cylindricus	Stylochlamydium venustum	Stylodictya asteriscus	S. validispina	Stylodictya sp. ?	Tetrapyle octacantha Gr.	Thalassoxanthium sp.	Tholospira cervicornis Gr.	Tholospira spp. ?	Xiphosphaera tesseractis ?	Spumellaria indet.	**TOTAL SPUMELLARIA**	Acanthodesmia vinculata	Acanthodesmiidae spp.	Androspyris hyxleyi	A. hyxleyi ?	Anthocyrtidium ophirense	A. zanguebaricum	Arachnocalpis sp. ?	Arachnocorys umbellifera	Botryostrobus elongatum ?	Callimitra sp.	Carpocanistrum spp.	Clathrocanium coarctatum	C. giltschii	C. murrai ?	Clathrocanium sp.	Clathrocorys sp.	Cycladophora bicornis	C. cornutoides	Eucecryphalus cervus	E. tricostatus	Eucecryphalus spp.	Eucyrtidium acuminatum	E. dictyopodium	E. hexastichum	Eucyrtidium spp.	Eucyrtidium spp. ?	Lamprocyclas maritalis Gr.	Lampromitra spp.	Lipmanella bombus	L. dictyoceras	L. dictyoceras ?	Liriospyris reticulata	Litharachnium eupilium	L. tentorium	Lophophaeninae spp.	Lophophaena spp.	Lophospyris pentagona	Lophospyris spp.
		3	2	3							5					15	**37**																																+			4	+		7
		+	1	4	3			+			10					13	**58**	2				+			2																				2								3		
	+	+		3	2	+		2			9	3		+		11	**49**																			+									8							1	+		2
+			+	1	+						+					1	**17**																																				+		
			+										+			+	**+**																																						
+	+	2	+	11	1			+			8		+			6	**66**	2																					+						+								2		2
			+	5							+		+			1	**17**																											+					+			+	+		+
			2		2				2		4					4	**44**		6																																				
			2	6							2					4	**23**																					2																	2
			+			+		2			+			+		4	**12**									+					+		+	+		1		1							+					1			2		+
	+		+		+		1	+			10					10	**44**	+				+											1			2	1	1	1		+								2	+			3		2
			+	6	3			+			3			2		7	**53**		1																	1		5															3		1
			2	+				+			8					4	**24**																					+																	1
			+			+					+		+	3		3	**19**																												+				+	+					
	+		3					1			5					5	**42**																					1											1				2	+	+
			+	+	+									+		2	**9**											+																	2								+		
	2	1	4			1		2	+		6		+	2		9	**52**				+															+									+				2						3
		+	+	1	+						+						**10**	+																																					
	+		+	+													**3**																																+				+		
3		+		1	+			+	+		5		+	+		1	**71**	+																						+		+											+	+	+
	+		+	+					+		1					1	**7**							+																													+		1
+		1		2	1			1			2		1	1		2	**50**	+				+	+	+	+				+					+		+	+	+		+		+			+					+		+	+	+	3
	+	+	1	+	+			+			5		+	+		1	**23**	+							+							+		1		+	+	+				+	+		+	+		+	+			+		+	+
		+	+			+		1					2	2		3	**28**					+			+					+				+				+							+				+				+		2
		+	+	+				1			9					8	**31**	+						+	+											+	+	3		+					+				+	+			1	+	8
								2					+			+	**13**	+	+																							+						+					2	+	
		2	2					+			15		+	6		7	**55**	+	+						+												+	+				+	+					+					2	2	5
			5			1										2	**18**																					1																	2
		1	2					1			5		1	16			**60**																			1																	4		1
	2	+	+	7	4	+		1			2		+			6	**52**																			1		+															1		2
			1	1	1						6					4	**27**																																+				1		
17																+	**24**																																						
																+	**76**																																						
+		1	2	+				2		1	3		1	+	+	6	**63**	+		+					+		1													+			+		+		+		+			+	+		5
		+		+	+						+					+	**8**																										1						+		+	+	+		+
1	1	4		1				3	2		3	2				3	**47**	1																		1							2		2										4
											3					1	**16**																												1								2		1
		1					1				1					6	**23**					1					5																										1	1	1
			8	1				1			1					12	**40**																					1																	1
								1								13	**24**																	2				2							2						1		3		2
											9					9	**21**																		2			2							2	2							4		
		1			1			1			1		1			5	**30**					1																1													1		6		1
											6					16	**45**																			1													1				2		
	+	2	4								5			2		5	**30**																													2							2		4
				+				+			6			8		9	**38**	2																		+																	2	+	

Table 2. (cont.)

	Nephrospyris renilla ?	Peridium spp.	Peripyramis circumtexta	Peromelissa phalacra	Phormospyris hexdisae	P. stabilis scaphipes	Plagoniidae spp.	Plectacantha spp.	Pseudocubus obeliscus	Pseudodictyophimus? spp.	Pterocanium praetextum	P. trilobum	Pterocanium sp.	Pterocorys zancleus	Pterocorys? spp.	Pteroconythidae spp.	Semantis glaciilis?	Spyrocyrtis scalaris	Stichopilium bicorne	Tetracorethra tetracorethra	Tetraphormis dodecaster	T. rotula	Theocorythium trachelium	Theoperidae spp.	Theoperidae sp. cf.	Zygocircus productus	Nassellaria spp.	Nassellaria spp. (juvenile)	**TOTAL NASSELLARIA**	Acantharia sp. 1	Acantharia sp. 2	Acantharia spp.	**TOTAL ACANTHARIA**	Aularia temaria	Aulosphaeridae spp.	Castanidium longispinum	Castanidium? or Castanella ? sp.	Challengeriidae spp.	Challengerium dicodon ?	Challengerium willemoesii	C. radians ?	Challengeron sp.	Conchellium capsula	C. caudatum	Conchidium argiope ?	Conchidium sp. ?	Euphycetta lucani	Medusetta ansata	Protocystis xiphodon	Phaeodaria spp.	**TOTAL PHAEODARIA**
		+					7		9						6					+							6	4	21	**63**				**1**																									
		1					3		6						+												+	+	23	**42**																									
		4					7		5						+					+							8	1	12	**50**	32	5	45	**82**																									
																												+	**+**	+			**+**																							
		+																										10	**10**	+			**+**																							
							+		+																		+	1	**6**																									
							7								6												6		**12**																									
														6														**15**	6			**6**																							
							2					+										+						**13**				**13**																						
							5			+					1					+								**25**				**25**																						
		4							+																		4	**20**				**20**																						
																			+									**2**				**2**																						
																											+	**3**	7	2	4	**14**																						
		+																										**10**	31	6	36	**74**																						
																												6	5	2	8	**15**																						
		+					+													+								**13**				**3**																						
		+					+																					**3**	+			**14**																						
		+					+													+								**14**				**11**																						
		+					+																					**11**				**5**																						
																												5	1			**1**																						
																												1				**1**																						
																												12				**12**																						
																												14				**14**																						
																												6				**6**																						
																																+																						
		+																										**22**				**22**																						
		+																										**7**				**7**																						
		+																										**22**				**22**																						
																												15				**15**																						
																												15				**15**																						
																												17				**17**																						
																												18				**18**																						
																												2				**2**																						
		1																										**34**				**34**																						
							2	4				2																**12**				**12**																						
																												6				**6**																						
																												7				**7**																						
		1																										**13**				**13**																						
																												12				**12**																						

3. Results and Discussion

3.1. Oceanographic conditions

Sea surface temperatures ranged from 25.3°C (Site M1) to 29.4°C (M7). According to the daily report on the Kuroshio Current provided by Japan Coast Guard, Site M5 on 7th August 2007 was located in the central part of the Kuroshio Current (Fig. 1). Site M7 was located in the southern part of the Kuroshio Current. While the southern edge of the Kuroshio Current was unclear, Site M9 appeared to be out side of the Kuroshio Current based on the on-site CTD vertical profiles. Water temperature became colder with increased water depth. Below 200 m the isotherm depth shoaled from Site M9 towards Site M5. Sea surface salinity was the lowest at Site M1 (33.1 psu) and the highest at Site M9 (34.5 psu). The high salinity waters (>34.5 psu) in the subsurface at Sites M5-M9 reflect the lateral advection of the central subtropical waters. The maximum of chlorophyll concentration was observed around the pycnocline depth at each site. In the plankton tow samples at Site M2, a diatom *Coscinodiscus* sp. was dominant and conspicuous in the net phytoplankton (>100μm).

3.2. Polycystine Radiolaria

Among the observed microzooplankton groups, polycystine Radiolaria represented the major component in all the samples except for the sea surface at Sites M5 and M7 (Fig. 2). The encountered polycystine radiolarian specimens in all the sample slides were categorized into the following two orders (Anderson et al., 2002): Spumellaria: 64 taxa; and Nassellaria 66 taxa (Table 2). While the sampled locations spans from 32.15°N to 33.43˚N, which are within the temperate climatic region of the world, the obtained polycystine radiolarian

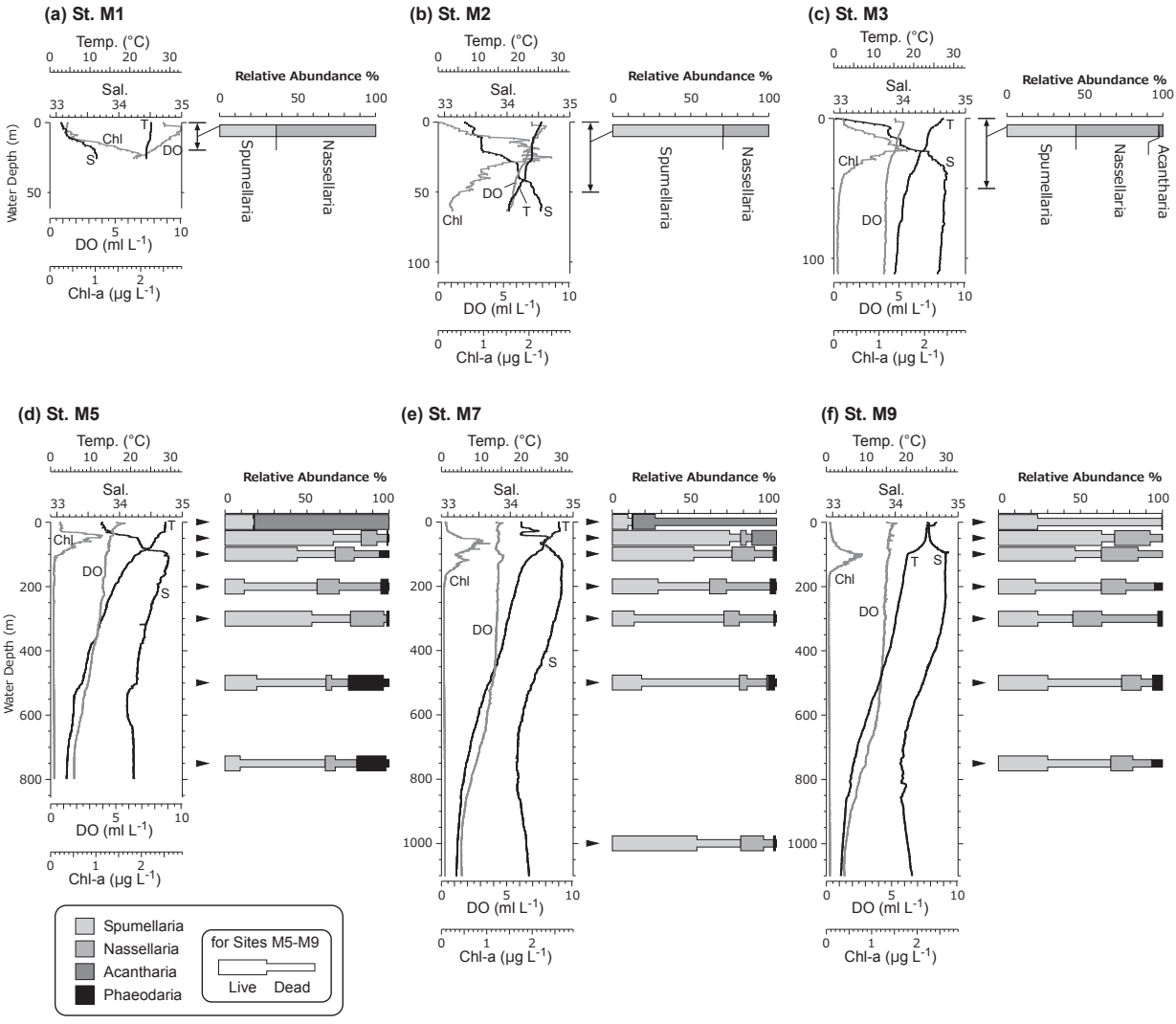

Fig. 2. CTD profiles and relative abundances of Polycystine Radiolaria, Acantharia, and Phaeodaria at Sites M1-M9. The distinction between live and dead specimens was given at Sites M5-M9.

assemblages clearly show the affinity to the subtropic to the tropic assemblages. This is due to the influence of the Kuroshio Current, which laterally advects the warm subtropical water mass from the lower latitudes along the western boundary of the North Pacific. The major encountered taxa in this study are essentially the same as those reported in the previous study at Station E in June 2002 (Fig. 1; Ishitani and Takahashi, 2007). However,the vertical distribution of characteristic species indicated by Ishitani and Takahashi (2007) were different from the results in this study. The differences in the vertical distribution of polycystine Radiolaria are primarily due to the seasonal difference in water mass conditions in the upper water column.

The relative abundance of Order Spumellaria was usually at similar level or higher than that of Order Nassellaria. The spumellarian assemblages were represented by *Didymocyrtis tetrathulumus, Tetrapyle octacantha* group. *Tetrapyle octacantha* group and *Didymocyrtis tetrathalamus*; they commonly occur in the subtropical and tropical oceans (Kling, 1979; Yamashita et al., 2002; Boltovskoy et al., 2010). In addition to Family Collosphaeridae, abundant Spaherozoum spicules were the main cause of high %Spumellaria in the shallow layers at Sites M5-M9. In particular, radiolarian assemblage at sea surface at Site M9 was characterized by the high abundance of *Sphaerozoum* with *Siphonosphaera* spp. and *Solenosphaera* spp., all of which belong to colonial radiolarians. Because that the colonial radiolarians prosper better in the pelagic waters than in more eutrophic waters the result shown here are conformable with the known distribution (Takahashi et al., 1995). Interestingly, *Tetrapyle octacantha* group and *Didymocyrtis tetrathalamus*, which commonly occur in the subtropical and tropical oceans (Kling, 1979; Yamashita et al., 2002; Boltovskoy et al., 2010), were commonly observed in many samples. Living *Dictyocoryne* spp. were observed in many samples at Sites M5 and M7 whereas the living specimens of this taxon were encountered only at 50 m at Site M9.

The vertical trend of %Nassellaria at Sites M5-M9 shows the maximum depth at 200 m or 300 m, which correspond to the lower part of high salinity layer (Fig. 2). The increase in %Nassellaria from the surface layer to the deeper layer is the same characteristics as in the previous observation in the oligotrophic tropical ocean (Yamashita et al., 2002). *Lophophaena* spp. and *Lophospyris* spp. were found in many samples. The high abundance of these taxa were also reported in the subtropical and tropical oceans (Kling, 1979; Yamashita et al., 2002). The nassellarian assemblage at Sites M1-M3 was mainly composed of *Pseudocubus obeliscus, Zygocircus productus*, Plagoniidae spp., and juvenile of Nassellaria spp. (Table 2). *Psudocubus obeliscus* and Z. *productus* were characteristically observed in the surface waters (Yamashita et al., 2002). The high abundances of P. *obeliscus* at coastal sites rather than pelagic sites appear to be related to the high primary productivity (Ishitani and Takahashi, 2007) and high nutrient supply in the equatorial upwelling (Yamashita et al., 2002). At Sites M5-M9, %Nassellaria was significantly minor at the sea surface. There are two possible reasons for the minor %Nassellaria representations. The first reason is the relative dominance of *Spaherozoum* spicules or Acantharia. Another reason is the limited standing stock of Nassellaria at sea surface at Sites M5-M9; Nassellaria were absent at Site M9 or 4-5 specimens only at Sites M5 and M7 whereas the encountered Spumellaria were greater than 100 specimens except for *Sphaerozoum* spicules. In the deep layer at Site M5-M9, *Eucecryphalus* spp. were encountered.

3.3. Phaeodaria

Seventeen phaeodarian taxa were observed mainly below the depth of chlorophyll concentration maximum at Sites M5-M9 (Fig. 2). The relative abundance of total Phaeodaria in the studied microplankton groups was higher than that of total Nassellaria at 500 m and 750 m at Site M5. The major taxon at Site M5 was *Challengeron willemoesii* in addition to *Protocystis xiphodon* and *Challengeriidae* spp. (Table 2). The depths with abundant *Challengeron willemoesii* were deeper than the previous result in the equatorial Pacific (as subsurface dwellers in 120-200 m: Yamashita et al., 2002). While phaeodarian specimens at Site M2 were absent in the census sample slides (Table 2), few skeletons of *Medusetta ansata* were found in the treated sample for photomicrographs (Plate 13, fig. 1).

The relative increase of phaeodarian abundance with respect to polycystine radiolarians in the deep layers is common in the tropical oceans (Dworetzky and Morley, 1987; Yamashita et al., 2002). When the relatively high standing stocks of Phaeodaria relative to polycystine Radiolaria were observed in the subsurface layers (40-200 m) around Japan, salinity and water temperature were about 34 psu and 5-13°C, according to the CTD profile figure in Ishitani and Takahashi (2007). Such values in salinity and water temperature were also observed in this study in the deep layers, which roughly correspond to the sampled depths with the observed living phaeodarian specimens (Fig. 2).

3.4. Acantharia

In spite of the fact that the studied samples had been stored in a refrigerator for seven months after sampling,

common to dominant acantharian specimens were encountered in the samples from the sea surface and upper waters of Sites M5 and M7 (Fig. 2). The dominant acantharian taxon at Sites M5 and M7 was Holacanthida(?) sp. as shown in Plate 13, figs. 7 and 8. Most acantharian specimens at Site M5 had the stained protoplasm, suggesting living conditions at the time of sampling. However, many specimens at the sea surface at Site M7 were dead without protoplasm (Fig. 2). The acantharian occurrences were trace level at Sites M3 and M9 and absent at Sites M1 and M2.

In general, acantharian skeletons are readily dissolved after death (Beers and Stewart, 1970) because of the unsaturated strontium sulfate concentrations in sea waters. The high abundance of acantharians at Sites M5 and M7 are unusual. This is because that addition of strontium for the sake of skeletal preservation (Michaels, 1988) was not proceeded to the acquired samples, which were kept in the buffered formaldehyde solution. Although the strontium concentration in the waters of the plankton net samples has not yet been analyzed, we suspect that some portion of acantharian skeletons may have been dissolved prior to the point where strontium concentration became saturated in the stored samples. The skeletal abundance ratios of acantharian versus polycystine radiolarians at sea surface at Sites M5 and M7 were two orders of magnitude less than those in the previous results without significant acantharian skeleton dissolution (Beers *et al*., 1975 in the central North Pacific gyre; De Deckker, 2004 in Indian Ocean). Therefore, the relative abundance of acanthaians at Sites M5 and M7 may originally have been significantly higher than our obtained results.

Based on the biogeographic occurrence pattern in this study, the high abundance of acantharians can be related to the summer surface waters of the Kuroshio Current. According to De Deckker (2004), the acantharian assemblage in the Mediterranean Sea around Italy suggested an ecological relationship to salinity gradient (Bottazzi, 1978; Bottazzi and Andreoli, 1978). In this study, the σ_t values determined by both salinity and water temperature were lower than that in the Mediterranean data when acantharians dominated relative to polycystine radiolarians and phaeodarians. Sigma-t (σ_t) at 0 m at Sites M5 and M7 were 21.2 and 21.3, respectively, which were lower than σ_t at sea surface at nearshore Site M1 (σ_t = 22.1) and offshore Site M9 (σ_t = 22.1). Not only salinity difference but also higher water temperature appear be related to the biogeographic patterns of acantharian distribution in this study. However, at Site M3 with the lowest σ_t at sea surface, %Acantharia was minor (Fig. 2). Such a low %Acantharia is explained by the difference in the sampling method (vertical towing for 0-50 m at Site M3). The previous study shows that the vertical distribution of acantharian abundance steeply decreases below 20 m water depth (Michaels, 1988). Therefore, the %Acantharia in the vertical tow sample at Site M3 appears to be suppressed, with the view that the standing stock of polycystine radiolarians just below the sea surface was relatively abundant compared to the acantharian standing stock.

4. Acknowledgements

We thank the captain, crew, technical staff, and scientists on board R/V Tansei-Maru of JAMSTEC for their efforts in the CTD observations and plankton two sampling employed in this study. We are grateful to Dr. Yoshiyuki Ishitani at JAMSTEC who reviewed the manuscript of this paper for his critical and constructive comments, which were greatly helpful in revising the manuscript. This work was financially supported by the Kochi University President's Discretionary Grant in 2007 and 2008.

5. References

Anderson, O. R., Nigrini, C., Boltovskoy, D., Takahashi, K., and Swanberg, N. R. (2002) Class Polycystina. *In: The Second Illustrated Guide to the Protozoa*, Lee, J.J., Leedale, G.F., and Bradbury, P., (eds.), Society of Protozoologists, Lawrence, KS. 994-1022.

Beers, J. R., and Stewart, G. L. (1970) The preservation of acantharians in fixed plankton samples. *Limnology and Oceanography*, **15**, 825-827.

Beers, J. R., Reid, F.M.H., and Stewart, G. L. (1975) Microplankton of the North Pacific Central Gyre. Population structure and abundance, June 1973. *Internationale Revue Gesamtes Hydrobiologie*, **60**, 607-638.

Boltovskoy, D., and Riedel, W.R. (1987) Polycystine Radiolaria of the California Current region: seasonal and geographic patterns. *Marine Micropaleontology*, **12**, 65-104.

Boltovskoy, D., Kling, S. A. Takahashi, K. and Bjørklund. K. (2010) World atlas of distribution of recent Polycystina (Radiolaria). *Paleotologia Electronica*, Article Number: 13.3.18A; http://palaeo-electronica.org/2010_3/215/index.html.

Bottazzi, E.M. (1978) Systematic-ecological aspects of Radiolaria with special reference to Acantharia. *Bolletino*

Zoologica, **45**, 133-144.

Bottazzi, E. M., and Andreoli, M.G. (1978) Distribuzione stagionale degli Acantari e dei Radiolari (Protozoa, Sarcodina) in diverse zone costiere dei mari italiani. *L'Ateneo Parmense Acta Naturalia*, **14**, 477-500.

De Deckker, P. (2004) On the celestite-secreting Acantharia and their effect on seawater strontium to calcium ratios. *Hydrobiologia*, **517**, 1-13.

Dworetzky, B.A., and Morley, J.J. (1987) Vertical distribution of radiolaria in the eastern Equatorial Atlantic: analysis of a multiple series of closely-spaced plankton tows. *Marine Micropaleontology,* **12**, 1-19.

Honjo, S., Manganini, S.J., Krishfield, R.A., Francois,R. (2008) Particulate organic carbon fluxes to the ocean interior and factors controlling the biological pump: A synthesis of global sediment trap programs since 1983. *Progress in Oceanography,* **76**, 217-285.

Ishitani, Y., and Takahashi, K. (2007) The vertical distribution of Radiolaria in the waters surrounding Japan. *Marine Micropaleontology,* **65**, 113-136.

Kling, A.S. (1979) Vertical distribution of polycystine radiolarians in the central North Pacific. *Marine Micropaleontology,* **4**, 295-318.

Michaels, A.F. (1988) Vertical distribution and abundance of Acantharia and their symbionts. *Marine Biology,* **97**, 559-569.

Motoda, S. (1957) North Pacific standard plankton net. *Information Bulletin on Planktology in Japan, **4,*** 13-*15*.

Motoda, S. (1971) Devices of simple plankton apparatus V. *Bulletin of the Faculty of Fisheries Hokkaido University, **22,*** 101-106.

Poulet, S., Berney, C., Fahrni, J., and Pawlowski, J.A.N. (2004) Small-subunit ribosomal RNA gene sequences of Phaeodarea challenge the monophyly of Haeckel's Radiolaria. *Protist,* **155,** 53-63.

Takahashi, K. (1991) Radiolaria: Flux, ecology, and taxonomy in the Pacific and Atlantic. In: Honjo, S. (Ed.), *Ocean Biocoenosis Series,* **3.** Woods Hole Oceanography Inst. Press, Woods Hole, MA. pp. 303.

Takahashi, K., Oba, T., Yamazaki, H., and Ohkouchi, N. (1995) Paleoceanographic changes based on radiolarian fossils during the past 80 ky in the western Tropical Pacific. *Kaiyo Monthly,* 27 (8), 466-473. [in Japanese with English fig. & table captions.]

Takahashi, K., and Anderson, O. R. (2002) Class Phaeodaria. *In: The Second Illustrated Guide to the Protozoa* , Lee, J.J., Leedale, G.F., and Bradbury, P., (eds.), Society of Protozoologists, Lawrence, Kansas. 981-994.

Yamashita, H., Takahashi, K., and Fujitani, N. (2002) Zonal and vertical distribution of radiolarians in the western and central Equatorial Pacific in January 1999. *Deep-Sea Research II,* **49,** 2823-2862.

.

Plate 1

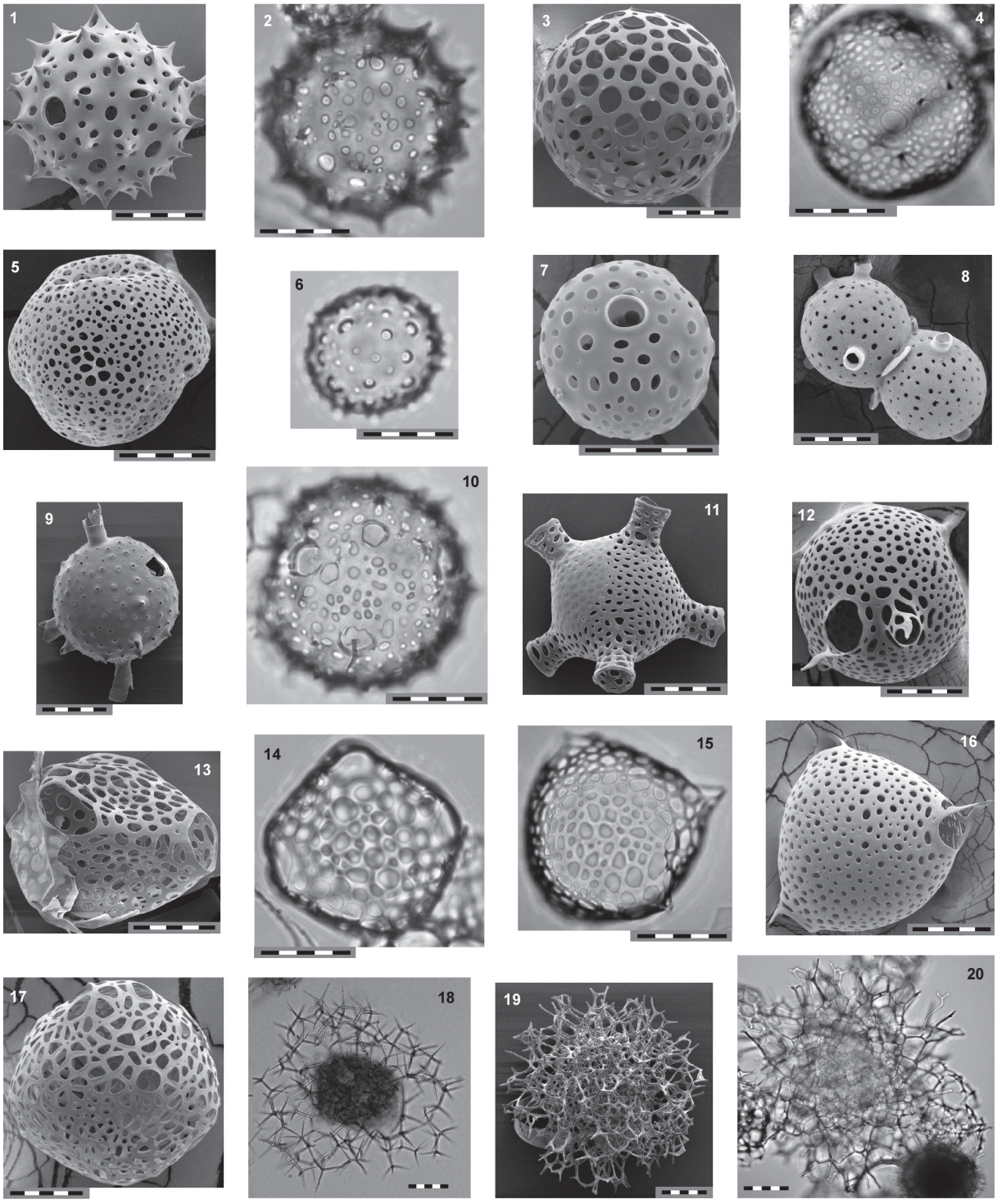

Plate 1. Spumellaria. All scale bars = 50 μm. The sample ID of each photomicrograph is represented in parenthesis. **1, 2.** *Acrosphaera spinosa,* **3.** *Collosphaera macropora,* **4, 5.** *Collosphaera tuberosa,* **6-10.** *Siphonosphaera* spp., **11. 12.** *Solenosphaera quadrata,* **13, 14.** *Solenosphaera zanquebarica,* **15-17.** *Solenosphaera* spp., **18.** *Sphaerozoum* sp., **19, 20.** *Plegmosphaera entodictyon* (figs. 1-3, 5, 6, 10-12, 14-17, 19, 20.: Sample Site M9, Multiple Core Sample (MC), 0-1 cm; figs. 4, 7, 8.: M5, MC, 0-1 cm; 9. M9,: MTD net sample (MTD), 50 m; 13. M7, MTD, 50 m; fig. 18.: M9, MTD, 0 m)

Plate 2

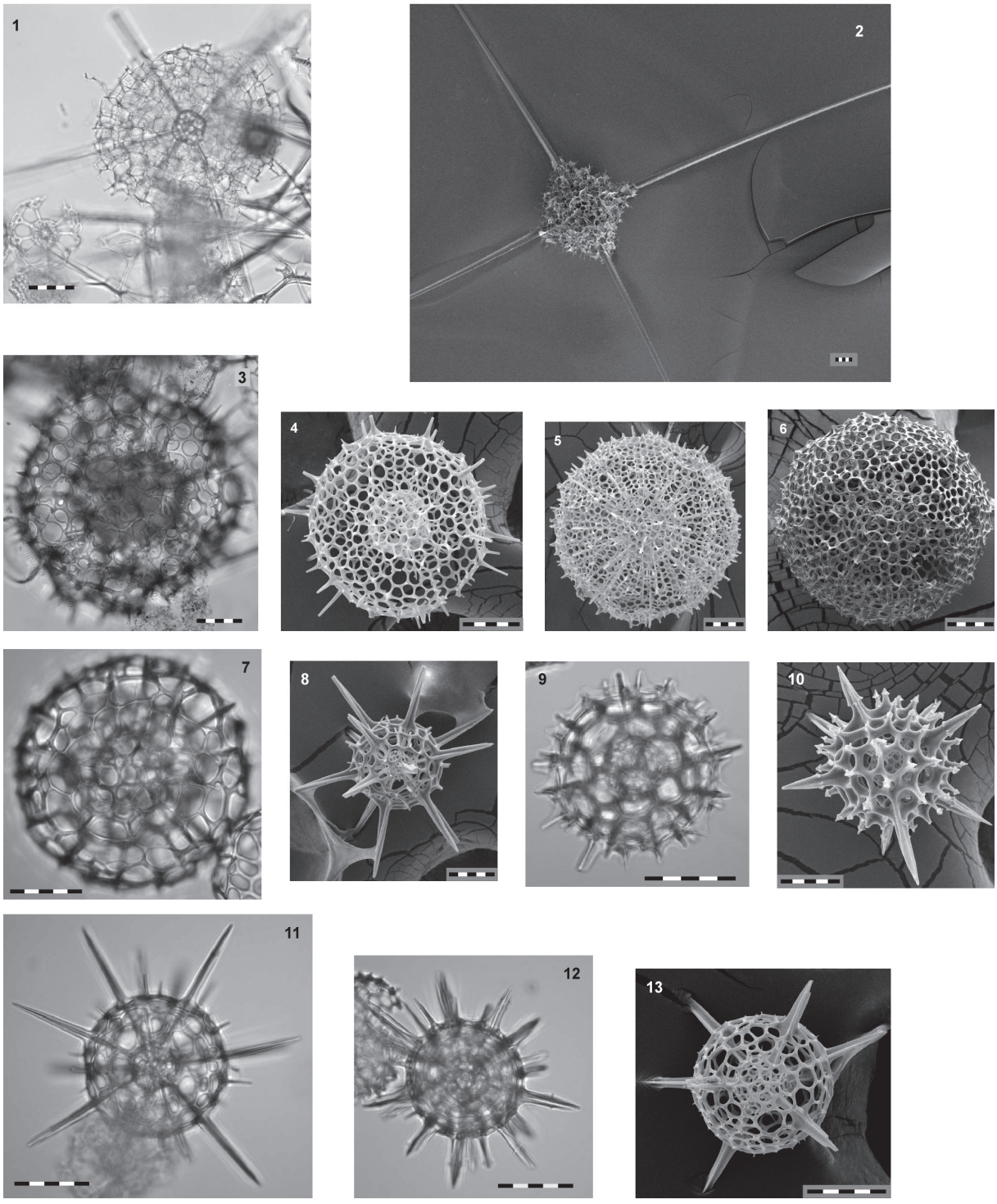

Plate 2. Spumellaria. All scale bars = 50 µm. *Spongosphaera polycantha,* **2.** *Spongosphaera streptacantha,* **3.** *Actinomma antarcticum* Group?, **4-5, 6?** *Actinomma arcadophorum,* **7-13.** *Actinomma* spp. (figs. 1, 2, 6, 7, 9, 11, 12.: M9, MC, 0-1 cm; fig.3.: M7, MC, 0-1 cm; figs. 4, 5, 8, 10, 13.: M5, MC, 0-1 cm)

Plate 3

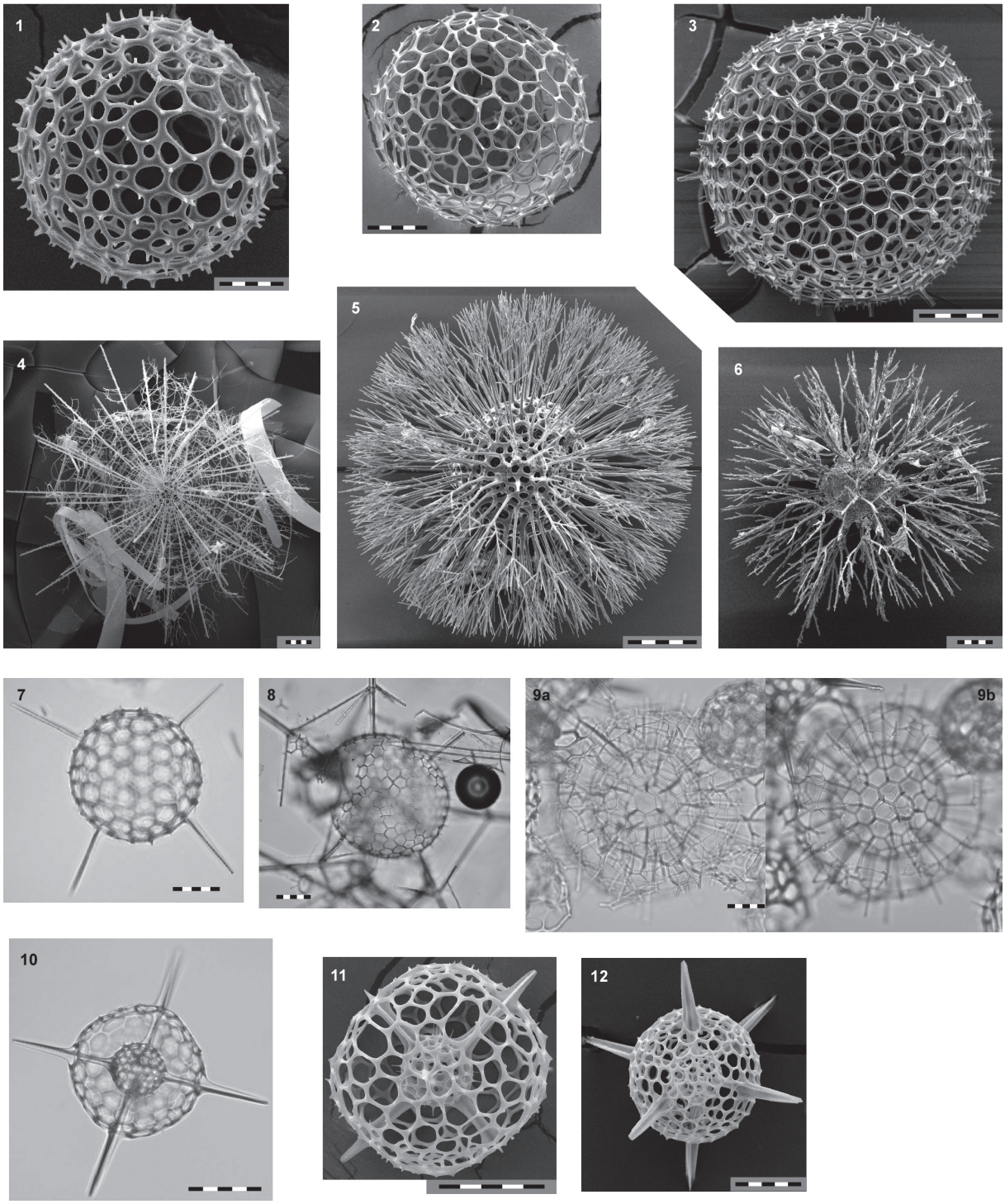

Plate 3. Spumellaria. All scale bars = 50 µm. 1. *Acanthosphaera actinota,* **2, 3.** *Actinoshapera* spp., **4.** *Arachnosphaera myriacantha,* **5.** *Cladococcus cervicornis,* **6.** *Cladococcus scoparius,* **7.** *Cladococcus viminalis,* **8.** *Astrosphaera hexagonalis,* **9.** *Drymosphaera dendrophora,* **10.** *Hexacontium hostile,* **11.** *Hexacontium melpomene,* **12.** *Hexacontium* spp. (figs. 1, 11.: M5, MC, 0-1cm; figs. 2, 7, 9, 10.: M9, MC, 0-1 cm; fig. 3.: M7, MTD, 300 m; fig. 4.: M2, NORPAC net sample (NORPAC), 0-50 m; fig. 5.: M7, MTD, 300 m; fig. 6.: M7, MTD, 50 m; fig. 8.: M7, MC, 0-1 cm).

Plate 4

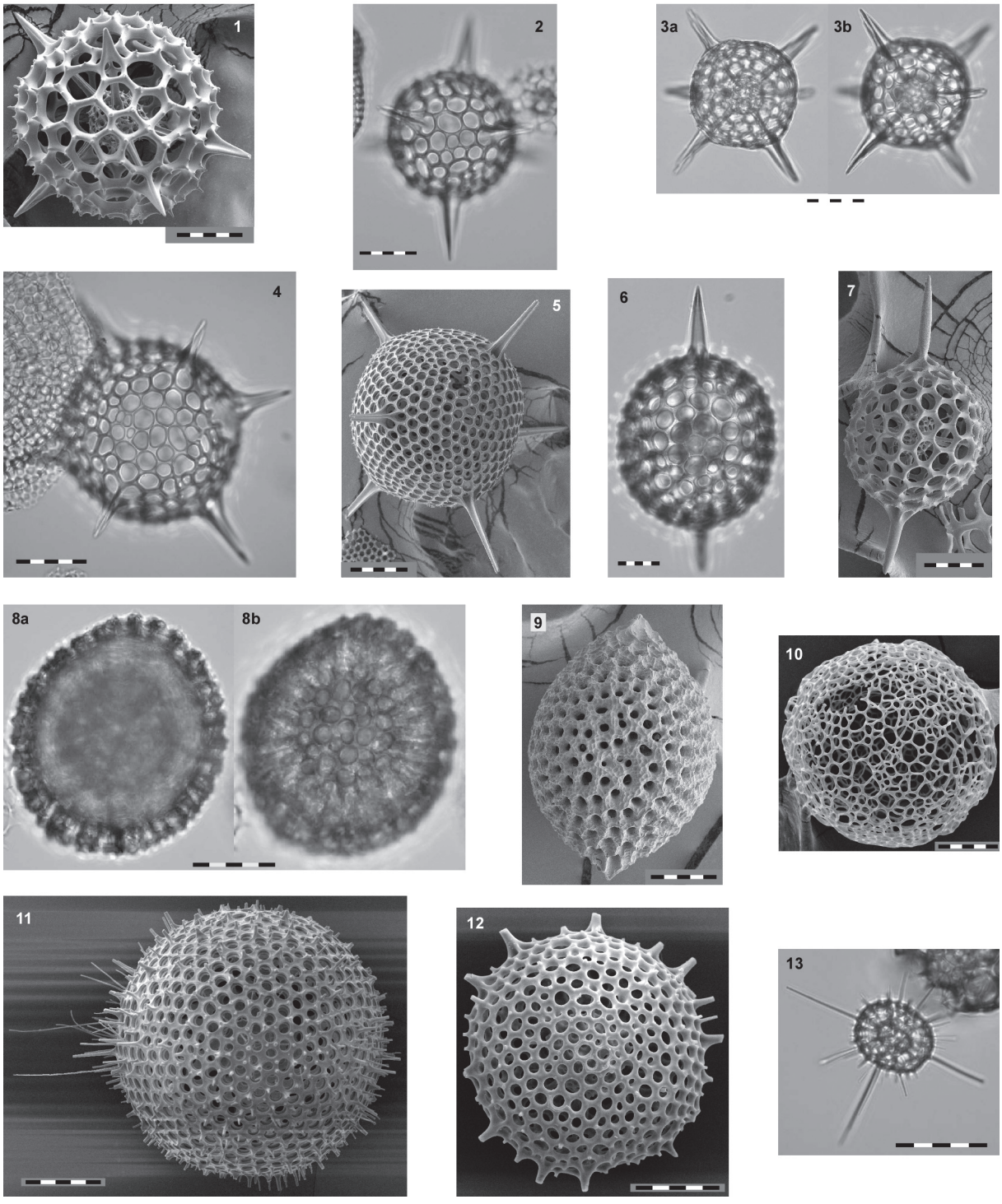

Plate 4. Spumellaria. All scale bars = 50 μm. **1-3.** *Hexacontium* spp., **4, 5.** *Hexalonche amphisiphon,* **6, 7.** *Axoprunum stauraxonium,* **8, 9.** *Druppatractus* sp., **10-13.** Actinomiidae spp.(figs. 1-9, 13.: M9, MC, 0-1 cm; fig. 10.: M5, MC, 0-1 cm; fig. 11.: M7, MTD, 300 m; fig. 12.: M9, MTD, 750 m)

Plate 5

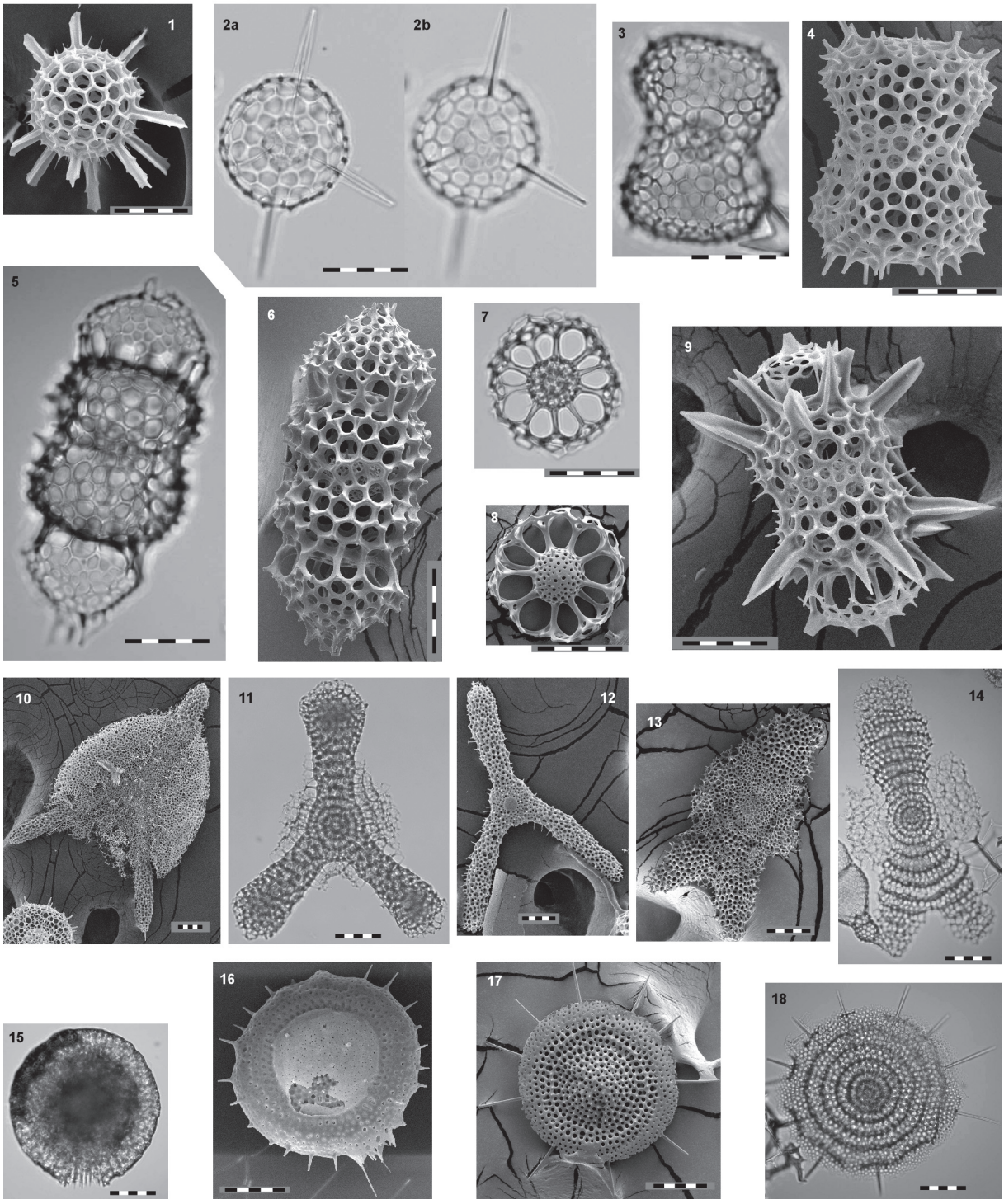

Plate 5. Spumellaria. All scale bars = 50 µm. **1, 2.** Actinomiidae spp., **3-8.** *Didymocyrtis tetrathalamus tetrathalamus,* **9.** *Didymocyrtis aff. tetrathalamus,* **10-12.** *Euchitonia elegans,* **13, 14.** *Amphirhopalum ypsilon,* **15.** *Spongopyle osculosa,* **16.** *Stylochlamydium venustum,* **17, 18.** *Stylodictya asteriscus,* (figs. 1, 4, 9, 10, 12.: M5, MC, 0-1 cm; figs. 2, 3. 5-8, 11, 13-15, 17, 18.: M9, MC, 0-1 cm; fig. 16.: M9, MTD, 750 m)

Plate 6

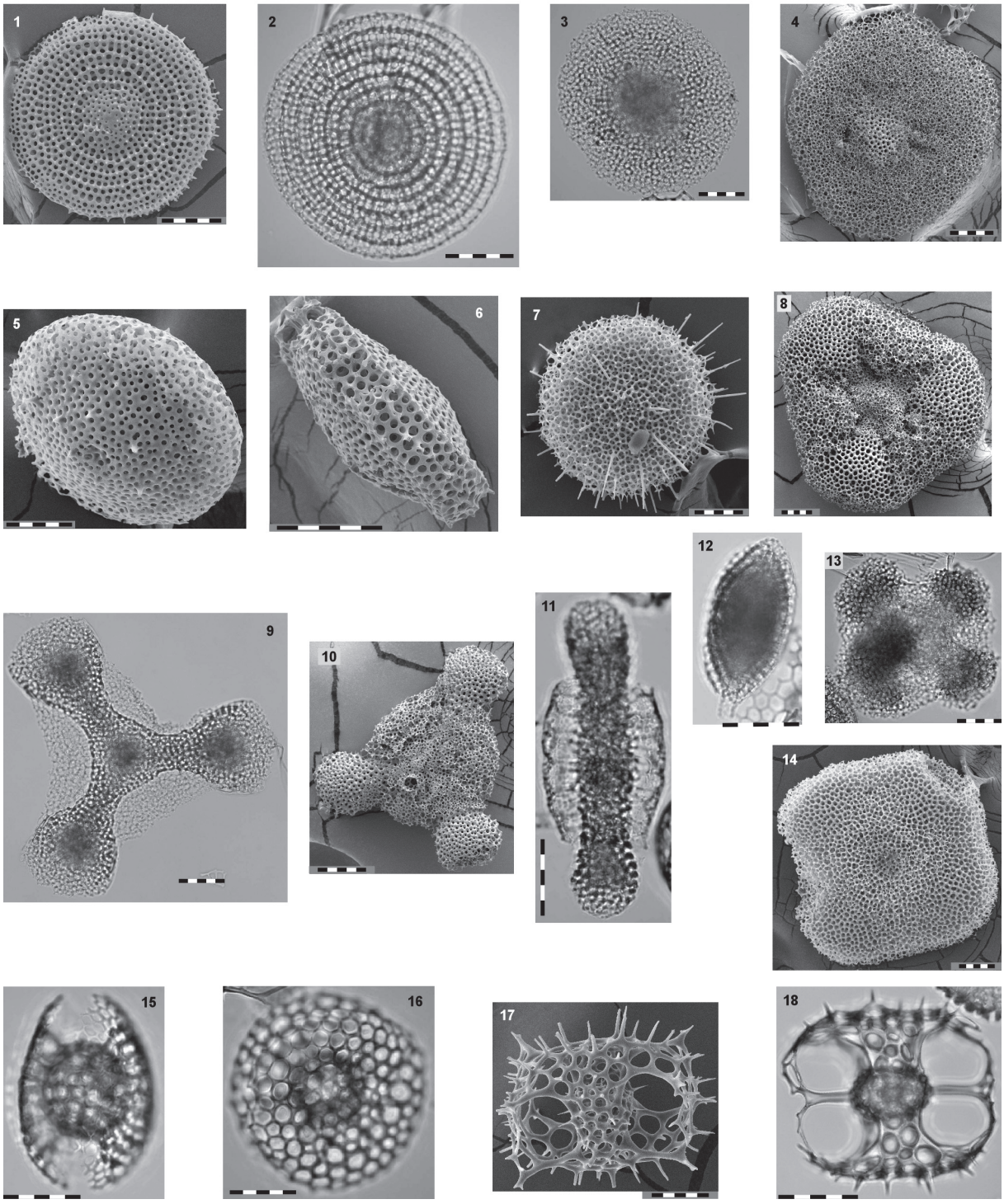

Plate 6. Spumellaria. All scale bars = 50 μm. **1, 2.** *Stylodictya validispina,* **3-7.** Spongodiscidae spp., **8-10.** *Dictyocoryne* spp., **11.** *Spongurus cylindricus,* **12.** *Spongurus spindalis,* **13, 14.** *Spongaster tetras tetras,* **15, 16.** *Heliodiscus macrococcus,* **17, 18.** *Tetrapyple octacantha* group (figs. 1, 5, 7, 14: M5, MC, 0-1 cm; figs. 2-4, 8-13, 15- 18.: M9, MC, 0-1 cm).

Plate 7

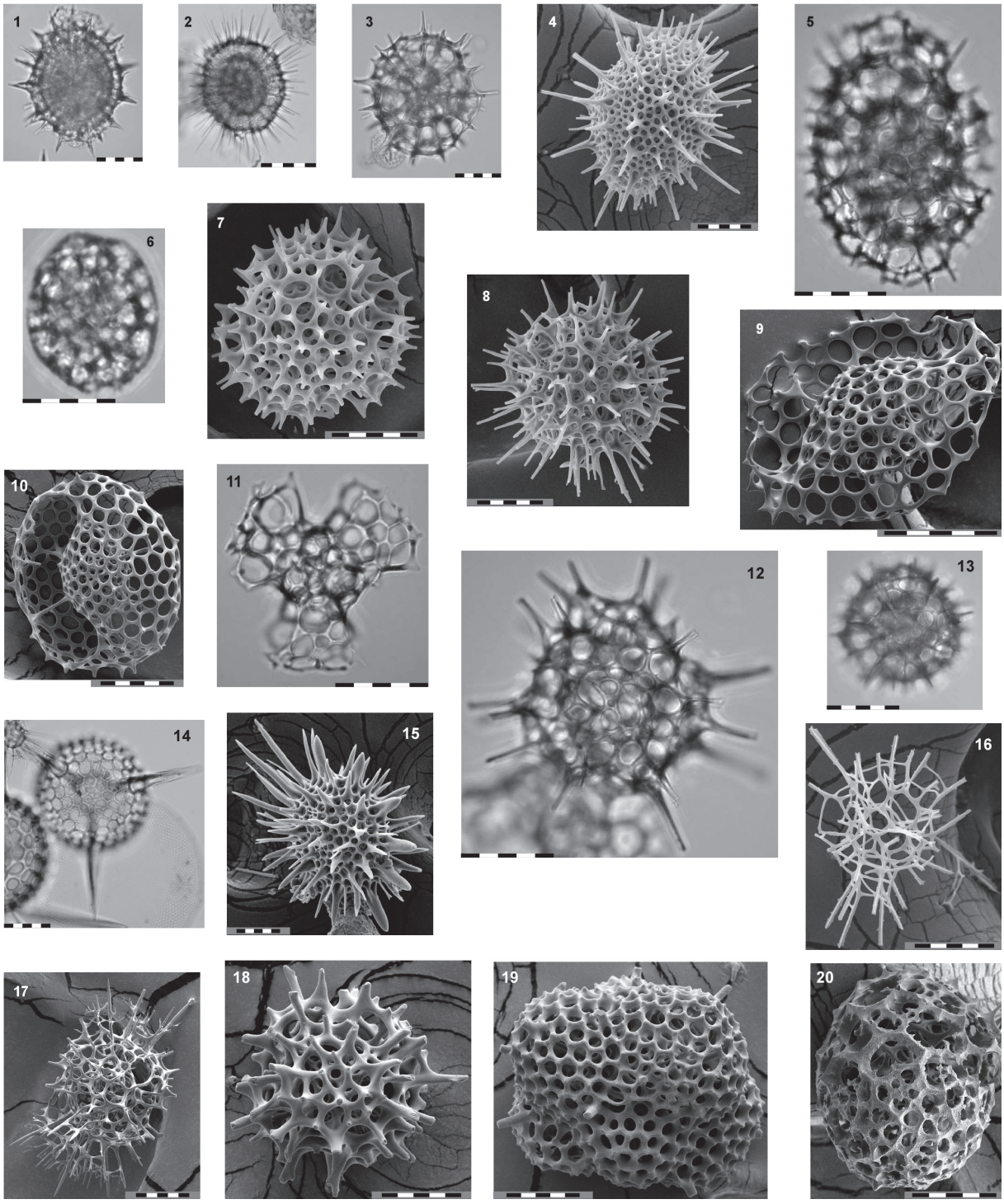

Plate 7. Spumellaria. All scale bars = 50 µm. **1, 2.** *Tholospira cervicornis* group, **3.** *Tholospira?* sp., **4-6.** *Larcopyle buetschlii,* **7, 8.** *Lithelius* spp.?, **9, 10.** *Larcospira quadrangular,* **11-20.** Spumellaria spp. (figs. 1-3, 5, 6, 9-13, 17-20.: M9, MC, 0-1 cm: figs. 4, 7, 8, 15, 16.: M5, MC, 0-1 cm; fig. 14.: M7, MC, 0-1 cm)

Plate 8

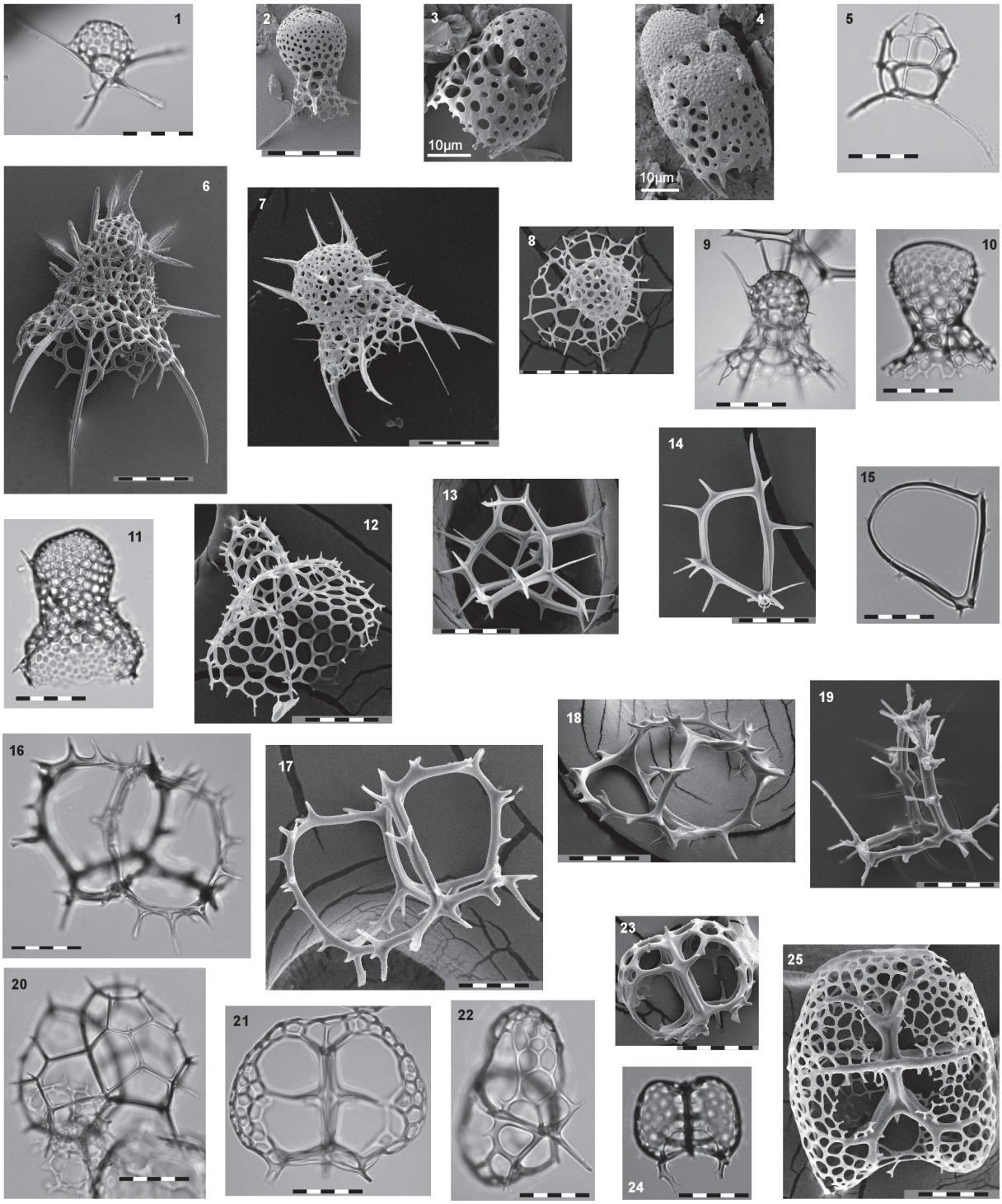

Plate 8. Nassellaria. All scale bars except for figs. 3 and 4 = 50µm. **1.** *Peridium* sp., **2.** *Peromelissa phalacra,* **3, 4.** Plagoniidae spp., **5.** *Plectacantha* sp., **6.** *Pseudodictyophimus* sp.?, **7-9.** *Arachnocorys umbellifera,* **10-12.** *Lophophaena* spp., **13.** *Pseudocubus obeliscus,* **14, 15.** *Zygocircus productus,* **16, 17.** *Acanthodesmia vinculata,* **18, 19.** *Lophospyris* spp., **20.** *Lophospyris pentagona pentagona,* **21, 22.** *Phormospyris herdisae,* **23.** *Ceratospyris borealis,* **24.** *Phormospyris stabilis scaphipes,* **25.** *Liriospyris reticulata?* (figs. 1, 5, 9-11, 18, 20-24.: M9, MC, 0-1 cm; figs. 2-4, 7, 8, 12-14, 17, 25.: M5, MC, 0-1 cm; fig. 6.: M7, MTD, 300 m; fig. 19.: M9, MTD, 50 m)

Plate 9

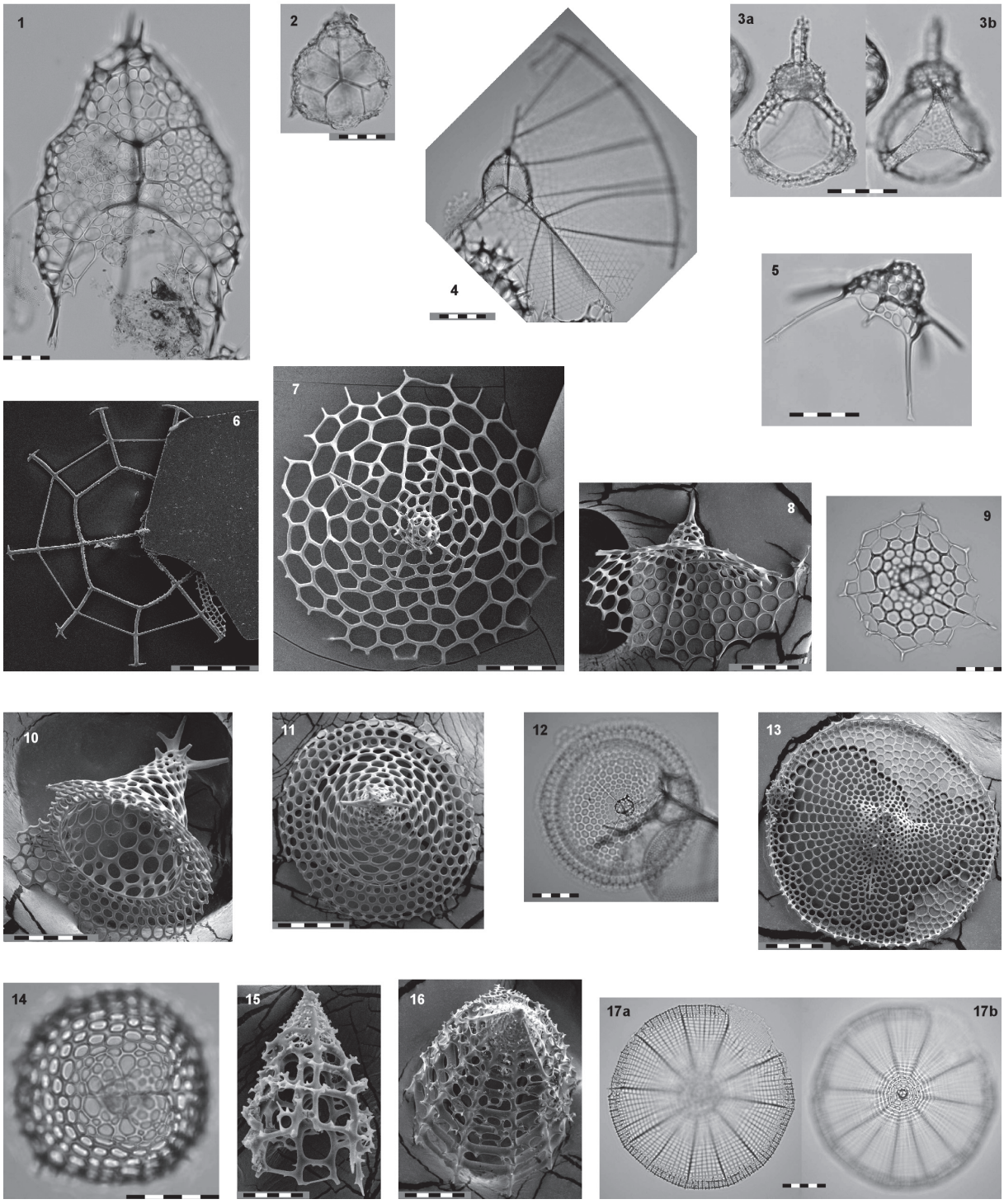

Plate 9. Nassellaria. All scale bars = 50µm. **1, 2**. *Androspyris huxley,* **3.** *Clathrocanium coarctatum,* **4.** *Callimitra* sp., **5.** *Tetraphormis rotula,* **6.** *Tetraphormis dodecaster,* **7-9.** *Lampromitra* spp., **10, 11.** *Eucecryphalus cervus,* **12.** *Eucecryphalus tricostatus* (inside view), **13, 14.** *Eucecryphalus* spp., **15, 16.** *Peripyramis circumtexta,* **17.** *Lithrachnium eupilium* (figs. 1, 2.: M7, MC, 0-1 cm; figs. 3-6, 8-10, 12-14, 16, 17.: M9, MC, 0-1 cm; fig. 7.: M7, MTD, 300 m; fig. 15.: M5, MC, 0-1 cm)

Plate 10

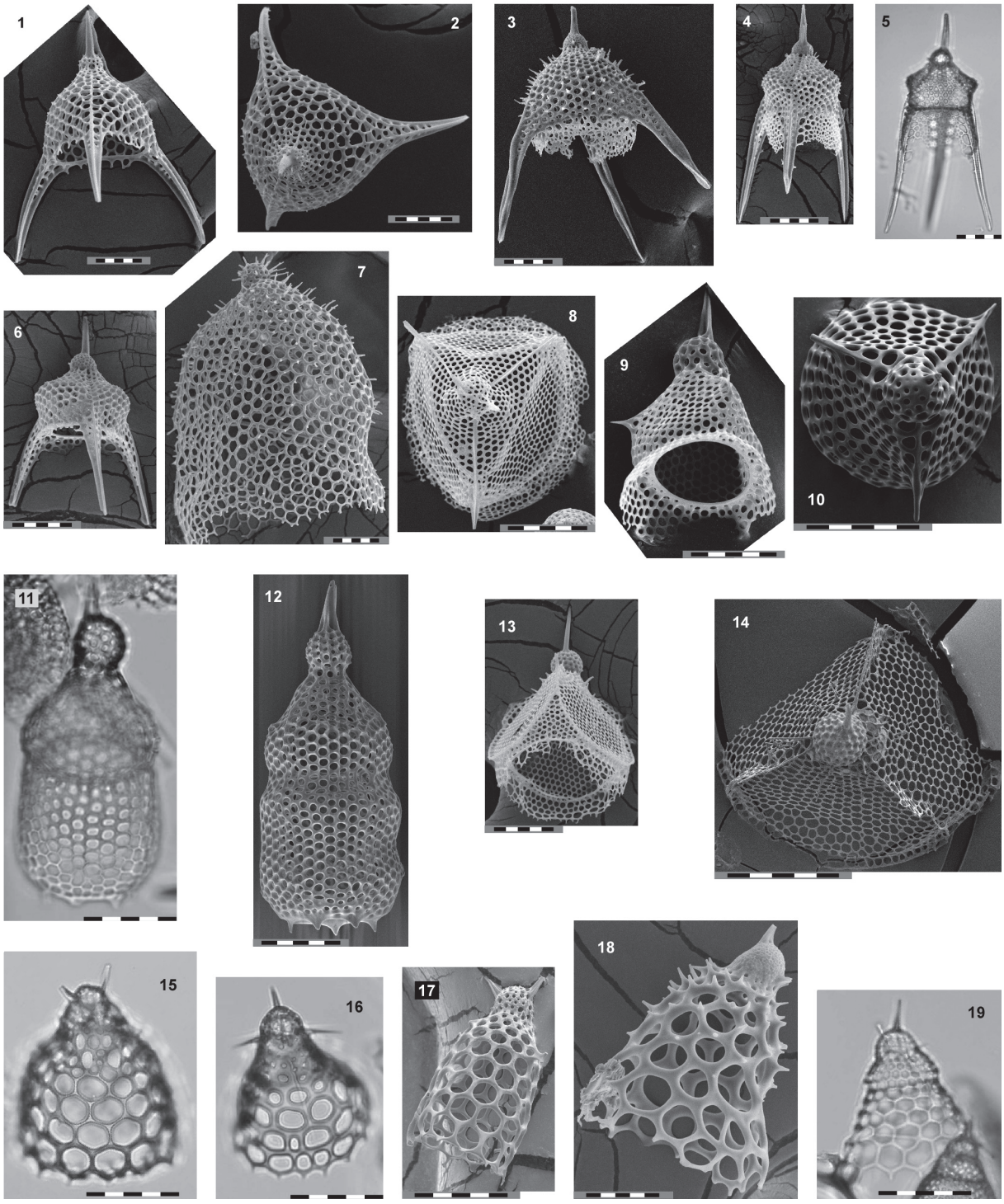

Plate 10. Nassellaria. All scale bars = 50µm. **1, 2.** *Pterocanium trilobum,* **3.** *Pterocanium praetextum eucolpum,* **4-6.** *Pterocanium praetextum praetextum,* **7.** *Conarachnium parabolicum,* **8-10.** *Stichopilium bicorne,* **11, 12.** *Theocorythium trachelium,* **13.** *Lipmanella bombus,* **14.** *Lipmanella* sp., **15.** *Cycladophora bicornis,* **16.** *Cycladophora davisiana,* **17.** *Cycladophora cornutoides,* **18.** *Pterocyrtidium dogieli,* **19.** Theoperidae sp., (figs. 1-4 , 6-9, 13, 18.: M5, MC, 0-1 cm; figs. 5, 10-12, 15-17, 19.: M9, MC, 0-1 cm; fig. 14.: M9, MTD, 50 m).

Plate 11

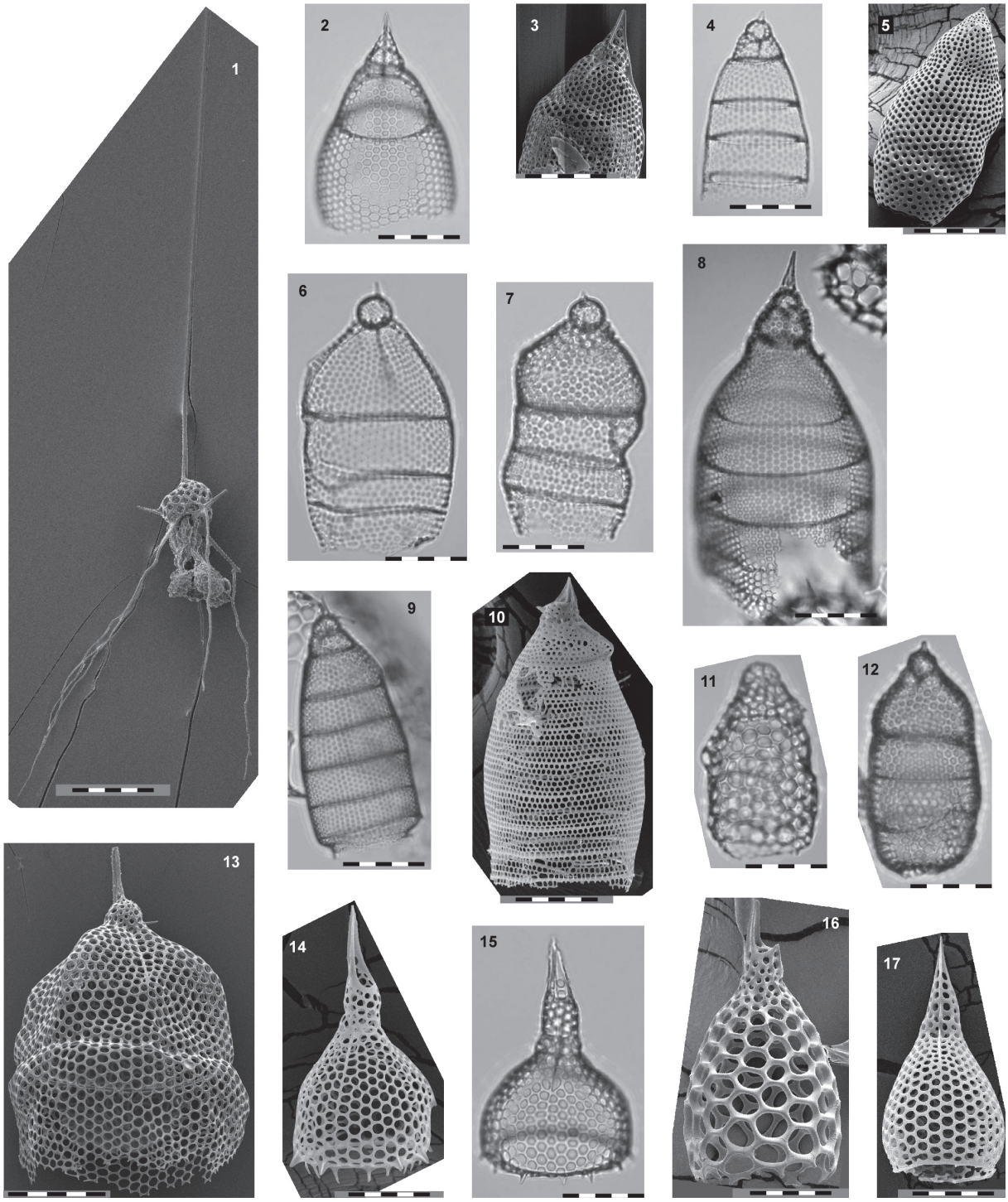

Plate 11. Nassellaria. All scale bars = 50 µm. **1.** *Tetracorethra tetracorethra,* **2, 3.** *Pterocorys zancleus,* **4, 5.** *Eucyrtidium acuminatum,* **6, 7.** *Eucyrtidium anomalum,* **8, 9.** *Eucyrtidium dictyopodium,* **10.** *Eucyrtidium hexastichum,* **11-13.** *Eucyrtidium* spp., **14, 15.** *Anthocyrtidium ophirense,* **16, 17.** *Anthocyrtidium zanguebaricum* (fig. 1.: M9, MTD, 50 m; figs. 2-9, 11, 12, 15, 16.: M9, MC, 0-1 cm; figs. 10, 14, 17.: M5, MC, 0-1cm; fig. 13.: M7, MTD, 300 m)

Plate 12

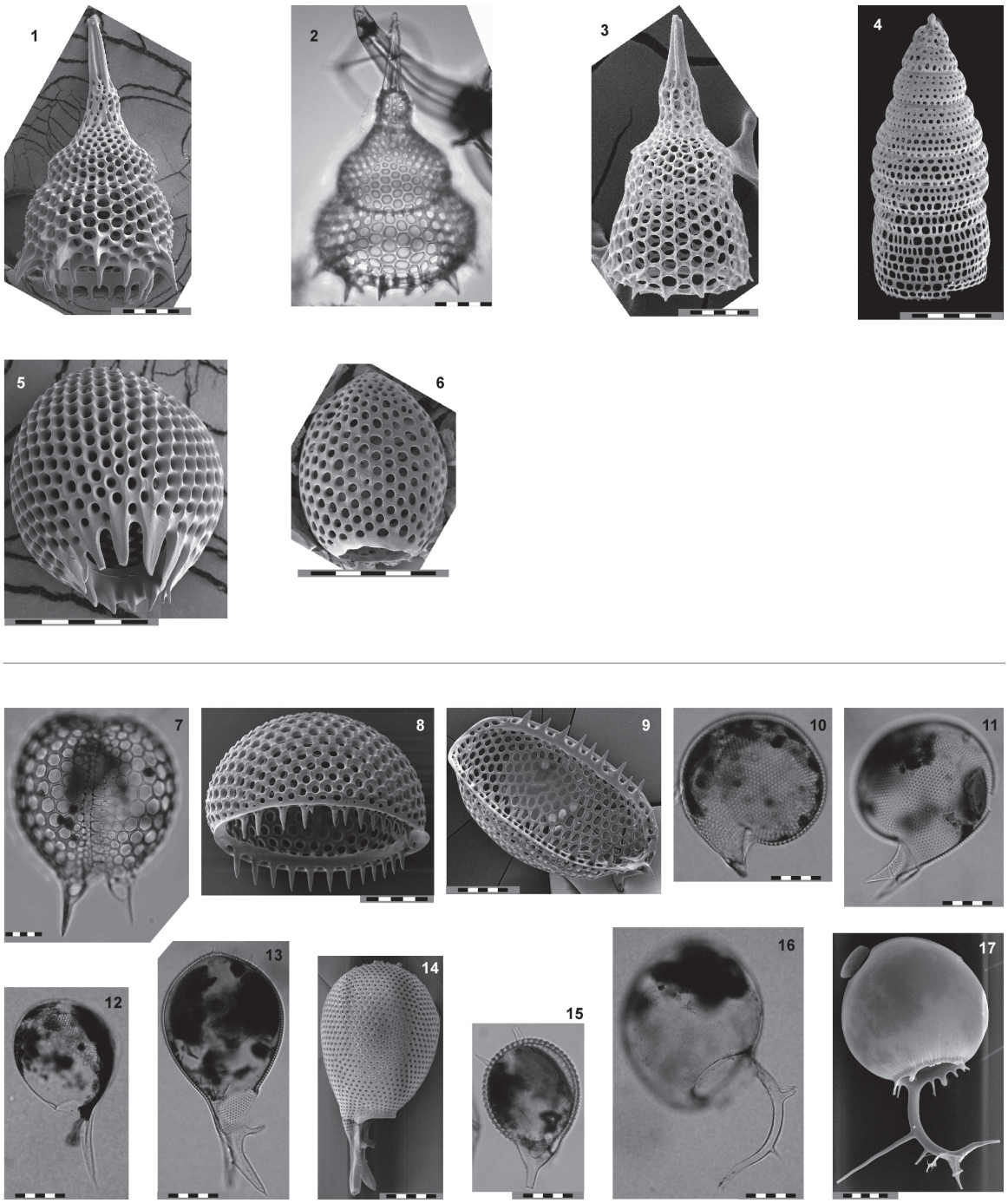

Plate 12. Nassellaria and Phaeodaria. All scale bars = 50 µm. **1-3.** *Lamprocyclas maritalis group*?, **4.** *Botryostrobus auritus/australis,* **5, 6.** *Carpocanistrum* spp., **7.** *Conchidium caudatum,* **8, 9.** *Conchellium capsula,* **10.** *Challengerosium*? sp., **11.** *Protocystis auriculata,* **12.** *Protocystis xiphodon,* **13, 14.** *Challengeron willemoesii,* **15.** *Challengellanium diodon*?, **16, 17**. *Euphycetta lucani* (figs. 1, 2, 5, 6.: M9, MC, 0-1 cm; figs. 3, 4.: M5, MC, 0-1 cm; fig. 7.: M9, MTD, 200 m; figs. 8, 9.: M7, MTD, 300m; fig. 10.: M5, MTD, 300 m; figs. 11, 15.: M5, MTD, 500 m; figs. 12, 13, 16.: M5, MTD, 200 m; fig. 14.: M7, MTD, 1000 m; fig. 17.: M9, MTD, 750 m)

Plate 13

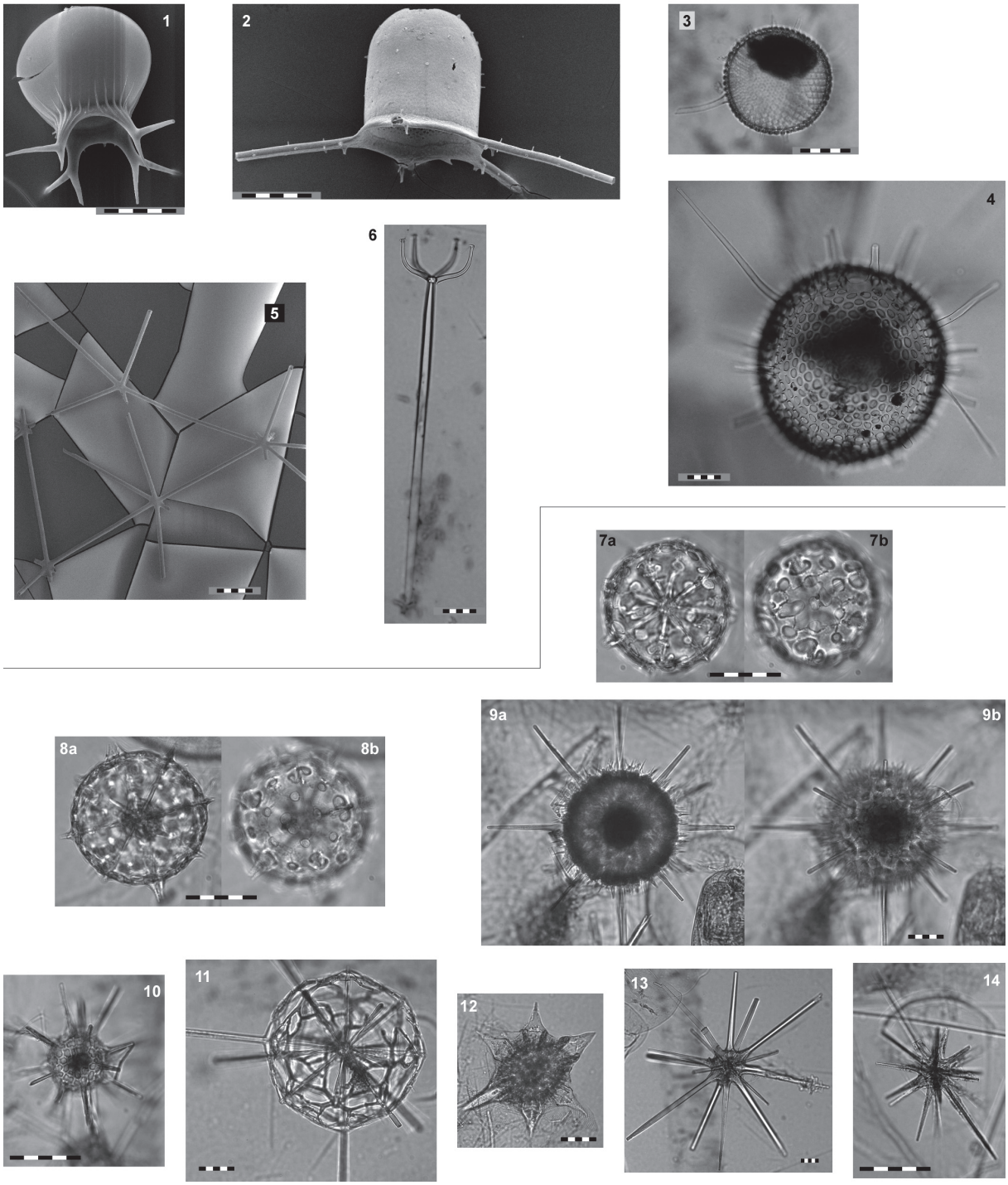

Plate 13. Phaeodaria and Acantharia. All scale bars = 50µm. **1.** *Medusetta ansata,* **2.** *Gazelletta cyrtonema,* **3.** *Porospathis*? sp., **4.** *Castanidium longispinum*?, **5.** *Aularia ternaria,* **6.** *Aulographis*? sp., **7, 8.** Acantharia sp. 1 , **9, 11-14.** Acantharia spp., **10.** Acantharia sp. 2, (fig. 1.: M2, NORPAC, 0-50 m; fig. 2.: M7, MTD, 50 m; fig. 3.: M7, MTD, 750 m; fig. 4.: M7, MTD, 100 m; fig. 5.: M7, MTD, 300 m; fig. 6.: M9, MTD, 750 m; figs. 7-14.: M5, MTD, 0 m)

Mem. Fac. Sci., Kyushu Univ., Ser. D, Earth & Planet. Sci., Vol. XXXII, No. 3,
pp. 63-73, March 10, 2011

Identification of full-substorm onset from ground-magnetometer data by singular value transformation

Terumasa Tokunaga*, Kiyohumi Yumoto**, Teiji Uozumi** and CPMN Group

Abstract

Pi 2 magnetic pulsations observed on the ground are a good indicator of the auroral breakup. However, they have not only corresponding full-substorm onsets but also most pseudobreakups. Another well-known substorm related phenomenon observed on the ground is positive bays. In order to identify full-substorm onsets from ground-magnetometer data, we developed a new algorithm based on "Singular Spectrum Analysis (SSA)". The algorithm enables us to screen Pi 2 pulsations accompanied by the magnetic positive bay. We applied proposed algorithm to ground-magnetometer data and compared to the obtained results with Polar/UVI data. As a result, we succeeded in identifying 62% of the full-substorm onsets from ground-magnetometer data obtained in the nighttime sector between 21 and 03LT.

Keywords: auroral substorm, Pi 2 pulsation, positive bay, Singular Value Transformation

1. Introduction

Pi 2 magnetic pulsations are defined as impulsive hydromagnetic oscillations with a period of 40-150s. It is well-known that Pi 2 pulsations has one-to-one correspondence with auroral breakups (Jacobs et al., 1964; Saito, 1969; Yumoto and CPMN Group, 2001). The excitation of the Pi 2 wave is closely related to the substorm trigger (Saito, 1976) and therefore Pi 2 onsets are often used for identifying substorm onsets. Although Pi 2 pulsations have been accepted as a good indicator of auroral breakups, they correspond to not only full-substorm onsets but also most pseudobreakups (Rostoker et al., 1980). Hsu and McPherron (2007) examined statistical properties of Pi 2 pulsations. They reported that the most probable number of Pi 2 bursts per substorm is 2. Pseudobreakups are characterized by short lifetimes, extreme locations, and weak magnetic perturbations on the ground (McPherron, 1991). In the previous substorm researches, geophysical differences between pseudobreakups and full substorms have been studied (Ohtani et al., 1993; Nakamura et al., 1994; Ohtani et al., 2002; Partamies et al., 2003). However, the physical difference in the magnetosphere and on the ground has not been clarified yet. In other words, to figure out the physical difference is a key subject for understanding the substorm onset mechanism. From this viewpoint, it is important to detect Pi 2 pulsations that correspond to full-substorm onset.

In 1990s, some studies have been made on the automatic detection of ground-observed Pi 2 pulsations. Takahashi et al. (1995) utilized wave power in the Pi 2 frequency band, which is calculated by applying the discrete Fourier transform, for selecting Pi 2 pulsations. An wavelet analysis has also been used to detect Pi 2 pulsations (Nose et al., 1998; Murphy et al., 2009). Recently, Hilbert-Huang Transformation used as ULF (Ultra Low Frequency) wave diagnosis of substorm expansion phase onset (Kataoka et al., 2009). Furthermore, the pattern recognition capabilities of artificial neural networks (ANN) have been used to identify Pi 2 pulsations (Sutcliffe, 2007). However, these methods cannot determine whether the Pi 2 pulsation corresponds to full-substorm onsets or to psedobreakups.

Another well-known substorm related phenomenon measured on the ground is positive bays. At the onset of

Manuscript received on 15 December 2010; accepted on 13 January 2011
* Department of Earth & Planetary Sciences, Graduate School of Sciences, Kyushu University, 6-10-1 Hakozaki, Higashi-ku, Fukuoka 812-8581, JAPAN; Corresponding author's e-mal: tokunaga@geo.kyushu-u.ac.jp
** Space Environment Research Center, Kyushu University, 6-10-1 Hakozaki, Higashi-ku, Fukuoka 812-8581, JAPAN

the substorm expansion phase, the crosstail current is diverted down the magnetic filed lines. The current then flows in the ionosphere as the westward electrojet and returns to the tail along the magnetic field line. The perturbation of tail current can be represented by an equivalent eastward current, which completes the three-dimensional current wedge. The mid-latitude and low-latitude signature of this wedge is a positive perturbation in the north-south component (McPherron et al., 1973a; Clauer and McPherron, 1974). The positive perturbation is called substorm positive bay (Akasofu and Meng, 1969; Meng and Akasofu, 1969). It is widely accepted that the sudden formation of the current wedge is essential to complete substorm onset. Hence, positive bays at mid and low latitudes could be an evidence for the occurrence of full substorms. From these arguments, we can say that Pi 2 pulsations accompanied by positive bays are one of the most reliable indicators of full-substorm onsets.

In order to identify full-substorm onsets from ground-magnetometer data, we propose a new algorithm to screen Pi 2 pulsations that accompanied by positive bays. As mentioned earlier, there are some works about automatic detections of Pi 2 pulsations. However, these methods are limited only to detecting wave packets. To screen Pi 2 pulsations that accompanied by positive bays, we should detect wave packets and changes of slopes simultaneously in ground-magnetometer data. Recently, singular spectrum analysis (SSA) has been used for change-point detections in time series (Moskvina and Zhigljavsky, 2003). Ide and Inoue (2005) developed the SSA-based change-point detection method, named singular spectrum transformations (SST), and showed that it was useful in knowledge discovery of causal relationships from a set of heterogeneous time series. Recently, the SST has been applied to determine the onset of positive bays (Tokunaga et al., 2010a, b). Unlike other conventional approaches, the SSA is data adaptive and does not employ any specific generative models. Further, SSA can extract simultaneously complex trends and periodic components. Hence, SSA-based change-point detection method likely fills our purpose, that is, to detect wave packets and changes of slopes simultaneously. In this paper, we introduce a new SSA-based change-point detection method, named Singular Value Transformation (SVT), to screen Pi 2 pulsations that accompanied by positive bays.

The outline of the rest of the paper is as follows. In Section 2, we describe the basic concept of SSA. Further, we introduce "bay-score" that provides information to determine whether the Pi 2 pulsation accompanied by the positive bay is present or not. Then, we define the framework of SVT. In Section 3, we apply our algorithm to the ground-magnetometer data and compare the result with auroral images obtained by Polar Ultra Violet Imager (Polar/UVI). Furthermore, we evaluated the practical performance of the algorithm in a statistical study.

2. Singular Value Transformation

In this section, we introduce the new method, named SVT, to detect substorm positive bays from ground-magnetometer data. The SVT can be regard as an applied technique of SSA. Thus, we first describe the basic concept of SSA.

2. 1. Pattern Extraction by SSA

First of all, let us consider a transformation of a sequence time series $Y = \{y_1, y_2, ..., y_K, ..., y_N\}$ into the multi-dimensional series $\mathbf{X} = [X_1, X_2, \ldots, X_K]$, where the X_i denotes a subsequence that can be described as $X_i = (y_i, \ldots, y_{i+K-1})$ $(1 \le i \le L)$. Vectors X_i's and the matrix $\mathbf{X}$ are called L-lagged vectors and an L-trajectory matrix, respectively. Note that an L-trajectory matrix $\mathbf{X}$ is an $L \times K$ Hankel matrix described as

$$\mathbf{X} = \begin{pmatrix} y_1 & y_2 & \cdots & y_K \\ y_2 & y_3 & \cdots & y_{K+1} \\ \vdots & \ddots & \vdots & \vdots \\ y_L & y_{L+1} & \cdots & y_N \end{pmatrix} \quad \cdots\cdots(1)$$

We call K and L a window width and an embedding dimension, respectively.

The second step of the SSA is the SVD of the Hankel matrix $\boldsymbol{X}$. Let us denote $(\lambda_1, \lambda_2, \ldots, \lambda_L)$ as squared singular values of $\mathbf{XX^T}$ in decreasing order of the magnitude $(\lambda_1 \ge \lambda_2 \ge \cdots \ge \lambda_L)$. Now the SVD of the Hankel matrix $\boldsymbol{X}$ can be described as $\mathbf{X}$=$\mathbf{ULV^T}$, where $\mathbf{\Lambda}$ denotes a diagonal matrix whose diagonal element equal to the squared singular values, $\mathbf{U}$ denotes a left singular matrix and $\mathbf{V}$ denotes a right singular matrix. Superscript T denotes the transpose of a matrix. Then, the Hankel matrix $\mathbf{X}$ can be described as a sum of rank-one bi-orthogonal

elementary matrices $\mathbf{X} = \mathbf{X}_1 + \mathbf{X}_2 + \cdots + \mathbf{X}_L$. The *i*th elementary matrix can be described by using the *i*th left singular vector and the *i*th right singular vector as $\mathbf{X}_i = \lambda_i U_i V_i^T (i = 1, \ldots, L)$. A set of these three notations consists of singular value λ_i, empirical orthogonal functions U_i and principal components V_i. Note that L corresponds to the number of singular vectors.

Now let us define *representative patterns* using empirical orthogonal functions U_i $(1 \le i \le L)$. As described above, the method to extract dominant structures in time series via the SVD on the Hankel matrix is referred to as the SSA.

2. 2. Preliminary procedure for SVT

Let us consider to create a $L \times K$ Hankel matrix $\hat{\mathbf{X}}$ according to the procedure shown in Figure 1.

$$\hat{\mathbf{X}} = \begin{pmatrix} y_1 & y_2 & \cdots & y_K \\ y_\tau & y_{\tau+1} & \cdots & y_{\tau+K} \\ \vdots & \ddots & \vdots & \vdots \\ y_{(L-1)\tau+1} & y_{(L-1)\tau+2} & \cdots & y_{(L-1)\tau+K} \end{pmatrix} \quad \cdots\cdots(2)$$

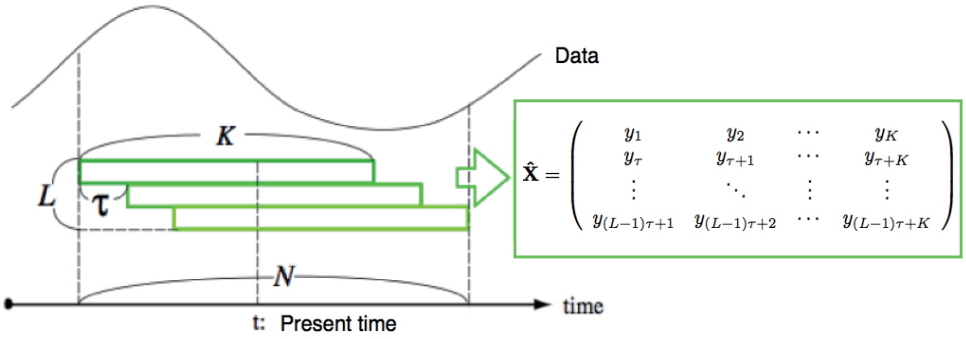

Fig. 1. Schematic illustration of the preliminary procedure for SVT.

Here, we call K and L a window width and an embedding dimension. τ represents a shift length. Next, we consider a SVD of the matrix $\hat{\mathbf{X}}$. Let us denote $(\hat{\lambda_1}, \hat{\lambda_2}, \ldots, \hat{\lambda_L})$ as squared singular values of $\hat{\mathbf{X}}\hat{\mathbf{X}}^T$ in decreasing order of the magnitude $(\hat{\lambda_1} \ge \hat{\lambda_2} \ge \cdots \ge \hat{\lambda_L})$, where the subscript T denotes transpose of a matrix. Now the SVD of the Hankel matrix $\hat{\mathbf{X}}$ can be described as $\hat{\mathbf{X}} = \hat{\mathbf{U}}\hat{\mathbf{\Lambda}}\hat{\mathbf{V}}^T$, where $\hat{\mathbf{\Lambda}}$ denotes a diagonal matrix whose diagonal element equal to the squared singular values, $\hat{\mathbf{U}}$ denotes a left singular matrix and $\hat{\mathbf{V}}$ denotes a right singular matrix. For simplicity, now we assume that $\hat{\mathbf{\Lambda}}$ is a square matrix, that is, K=L. Then, $\hat{\mathbf{\Lambda}}$ can be described as

$$\hat{\mathbf{\Lambda}} = \begin{pmatrix} \hat{\lambda_1} & 0 & \cdots & 0 \\ 0 & \hat{\lambda_2} & \cdots & 0 \\ \vdots & \ddots & \vdots & \vdots \\ 0 & 0 & \cdots & \hat{\lambda_L} \end{pmatrix}. \quad \cdots\cdots(3)$$

Now let the *i*th column vector of matrix $\hat{\mathbf{U}}$ and the *i*th row vector of matrix $\hat{\mathbf{V}}$ be $\hat{U_i}$ and $\hat{V_i}$, respectively. $\hat{U_i}$ and $\hat{V_i}$ called empirical orthogonal functions and principal components, respectively. The magnitude of $\hat{\lambda_i}$ correspond to powers of empirical orthogonal functions and principal components.

Next, we focus attention on the time variation of $\hat{\lambda}_i$. In Figure 2, we show the test data, which we created based on a mid- and low-latitude magnetic variation around a substorm onset. Figure 3a shows the time variation of $\hat{\lambda}_i$ $(i = 1, \cdots, 20)$. Figure 3b shows $\hat{\lambda}_i$ $(i = 1, \cdots, 20)$ at *t=250*s and Figure 3c shows $\hat{\lambda}_i$ $(i = 1, \cdots, 20)$ at *t=1400*s.

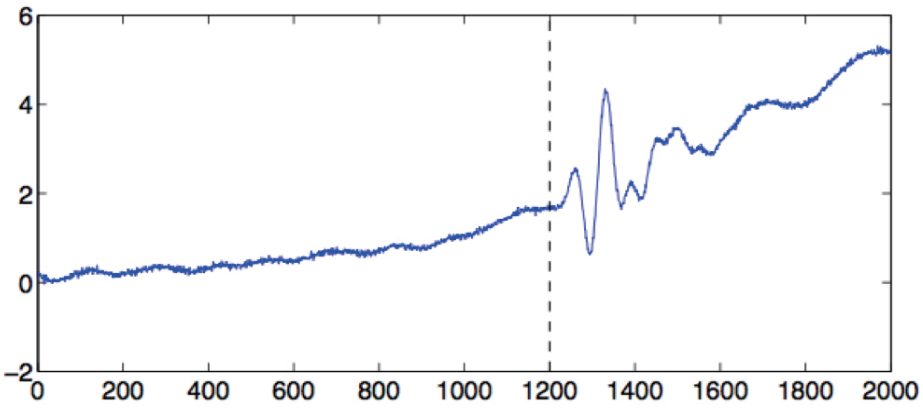

Fig. 2. Test data, which we created based on a mid- and low-latitude magnetic variation around a substorm onset. The vertical dashed line at t=1200s represents the start time of extraordinary oscillations.

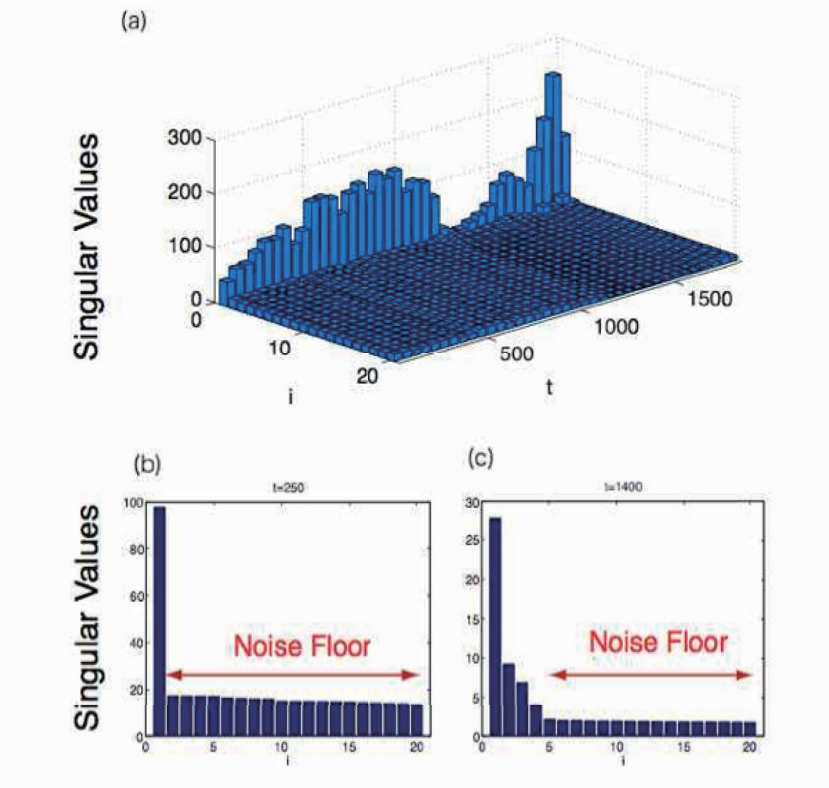

Fig. 3. (a) A time variation of singular values for the test data shown in Fig. 2 calculated with the procedure described in Section 2.2. Hankel matrices were created with *K*=80, *L*=80, *M*=20, τ=30. (b) Singular values at t=250s. (c) Singular values at t=1400s.

As shown in Figure 3b, we see that the first eigenvalue $\hat{\lambda}_1$ is extraordinary large. In contrast, $\hat{\lambda}_i$ $(i = 2, \cdots, 20)$ are almost the same. So it is likely that empirical orthogonal functions $\hat{U}_i$ $(i = 2, \cdots, 20)$ or principal components $\hat{V}_i$ $(i = 2, \cdots, 20)$ represent noise. Also, this indicates that the essential structure of the test data around *t=250*s can be represented by the first empirical orthogonal functions or the first principal component.

Next, let us focus on Figure 3c which shows $\hat{\lambda}_i$ $(i = 1, \cdots, 20)$ at *t=1400*s. At this time, the extraordinary oscillation has already begun. We see that the magnitudes of singular values decrease from *i=1* to *i=4*. However, $\hat{\lambda}_i$ $(i = 5, \cdots, 20)$ are the almost same. So it is likely that empirical orthogonal functions $\hat{U}_i$ $(i = 5, \cdots, 20)$ or principal components $\hat{V}_i$ $(i = 5, \cdots, 20)$ represent noise. This indicates that the essential structure of the test data around *t=1400*s can be represented by a linear combination of first to fourth empirical orthogonal functions $\hat{U}_i$ $(i = 1, \cdots, 4)$ or of first to fourth principal components V_i $(i = 1, \cdots, 4)$. From what we have seen, it is clear that the distribution of singular values obtained by SVD of the Hankel matrix reflects the complexity of the subsequence.

2. 3. Bay-score

We introduce a relative anomaly metric of time series at the present time, named *"bay-score"*. It provides information to determine whether the Pi 2 pulsation that accompanied by the positive bay is present or not. As we discussed in Section 2.2, the distribution of singular values calculated by SVD of the Hankel matrix reflects the complexity of the subsequence. The top panel of Figure 4 shows H-component of ground-magnetometer data obtained at KAG. The second panel of Figure 4 shows the time variations of the largest singular value calculated by the procedure described in Section 2.2. Similarly, the third panel and the fourth panel of Figure 4 shows the time variations of the second-largest singular value and that of the third-largest singular value, respectively. The vertical dashed lines in red show Pi 2 pulsations accompanied by positive bays selected by visual inspection. We see that singular values around substorm positive bays decreased. By taking account into the feature, we define the bay-score *Z*(t) as

$$Z = \frac{1}{\left(\sum_{i=1}^{M} \frac{\hat{\lambda}_i}{\|\hat{\lambda}_i\|}\right)^3}. \quad \cdots\cdot(4)$$

Here, *M* is the number of singular values to be included for the bay-score. The selection of *M* affects the sensibility of the SVT. $\|\cdot\|$ is the usual Euclidean norm. $\hat{\lambda}_i$ is the *i*th-largest singular value. Note that *Z(t)* is non-dimensional parameter and positive value by definition. The calculation of the bay-score can be viewed also as a nonlinear transformation from an original time-series $\mathcal{T}$ to a new time-series $\mathcal{T}_v$, i.e.

$$\mathcal{T} \rightarrow \mathcal{T}_v(K, L, M, \tau). \quad \cdots\cdot(5)$$

We call this transformation *"Singular Value Transformation (SVT)"*. The algorithm detects Pi 2 pulsations that accompanied by positive bays, if the bay-score *Z(t)* be larger than a predetermined threshold value.

2.4. Choice of parameters

As shown in Eq. 5, the SVT algorithm includes four parameters, namely, *K, L, M* and $\mathcal{T}$. By nature of SVT, these parameters needed to be determined experimentally. In change-point detection methods based on SSA, the choice of *K* depends on the kind of structural changes to be detected (Moskvina and Zhigljavsky, 2003). A general rule is to choose *K* reasonably large. However, if we allow small gradual changes in the time series then we could not take *K* very large. The feature is most likely valid in the SVT. Since the onset of Pi 2 pulsations is gradual, we should not take *K* as a large value. In this paper, we set to *K=80*s, which is the typical period of Pi 2 pulsations. Remaining parameters, *K*=80, *L*=80, *M*=20, τ=30 were determined empirically. In the following application, these parameters were set to *L*=*K*, *M*=20, τ=30s.

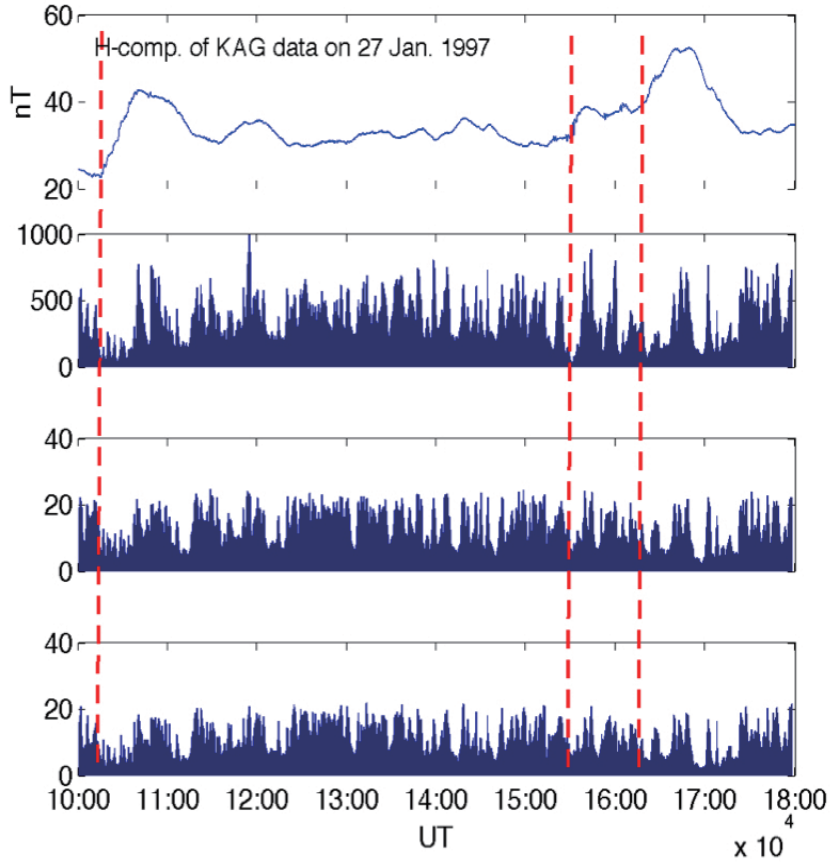

Fig. 4. (Top panel) H-component of ground-magnetometer data obtained at KAG station on 10:00-18:00UT 27 January 1997. The vertical dashed lines in red show the onset of positive bays determined by visual inspection. (Second panel) The largest singular values calculated with K=80, L=80, M=20, τ=30 for the ground-magnetometer data that shown in the top panel. (Third panel) The second-largest singular values. (Fourth panel) The third-largest singular values.

3. Application to Ground-magnetometer Data

3. 1. Data Sets

3. 1. 1. Ground-magnetometer data

Ground magnetometer data obtained from the CPMN (Circum-pan Pacific Magnetometer Network) stations in the 210° magnetic meridian (MM) chain (Yumoto and CPMN Group, 2001) have been used in the following applications. CPMN consists of about 50 stations. In this study, the data obtained at KAG were used for the analysis. The locations of these stations are listed in Table 1. The observations were based on vector measurements by fluxgate magnetometers with a sampling rate of 1Hz.

Table 1. Locations of geomagnetic observatories used in this paper.

Station	Geographic Latitude	Geographic Longitude
KAG	31.48	130.72

3. 1. 2. Polar Ultra Violet Imager

In this study, Polar Satellite Ultra Violet Imager (Polar/UVI) to check the global auroral activities. The Polar satellite is in a highly elliptical polar orbit with an apogee at about $9R_E$, and it collects data from a high-altitude perspective on auroral activities. In this paper, we referenced the specification of Polar/UVI is described in Liou et al. (1999). UVI is a narrow-angle larger-aperture design. In Figure 5a, we present a sequence of nightside UV auroral images from Polar/UVI. The images were obtained by a combination of Lyman-Birge-Hopfield bands (1400-1600 $\overset{0}{A}$) on 4 January 1997. We see that the auroral intensity started to enhance exponentially between 15:45:08UT and 15:46:22UT.

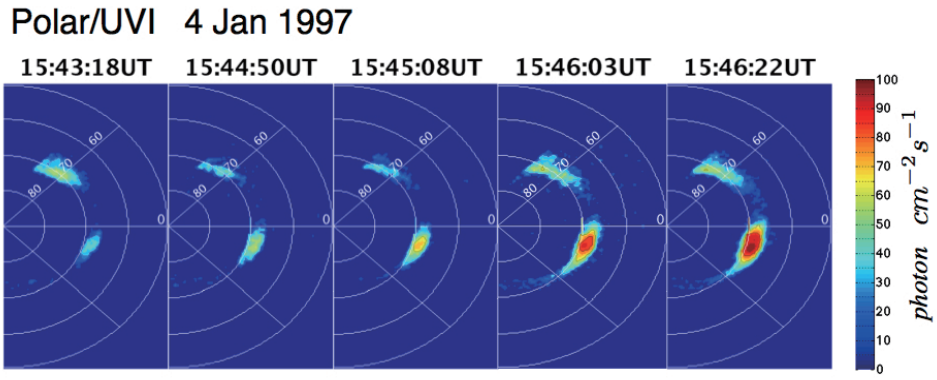

Fig. 5. Polar/UVI images at N2 Lyman-Birge-Hopfield bands (1400-1600 $\overset{0}{A}$) on 4 January 1997.

3. 2. Case Studies

In two case studies, we evaluate the performance of the SVT. The top panel of Figure 6 shows the keogram of auroral brightening observed by Polar/UVI in the Southern Hemisphere on 8 January 1997. The luminescence intensity averaged over magnetic local time of 21-03 h. The vertical axis shows magnetic latitude. The vertical dashed line in red shows full-substorm onsets visually identified by checking the keogram. Here, we define the full-substorm onset as the auroral breakup that is followed by rapid poleward motion of the brightened arc. The middle panel of Figure 6 shows H-component of ground-magnetometer data obtained at KAG station on 8 January 1997. The bottom panel of Figure 6 shows the resulting SVT series calculated with K=80, L=80, M=20, τ=30. The dashed horizontal line in blue shows the threshold value (0.05) for the detection of Pi 2 pulsations accompanied by positive bays.

We can see that the result shows two high scores that exceed 0.05 at around 14:20UT and at around 14:40UT. These two high scores most likely correspond to second and third full-substorm onsets shown as vertical dashed lines. However, we see that the first full-substorm onset at around 13:10UT was not detected. This is likely due to the fact that the amplitude of the positive bay at around 13:10UT was small.

Similarly, the top panel of Figure 7 shows the keogram of auroral brightening observed by Polar/UVI in the Southern Hemisphere on 27 January 1997. The middle panel of Figure 7 shows H-component of ground-magnetometer data obtained at KAG station on 27 January 1997. The bottom panel of Figure 7 shows the resulting SVT series calculated with K=80, L=80, M=20, τ=30. The presentation format is the same as Figure 6. We can see that the result shows two high scores that exceed 0.05 at around 10:00UT, at around 15:30UT, at around 15:15UT and at around 17:10UT. It is likely that four full-substorm onsets were detected successfully by the proposed algorithm.

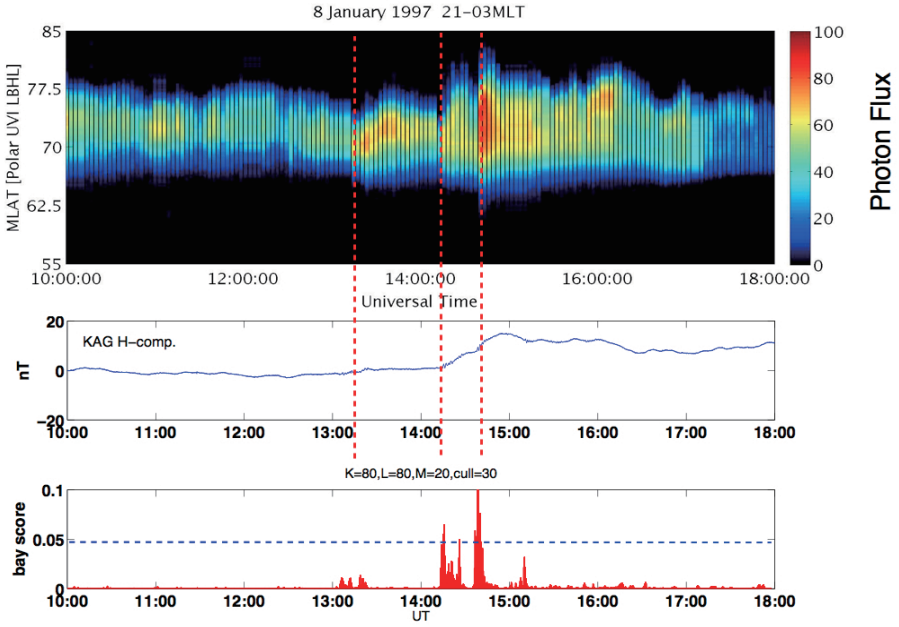

Fig. 6.(Top) Keogram of auroral brightening observed by Polar/UVI in the Southern Hemisphere on 8 January 1997. The luminescence intensity averaged over magnetic local time of 21-03LT. (Middle) H-component of ground-magnetometer data observed at KAG station on 8 January 1997. (Bottom). The resulting SVT series calculated from H-component of KAG data. The SVT parameters were set to K=80, L=80, M=20, τ=30. The dashed horizontal line in blue shows the threshold value for the detection of Pi 2 pulsations accompanied by positive bays.

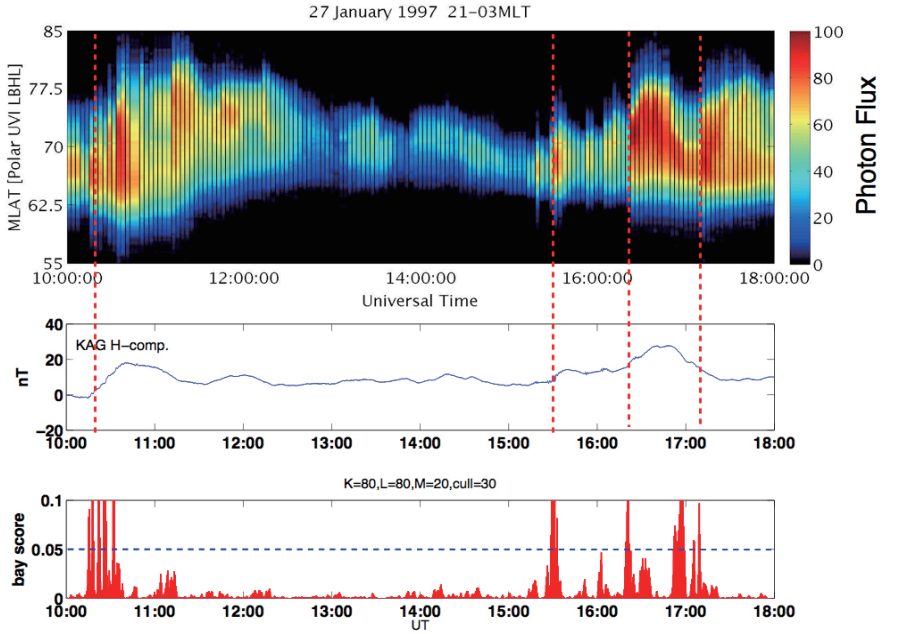

Fig. 7.(Top panel) Keogram of auroral brightening observed by Polar/UVI in the Southern Hemisphere on 27 January 1997. The luminescence intensity averaged over magnetic local time of 21-03LT. (Middle) H-component of ground-magnetometer data observed at KAG station on 27 January 1997. (Bottom panel) The resulting SVT series calculated from H-component of KAG data. The SVT parameters were set to K=80, L=80, M=20, τ=30. The dashed horizontal line in blue shows the threshold value for the detection of Pi 2 pulsations accompanied by positive bays.

3. 3. Statistical Evaluation

Next, let us evaluate the performance of the full-substorm onset detection algorithm based on SVT in a statistical study. By checking the keogram of auroral brightening observed by Polar/UVI, we identified 69 auroral breakups for the period from 3 January 1997 through 4 February 1997. We applied the SVT to H-component of ground-magnetometer data obtained at KAG. The investigation was limited in a time period from 10:00-18:00UT, which KAG was located in/around the midnight sector in the period. The SVT parameters were set to K=80, L=80, M=20, τ=30. The threshold value for detecting auroral breakups was set to 0.05. The evaluation procedure is as follows. (1) Detected Events: If the bay-score exceed 0.05 during poleward motion of aurora. (2) False Positive: If the bay-score exceed 0.05 during there is no poleward motion of aurora. (3) False Negative: If the bay-score does not exceed 0.05 during poleward motion of aurora. As we mentioned in Section 1, the most probable number of Pi 2 bursts per substorm is 2 (Hsu and McPherron, 2007). In other words, about half of Pi 2 pulsations is not accompanied by poleward expansion and positive bays. Thus, it is our expectation that the algorithm possibly detect almost equal numbers of full-substorm onsets and false positives.

A test result of the algorithm is summarized in Table 2. The algorithm detected 51 possible full-substorm onsets. Forty three out of 51 events were in good agreement with full-substorm onsets. Eight out of 51 events were false positives. The number of false positive was lower than expected. Twenty six out of 69 events were overlooked. Thus the rate of successful detection is calculated to be about 62%. We consider that our algorithm gives fairly good results on the nightside (21-03LT).

Table 2. Test result of the full-substorm onset detection algorithm based on SVT for the KAG data in the nighttime (21--03LT).

Date	Event Number	Successful Detection	False Negative	False Positive
3 Jan. 1997	1	1	0	0
4 Jan. 1997	1	1	0	0
5 Jan. 1997	2	2	0	0
6 Jan. 1997	1	0	1	0
7 Jan. 1997	4	4	0	3
8 Jan. 1997	3	2	1	0
9 Jan. 1997	0	0	0	0
11 Jan. 1997	4	3	1	1
12 Jan. 1997	3	3	0	0
13 Jan. 1997	5	3	2	0
14 Jan. 1997	2	2	0	0
15 Jan. 1997	1	1	0	0
16 Jan. 1997	0	0	0	0
17 Jan. 1997	3	1	2	0
18 Jan. 1997	0	0	0	0
19 Jan. 1997	3	1	2	0
20 Jan. 1997	1	0	1	0
21 Jan. 1997	5	3	2	1
22 Jan. 1997	1	1	0	0
23 Jan. 1997	0	0	0	0
24 Jan. 1997	4	1	3	0
25 Jan. 1997	1	0	1	0
27 Jan. 1997	4	4	0	0
28 Jan. 1997	4	4	0	2
29 Jan. 1997	1	1	0	0
30 Jan. 1997	4	2	2	0
31 Jan. 1997	1	0	1	0
1 Feb. 1997	1	0	1	0
2 Feb. 1997	4	1	3	0
3 Feb. 1997	1	1	0	0
4 Feb. 1997	4	1	3	1
Total	69	43	26	8

4. Conclusions

In order to identify the onset of full-substorms from ground-magnetometer data, we developed a new algorithm to detect Pi 2 pulsations that accompanied by positive bays. There are some works about automatic detection of Pi 2 pulsations. However, the previous studies are limited in detecting only wave packets. Thus, we defined the "bay-score" which provides information to determine whether positive bay is present or not. The transformation from an original time-series to a new time series of the bay-score named "Singular Value Transformation (SVT)". We have applied the SVT to ground-magnetometer data and showed that high scores of resulting SVT series are in good agreement with that full-substorm onsets. Further, we evaluated the practical performance of the SVT in a statistical study. By checking the keogram of auroral brightening observed by Polar/UVI, 69 full-substorm onsets were identified for the period from 3 January 1997 through 4 February 1997. Forty three events of them were detected successfully from ground-magnetometer data by proposed algorithm. On the other hand, 26 events were overlooked. This is mainly due to a local time dependence of positive bays (McPherron, 1973b). As mentioned in Section 1, it is thought that the substorm positive bay is caused by the substorm current wedge. Hence, the positive bay intensity strongly depends the positional relationship between the auroral breakup and the station. If KAG station was located outside the current wedge, the detection of positive bay likely failed regardless of the SVT parameter setting. By using the network data that covers wide range of longitude, the detection ratio will be improved. Whereas, the number of false positive was lower than expected. Hence, we conclude that the proposed algorithm is a strong method to detect positive bays from ground-magnetometer data. In other words, it will enable us to identify full-substorm onsets from ground-magnetometer data.

5. Acknowledgments

We would like to thank Prof. J. Dowell of the University of Iowa for providing the Polar/PWI data, Dr. C. Meng and Dr. K. Liou of Johns Hopkins University for providing Polar/UVI data. We thank all the members of the CPMN project (PI; K. YUMOTO) for their ceaseless support. The CPMN project is financially supported by the Ministry of Education, Science, and Culture of Japan (and Japan Society for the Promotion of Science (JSPS)) as the Grants-in-Aid for Overseas Scientific Survey (05041060, 0841105, 10041122, 12373003). The senior author (T. Tokunaga) was supported by the JSPS under Grant-in-Aid for Scientific Research 2005443. We would like to thank Dr. H. Kawano for his great assistance in evaluating and improving this paper as a reviewer.

6. References

Akasofu, S.-I., and Meng, C.-I. (1969) A study of polar magnetic substorm. *J. Geophys. Res*., **74**(1), 293-313, doi:10.1029/ JA074i001p00293.

Clauer, C.-R., and McPherron, R.-L. (1974) Mapping the local time-universal time development of magnetospheric substorms using mid-latitude magnetic observations. *J. Geophys. Res*., **79**(19), 2811-2820.

Hsu, T.-S., and McPherron R.-L. (2007) A statistical study of the relation of Pi 2 and plasma flows in the tail. *J. Geophys. Res*., **112** (A5), doi:10.1029/2006JA011782.

Ide, T., and Inoue, K. (2005) Knowledge discovery from heterogeneous dynamic systems using change-point correlations. *In Proceedings of 2005 SIAM International Conference on Data Mining*, Society for Industrial and Applied Mathematics, 571-576.

Jacobs, J.-A., Kato, Y., Matsushita, S., and Troitskaya, V.-A. (1964) Classification of geomagnetic micropulsations. *J.Geophys. Res*., **69**(1), 180-181.

Kataoka, R., Miyoshi, Y., and Morioka, A. (2009) Hilbert-huang transform of geomagnetic pulsations at auroral expansion onset. *J. Geophys. Res*., **114**, doi: 10.1029/2009JA014214.

Liou, K., Meng, C.-I., Lui, A.-T., and Newell, P.-T. (1999) On relative timing in substorm onset signatures. *J. Geophys. Res*., **104** (A10), 22807-22817.

McPherron, R.-L., Russell, C.-T., and Aubry, M.-P. (1973a) Satellite studies of magnetospheric substorms on August 15, 1968, 9, Phenomenological model for substorms. *J. Geophys Res*, **78**(16), 3131- 3149.

McPherron, R.-L., Russell, C.-T., Kivelson, M.-G., and Coleman Jr., P.-J. (1973b) Substorms in space: The correlation between ground and satellite observations of the magnetic field. *Radio Science*, **8**(11), 1059-1076.

McPherron, R.-L. (1991) Physical process producing magnetospheric substorms and magnetic storms. in Geomagnetism, 4, 593-739.

Meng, C.-I. and Akasofu, S.-I. (1969) A Study of Polar Magnetic Substorms 2. Three-Dimensional Current

System. *J. Geophys. Res*., **74**(16), 4035-4053, doi:10.1029/JA074i016p04035.

Moskvina, V., and Zhigljavsky, A. (2003) An algorithm based on singular spectrum analysis for change-point detection. *Communications in Statistics—Simulation and Computation*, **32**(2), 319-352.

Murphy, R.-K, Rae, I.-J., Ian, R.-M, Milling, D.-K., Watt, C.-E., Ozeke, L., Frey, H.-U., Angelopoulos, V., and Russel, C.-T. (2009) Wavelet-based ULF wave diagnosis of substorm expansion phase onset. *J. Geophys. Res*., **114**, doi:10.1029/2008JA013548.

Nakamura, R., Baker, D.-N., Yamamoto, T., Belian, R.-D., Bering III, E.-A., Benbrook, J.-R., and Theall, J.-R. (1994) Particle and field signatures during pseudobreakup and major expansion onset. *J. Geophys. Res*., **99**(A1), 207-221.

Nose, M., Iyemori, T., Takeda, M., Kamei, T., Milling, D.-K., Orr, D., Singer, H.-J., Worthington, E.-W., and Sumitomo, N. (1998) Automated detection of Pi 2 pulsations using wavelet analysis: 1. Method and an application for substorm monitoring. *Earth, Planetary and Space Sciences*, **50**(9), 773-783.

Ohtani S., Anderson, B.-J., Sibeck, D.-G., Newell, P.-T., Zanetti, L.-J., Potemura, T.-A., Takahashi, K., Lopez, R.-E., Angelopoulos, V., Nakamura, R., Klumper, D.-M., and Russell, C.-T. (1993) A multisatellite study of a pseudo-substorm onset in the near-Earth magnetotail. *J. Geophys. Res*., **98**(A11), 19355-19367.

Ohtani, S., Yamaguchi, R., Nose, M., Kawano, H., Engebretson, M., and Yumoto, K. (2002) Does the braking of the fast plasma flow trigger a substorm?: a study of the August 14, 1996, event. *Geophys. Res*. Lett., **29**(15), doi: 10.1029/2001GL013785.

Partamies, N., Amm, O., Kauristie, K., Pulkkinen, T.-I., and Tanskanen, E. (2003) A pseudo-breakup observation: Localized current wedge across the postmidnight auroral oval. *J. Geophys. Res*., **108**(A1), doi: 10.1029/2002JA009276.

Rostoker, G., Akasofu, S.-I., Foster, J., Greenwald, R.-A., Kamide, Y., Kawasaki, K., Lui, A.-T.-Y., McPherron, R.-L., Russell, C.-T. (1980) Magnetospheric substorms - Definition and signatures. *J. Geophys. Res*., **85**(NA4), 1663-1668.

Sato, T. (1969) Geomagnetic pulsations. *Space Science Review*, **10** (3), 319-412.

Saito, T., Yumoto, K., and Koyama, K. (1976) Magnetic pulsations pi2 as a sensitive indicator of magnetospheric substorm. *Planet. Space Sci*., **24**(11), 1025-1029, doi:10.1016/0032-0633(76)90120-3.

Sutcliffe, P. R. (2007) Substorm onset identification using neural networks and Pi2 pulsations. *Ann. Geophysicae*, **15**(10), 1257-1264.

Takahashi, K., Ohtani, S., and Anderson, B.-J. (1995) Statistical analysis of Pi 2 pulsations observed by the AMPTE CCE spacecraft in the inner magnetosphere. *J. Geophys. Res*., **100**(A11), 21929-21941.

Tokunaga, T., Ikeda, D., Nakamura, K., Higuchi, T., Yoshikawa, A., Uozumi, T., Fujimoto, A., Morioka, A., and Yumoto, K. (2010a) Detecting precursory events in time series data by an extension of singular spectrum transformation. *In: Proceedings of the 10th WSEAS International Conference on Applied Computer Science*, Fujita, H., Sasaki, J., and Guizzi, G. (eds.), WSEAS Press, 366-374.

Tokunaga, T., Ikeda, D., Nakamura, K., Higuchi, T., Yoshikawa, A., Uozumi, T., Fujimoto, A., Morioka, A., and Yumoto, K. (2010b) Onset time determination of precursory events in time series data by an extension of singular spectrum transformation. *International Journal of Circuits, System and Signal Processing*, **5**, 46-60.

Yumoto, K., and the CPMN Group. (2001) Characteristics of Pi 2 magnetic pulsations observed at the CPMN stations: a review of the STEP results. *Earth Planets Space*, **53**(10), 981-992.

Memoirs of the Faculty of Sciences, Kyushu University
Series D, Earth and Planetary Sciences

This publication is published irregularly. All the back issues are listed below.

Back Issues

Memoirs of the Faculty of Science, Kyushu Imperial University. Series D, Geology.
Vol. 1 No. 1 (July, 1940), No. 2 (Mar., 1941), No. 3 (July, 1942).
Vol. 2 No. 1 (Feb., 1943), No. 2 (Aug.,1944).
Vol. 3 No. 1 (Apr., 1947).
Memoirs of the Faculty of Science, Kyushu University. Series D, Geology.
Vol. 3 No. 2 (Nov., 1949), No. 3 (May.,1952), No. 4 (Dec.,1952).
Vol. 4 No. 1 (June, 1954), No. 2 (July, 1954).
Vol. 5 No. 1 (Aug., 1954), No. 2 (Oct., 1954), No. 3 (Dec.,1955), No. 4 (Jan., 1957).
Vol. 6 No. 1 (Feb., 1957), No. 2 (May.,1957), No. 3 (May.,1958).
Vol. 7 No. 1 (Mar., 1958).
Vol. 8 No. 1 (Mar., 1958), No. 2 (May.,1958), No. 3 (Mar.,1959), No. 4 (May.,1959).
Vol. 9 No. 1 (Dec., 1959), No. 2 (Nov.,1959), No. 3 (Mar.,1960).
Special Issue No. 1 (Nov., 1959), No. 2 (Jan., 1960).
Vol. 10 No. 1 (Dec., 1960), No. 2 (Mar.,1961).
Vol. 11 No. 1 (Mar., 1961), No. 2 (Nov.,1961), No. 3 (Dec.,1961).
Vol. 12 No. 1 (Mar., 1962), No. 2 (June,1962), No. 3 (June,1962).
Vol. 13 No. 1 (Feb., 1963).
Vol. 14 No. 1 (Jan., 1963), No. 2 (Mar.,1963), No. 3 (Jan., 1964).
Vol. 15 No. 1 (June, 1964), No. 2 (Mar.,1965).
Vol. 16 No. 1 (Mar., 1965), No. 2 (May.,1965), No. 3 (Nov.,1965).
Vol. 17 No. 1 (Nov., 1965), No. 2 (Dec.,1965), No. 3 (Sept.,1966).
Vol. 18 No. 1 (Feb., 1967), No. 2 (Dec.,1967).
Vol. 19 No. 1 (Jan., 1969), No. 2 (Jan., 1969), No. 3 (Nov.,1969).
Vol. 20 No. 1 (Jan., 1970), No. 2 (Nov.,1970).
Vol. 21 No. 1 (Oct., 1971), No. 2 (Dec.,1972).
Vol. 22 No. 1 (Nov., 1973), No. 2 (Feb.,1975).
Vol. 23 No. 1 (Mar., 1975), No. 2 (Nov.,1975), No. 3 (Feb.,1977).
Vol. 24 No. 1 (Nov., 1978), No. 2 (Nov.,1979), No. 3 (Jan., 1981), No. 4 (Dec.,1981).
Vol. 25 No. 1 (Nov., 1983), No. 2 (Nov.,1984), No. 3 (Feb.,1985).
Vol. 26 No. 1 (Jan., 1986), No. 2 (Jan., 1988), No. 3 (Dec.,1989).
Memoirs of the Faculty of Science, Kyushu University. Series D, Earth and Planetary Sciences.
Vol. 27 No. 1 (Jan., 1991), No. 2 (Feb.,1992).
Vol. 28 No. 1 (Dec., 1993), No. 2 (Dec.,1994).
Vol. 29 No. 1 (Dec., 1995), No. 2 (Dec.,1996).
Vol. 30 No. 1 (Jan., 1998), No. 2 (Dec.,1998), No. 3 (Dec.,1999).
Vol. 31 No. 1 (Dec., 2000), No. 2 (Feb.,2002), No. 3 (Feb.,2005), No. 4 (Feb.,2007).
Vol. 32 No. 1 (Feb., 2008), No. 2 (Mar.,2009), No. 3 (Mar.,2011).

Published by
FACULTY OF SCIENCES
Kyushu University
Fukuoka, Japan

平成23年3月10日　発行

編 集 兼　九州大学大学院理学研究院
発 行 者　〒812-8581
福岡市東区箱崎6丁目10番1号

編　　集　株 式 会 社 ミ ド リ 印 刷
福岡市博多区西月隈1丁目2番11号

TYPESETTING PERFORMED AT MIDORI PRINTING CO., LTD., FUKUOKA